



## Durham E-Theses

---

### *Some applications of regge theory to high energy cross sections*

O'Hara, Donald William

#### How to cite:

---

O'Hara, Donald William (1973) *Some applications of regge theory to high energy cross sections*, Durham theses, Durham University. Available at Durham E-Theses Online: <http://etheses.dur.ac.uk/8591/>

#### Use policy

---

The full-text may be used and/or reproduced, and given to third parties in any format or medium, without prior permission or charge, for personal research or study, educational, or not-for-profit purposes provided that:

- a full bibliographic reference is made to the original source
- a [link](#) is made to the metadata record in Durham E-Theses
- the full-text is not changed in any way

The full-text must not be sold in any format or medium without the formal permission of the copyright holders.

Please consult the [full Durham E-Theses policy](#) for further details.

SOME APPLICATIONS OF REGGE THEORY TO  
HIGH ENERGY CROSS SECTIONS

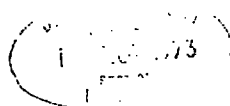
by

Donald William O'Hara

A thesis presented for the degree of  
Doctor of Philosophy  
at the University of Durham.

August 1973

Mathematics Department,  
University of Durham.



## PREFACE

The work presented in this thesis was carried out in the Department of Mathematics at the University of Durham between October 1970 and August 1973 under the supervision of Professor E.J. Squires.

The material in this thesis has not been submitted for any degree in this or any other university. No claim of originality is made for chapter one or chapter five. Chapters two and three are based on two papers by the author in collaboration with Professor Squires, together with some unpublished material by the author. Chapter four is based on unpublished work by the author.

The author wishes to express his sincere gratitude to Professor Squires for his patient help and guidance throughout this work. He wishes to thank Miss A.R. Ward and Mr. G.W. Bennett for valuable discussions, and Mrs. D. Kipling for her accurate typing. He is grateful also to the Science Research Council for a Research Studentship.

## ABSTRACT

This thesis deals with some applications of Regge Theory to  $K^{\pm} p$  and  $pp$  elastic scattering.

Chapter one is an introduction. The important results and problems of Regge theory are discussed, together with some recent developments.

In chapter two a model incorporating doubled trajectories is proposed and compared to  $K^{\pm} p$  elastic scattering data. The model supports  $t$  channel helicity conservation for the pomeron near the forward direction. The results for  $K^{-} p$  agree in part with those of Hayot and Navelet at 10 GeV/c, and those for  $K^{+} p$  agree well with the CERN beta phase shift solution at 2.5 GeV/c.

In chapter three a  $j$ -plane analysis technique is introduced. It is applied to  $pp$  elastic scattering, where the results do not allow an interpretation in terms of simple poles. Evidence is presented that the curvature of the  $pp$  total cross section is not due to exchange degeneracy breaking.

In chapter four the  $j$ -plane structure of  $pp$  scattering in the absorption model is investigated. Many of the puzzling features of the results of chapter three are explained.

Chapter five is concerned with the recent data on  $pp$  scattering at high energies. Several models which have been proposed to explain these data are discussed, and some conclusions are drawn.

## CONTENTS

	<u>Page</u>
PREFACE	
ABSTRACT	
CHAPTER 1 INTRODUCTION	
1.1 Regge Theory	1
1.2 Problems of Regge Pole Theory	5
1.3 Duality	8
1.4 The Veneziano Model	12
1.5 Doubled Trajectory Models	15
1.6 Regge Cuts	17
FIGURES	22
CHAPTER 2 DOUBLED TRAJECTORIES AND $K \rightleftharpoons P$ ELASTIC SCATTERING	
Introduction	23
2.1 Amplitudes and Formalism	24
2.2 Ambiguities in Regge Analysis	27
2.3 The Model.....	30
2.4 Comparison with the Amplitude Analysis of Heyot and Navelet	44
2.5 Comparison with $K - p$ Phase Shift Analysis	47
2.6 Conclusions	53
FIGURES	55
CHAPTER 3 J-PLANE ANALYSIS OF PP ELASTIC SCATTERING	
Introduction	56
3.1 Amplitudes and Formalism	58
3.2 The Total Cross Section	61
3.3 The Differential Cross Section	66
3.4 Conclusions	76
FIGURES	77

	<u>Page</u>	
CHAPTER 4	THE J-PLANE STRUCTURE OF PP ELASTIC SCATTERING IN THE ABSORPTION MODEL	
	Introduction	78
4.1	Formalism and Definitions	80
4.2	The Model	82
4.3	Comparison with the Data Analysis of Chapter 3	85
4.4	Conclusions and Discussion	90
	FIGURES	91
CHAPTER 5	THE PP DATA AT VERY HIGH ENERGIES AND CONCLUDING REMARKS	
	Introduction	92
5.1	The Experimental Situation	93
5.2	Field Theoretic Models	95
5.3	The Triple Pomeron Vertex	97
5.4	The Reggeon Calculus	98
5.5	Discussion and Conclusions	99
	FIGURES	101
APPENDIX	ELASTIC SCATTERING KINEMATICS	102
	REFERENCES	104

1.1 Regge theory

The complex angular momentum plane has been central in most recent approaches to strong interaction physics. In Regge theory, scattering amplitudes are analytic functions of the angular momentum  $j$ , and a particle of mass  $m$  lies on a Regge trajectory  $\alpha(t)$ , where the spin of the particle is  $\alpha(m^2)$ . The partial wave amplitude then has a pole at  $j = \alpha(t)$  and it is the exchange of these Regge Poles which is supposed to dominate the amplitudes at high energies.

A Regge trajectory  $\alpha(t)$  has associated with it a signature  $\tau$ , which may be  $+1$  or  $-1$  (called even or odd signature respectively). In general many particles will lie on the same trajectory, but only particles of even (odd) spin can lie on a trajectory of even (odd) signature.

If a trajectory  $\alpha(t)$  is allowed by its quantum numbers to be exchanged in the process  $ab \rightarrow a'b'$ , then its contribution to the amplitude for this process at high energies is given by

$$A_{\alpha}(s, t) = \beta_{\alpha}(t) \gamma_{\alpha}^{ab \rightarrow a'b'}(t) \left(\frac{s}{s_0}\right)^{\alpha(t)} \quad (1.1)$$

This is often represented by the diagram in fig.(1.1). Here

$\beta_{\alpha}(t)$  is the signature factor

$$\beta_{\alpha}(t) = - \frac{(e^{-i\pi\alpha(t)} + \tau_{\alpha})}{\sin(\pi\alpha(t))} \quad (1.2)$$

$\tau_{\alpha}$  is the signature of the trajectory,  $\gamma_{\alpha}^{ab \rightarrow a'b'}(t)$

is the residue function, and  $s_0$  is the scale factor.

Properties of the trajectory function

(i)  $\alpha(t)$  is universal, that is it depends on the quantum numbers, but not on the external particles.

(ii)  $\alpha(t)$  is an analytic function of  $t$ , except for a cut on the positive real axis starting at the  $t$  channel threshold  $t_{TH}$ . (In all cases relevant to this thesis  $t_{TH} = 4m^2$ ).

(iii) As mentioned above, a particle of mass  $m$  which lies on the trajectory has spin  $\sigma = \alpha(m^2)$ , and satisfies

$$(-1)^\sigma = \tau_\alpha$$

(iv) Unitarity, via the Froissart Bound, i.e.

$$\sigma_T \lesssim (\log s)^2 \tag{1.3}$$

implies that  $\alpha(s) \lesssim 1$

(v) Experimentally it is found that trajectories seem to be linear in  $t$  up to the highest spins detected.

(vi) From the above properties it can be deduced that  $\alpha(t)$  is a Herglotz function of  $t$  for  $t < t_{TH}$ .

Using (v) and (ii) we may write the dispersion relation

$$\alpha(t) = \alpha(0) + \alpha' t + \frac{1}{\pi} \int_{t_{TH}}^{\infty} dt' \frac{\text{Im} \alpha(t')}{t' - t} \tag{1.4}$$

from which

$$\frac{d^n \alpha}{dt^n} = \frac{n!}{\pi} \int_{t_{TH}}^{\infty} dt' \frac{\text{Im} \alpha(t')}{(t' - t)^{n+1}} \tag{1.5}$$

(Note that this result is unchanged if a subtraction is necessary in the integral in e.g. (1.4).)

Unitarity requires that

$$\text{Im} \alpha(t) > 0 \tag{1.6}$$

which implies

$$\frac{d^n \alpha(t)}{dt^n} > 0 \text{ for all } t < t_{TH} \tag{1.7}$$

i.e. that  $\alpha(t)$  is a Herglotz function. This property will be useful in calculating Regge Cut discontinuities.

Properties of the Residue Function

(i) Apart from kinematic singularities, which may be removed explicitly,  $\gamma_\alpha(t)$  is a real analytic function of  $t$ , except for a cut along the positive real axis starting at  $t_{TH}$ .

(ii)  $\gamma_\alpha^{ab} \rightarrow a'b'$  (t) factorises into functions at the vertices of fig.(1.1) i.e.

$$\gamma_\alpha^{ab} \rightarrow a'b' (t) = \gamma_\alpha^{a\bar{a}'}(t) \gamma_\alpha^{b\bar{b}'}(t) \tag{1.8}$$

(iii) For a particle of mass  $m$  on the trajectory  $\alpha$ ,  $\gamma_\alpha(m^2)$  is proportional to its coupling constant.

(iv) Behaviour near Integral Values of  $\alpha$

When the initial state of a process can couple to a particle of spin  $j$ , but the final state cannot,  $j$  is known as a sense-nonsense point, and vice versa. If both initial and final states can couple,  $j$  is a sense-sense point, and if neither,  $j$  is a nonsense-nonsense point. Values of  $j$  to which either the initial or final state cannot couple are known collectively as nonsense values. Values of  $j$  satisfying

$$(-1)^j = \tau_\alpha$$

are known as right-signature points, and values not satisfying this are wrong-signature points.

We consider the behaviour of the leading Regge Pole contributions to helicity amplitudes which are sense-sense, sense-nonsense, and nonsense-nonsense at  $\alpha(t) = n$  ( $n$ : integer).

$$A_{ss} \sim \beta_\alpha \gamma_\alpha^{ss} \left(\frac{s}{s_0}\right)^\alpha \tag{1.9}$$

$$A_{sn} \sim (\alpha - n)^{\frac{1}{2}} \beta_\alpha \gamma_\alpha^{sn} \left(\frac{s}{s_0}\right)^\alpha \tag{1.10}$$

$$A_{nn} \sim (\alpha - n) \beta_\alpha \gamma_\alpha^{nn} \left(\frac{s}{s_0}\right)^\alpha \tag{1.11}$$

The factors  $(\alpha - n)^{\frac{1}{2}}$ ,  $(\alpha - n)$  come from the behaviour of the rotation functions  $d_{\lambda\lambda'}^j(\theta)$  near  $j = n$  (see ref.1). (1.10) implies, by analyticity of  $A_{sn}$ , that

$$\gamma_\alpha^{sn} \sim (\alpha - n)^{\frac{1}{2}} \quad \text{near } \alpha = n \tag{1.12}$$

and since by factorisation

$$\gamma_\alpha^{ss} \gamma_\alpha^{nn} = (\gamma_\alpha^{sn})^2 \sim (\alpha - n) \tag{1.13}$$

either  $\gamma_\alpha^{ss}$  or  $\gamma_\alpha^{nn}$  must contain a factor  $(\alpha - n)$ .

If  $\alpha(t)$  is a right signature point with  $t < 0$   $\gamma_\alpha^{ss}$  must vanish, since otherwise  $A_{ss}$  would have the pole in the signature factor, implying the existence of a particle of imaginary mass, called a ghost or tachyon. At wrong-signature points, however,  $\beta_\alpha$  does not have a

pole, so that one of the amplitudes will vanish at these points. Such behaviour is known as a Wrong Signature Zero, and has been extensively used to explain the dips found in the differential cross sections of many processes at  $t \approx -0.6 \text{ GeV}^2$ , where one expects  $\alpha_{\sqrt{s}} \approx 0$ .

Unfortunately for this explanation, it can be shown from unitarity (9,20) that there are also fixed poles at these points, but the effect of these poles is difficult to estimate, and they are often neglected. In any case Mandelstam (21) has argued that they are shielded (i.e. moved onto unphysical sheets) by Regge Cuts.

## 1.2 Problems of Regge Pole Theory

### (i) The Charge Exchange Polarisation

The process  $\pi^- p \rightarrow \pi^0 n$ , known as  $\pi N$  charge exchange, has attracted a great deal of attention, since the only known trajectory which is allowed to be exchanged is the  $\rho$ . Regge theory therefore predicts the following forms for the invariant amplitudes  $A', B$  (see section 2.1) at high energy:

$$A'(s, t) = \beta_\rho(t) \gamma_\rho(t) \left(\frac{s}{s_0}\right)^{\alpha_\rho(t)} \quad (1.14)$$

$$B(s, t) = \beta_\rho(t) \beta'_\rho(t) \left(\frac{s}{s_0}\right)^{\alpha_\rho(t)-1} \quad (1.15)$$

The polarisation parameter is given by

$$P \frac{d\sigma}{dt} = 2C(s, t) \operatorname{Im}(A'B^*) \quad (1.16)$$

(where  $C(s, t)$  contains only kinematic factors) so that the prediction of Regge Theory is

$$P \frac{d\sigma}{dt} = 2C \gamma_\rho(t) \beta'_\rho(t) \left(\frac{s}{s_0}\right)^{2\alpha_\rho-1} \operatorname{Im}(|\beta_\rho|^2) \quad (1.17)$$

Experimentally, however, the polarisation is quite large and positive over a wide range of  $s$  and  $t$ .

To explain this phenomenon some authors (3, 4, 5, 22) have postulated the existence of another trajectory, called the  $\rho'$ , half a unit below the  $\rho$  in the angular momentum plane, i.e.

$$\alpha_{\rho'}(0) = 0 \quad (1.18)$$

with which they are able to fit all the available data. Such an explanation cannot be completely dismissed, especially in the light of the discovery of an apparently suitable candidate for this particle<sup>(22)</sup>, although the coupling of this experimental  $\rho'$  to  $\pi\pi$  appears to be small.

Many more recent attempts to solve this problem have involved Regge cuts, and in particular the absorption model. (for a list of some of the references see ref.12). These have all failed to reproduce the

angular structure of the data, producing quite unnecessary wild fluctuations and zeros. The amplitude analysis by Halzen and Michael<sup>(23)</sup> of the  $\pi N$  system has shown that the amplitudes produced by these models are also wrong, and it seems that this explanation is not correct. It may be, however, that Regge cuts are still the answer, and that it is merely the absorption model which is too crude to be useful in calculating such a sensitive parameter as the polarisation.

(ii) The crossover phenomenon.

The differential cross sections for  $\pi^+p$  and  $\pi^-p$  are found experimentally to be equal at  $t_c \cong -0.16 \text{ GeV}^2$  independent of energy. The same result is found in  $Kp$  and  $pp$  scattering.

Consider as an example  $\pi p$  scattering. The allowed exchanges are

$$\pi^+ p = p \leftrightarrow \rho^+ \rho^- \quad (1.19)$$

and it is quite easy to show that for the quantity

$$\Delta \frac{d\sigma}{dt} (\pi) \cong \frac{d\sigma}{dt} (\pi^-p) - \frac{d\sigma}{dt} (\pi^+p) \quad (1.20)$$

to vanish at  $t = t_c$ , it is necessary that the  $\rho$  residue has a zero there, i.e.

$$\gamma_{\rho}^{\pi p}(t_c) = 0 \quad (1.21)$$

From  $Kp$  and  $pp$  one may deduce a similar zero in the  $w$  residue.

The problem arises when we use factorisation to predict similar zeros in  $\pi p \rightarrow \rho n$  and  $\rho p \rightarrow \pi^0 p$ , where experimentally none are observed.

Regge cut models have been used to explain this phenomenon. In these models crossover zeros are generated by cancellations between the pole and cut terms. The problem with this explanation is that, since the energy dependence of the pole and cut are not the same, the crossover zero should move with energy. Phenomenologically this is not a serious problem, since the rate at which the zero moves will be dependent only on  $\log s$ , but it seems an odd coincidence that the zero remains in the same position for all processes.

(iii) The Pion Conspiracy Problem

We just mention this for completeness, as another well-known problem of Regge pole theory caused by factorization. The subject is discussed in detail in ref. (12).

What happens is that angular momentum conservation and the unnatural parity of the pion imply that its contribution to the processes  $\gamma p \rightarrow \pi^+ n$  and  $np \rightarrow pn$ , among others, should vanish in the forward direction. Experimentally, however, the differential cross sections for these processes exhibit sharp forward spikes of width about  $m \frac{2}{k}$ , for which the most natural explanation seems to be the pion exchange.

The conspiracy explanation (56, 57) requires the invention of an even-parity "conspirator" with the same residue and trajectory as the pion at  $t = 0$ , which allows the angular momentum constraint to be satisfied while the pion is finite at  $t = 0$ .

Apart from the fact that no such scalar particle has been observed, this explanation runs into serious trouble through factorisation<sup>(58)</sup>. This implies that the forward cross sections for  $\pi N \rightarrow \rho \Delta$  and  $N\bar{N} \rightarrow \Delta\bar{\Delta}$  should vanish, which experimentally does not seem to be the case.

Cut models have also been put forward as a solution to this problem. Extremely strong cuts are necessary, in some cases the enhancement factor  $\lambda$  being as much as 3.5 (see, for example ref. (59)), which is somewhat difficult to justify.

### 1.3 Duality

It is well known that at low energies the scattering amplitude is conveniently described by a sum of s channel resonances, whereas at high energies the exchange of t channel Regge poles provides a more economical description. For intermediate energy regions, it might be thought reasonable to take a sum of these descriptions;

$$A(s,t) = A^{\text{Regge}}(s,t) + A^{\text{Resonance}}(s,t) \quad (1.25)$$

This approach, called the Interference model, was criticised by Dolan, Horn & Schmid<sup>(8)</sup>. They added the known resonances in

$\pi\text{-p} \rightarrow \pi^0\text{n}$  to the  $\rho$  Regge-Pole amplitude obtained from a high-energy fit, and found that the sum was much larger than the actual amplitude. This led them to formulate the principle of Duality, that the s-channel resonances are contained in the t-channel Regge Poles, and vice versa. The interference model is then wrong because it commits double counting.

Important to this sort of Duality is the concept of the Finite Energy Sum Rule. We consider the contour C of fig.(1.2) in the complex plane, where the variable  $v$ , defined by

$$v = \frac{s-u}{2S_0} \quad (1.26)$$

is convenient because of its simple crossing behaviour. We write Cauchy's theorem for  $v^n A(v,t)$  around the contour as

$$\oint_C v^n A(v,t) dv = 0 \quad (1.27)$$

If A is an amplitude with Regge asymptotic behaviour, (see e.g.(1.4))  
i.e.

$$A(v,t) \underset{|v| \rightarrow \infty}{\sim} \sum_{\alpha} -\delta_{\alpha}(t) \frac{e^{-i\pi\alpha} + \tau_{\alpha}}{\sin \pi\alpha} v^{\alpha} \quad (1.28)$$

we may substitute this form for  $A(v, t)$  on the large circle (radius  $N$ ) we obtain the following sum rule:

$$\frac{1}{N^{n+1}} \int_{v_{TH}}^N v^n dv \operatorname{Im} A(v, t) = \sum_{\alpha} \frac{\gamma_{\alpha}(t) N^{\alpha(t)}}{\alpha(t) + n + 1} \quad (1.29)$$

Now since at low energies  $A(v, t)$  is given by the direct channel resonances, if we choose  $N$  sensibly we may write

$$\frac{1}{N^{n+1}} \int_{v_{TH}}^N v^n dv \operatorname{Im} A^{\text{RESONANCE}}(v, t) = \sum_{\alpha} \frac{\gamma_{\alpha}(t) N^{\alpha(t)}}{\alpha(t) + n + 1} \quad (1.30)$$

This means that the Regge Pole term averages the direct channel resonances. This defines what is known as Global Duality.

Finite Energy Sum Rules can also be used to predict high energy parameters from the behaviour of direct channel resonances at low energies. For example, if we define

$$S_n(t) = \frac{1}{N^{n+1}} \int_{v_{TH}}^N v^n dv \operatorname{Im} A^{\text{RESONANCE}}(v, t) \quad (1.31)$$

and consider, for example,  $\pi-p \rightarrow \pi^0 n$ , where only the  $\rho$  can be exchanged, we find, from e.q. (1.30)

$$\alpha_{\rho}(t) = \frac{(m+1) S_m - (n+1) S_n}{S_n - S_m} \quad (1.32)$$

The values of  $\alpha_{\rho}(t)$  found in this way agree well with those obtained from high energy fits.

At this stage a problem arises, namely the role of the pomeron in these sum rules. If we consider, for example,  $K+p$  scattering, there are no known direct-channel resonances, but the high energy behaviour is supposed to be pomeron dominated. E.q.(1.30) clearly cannot be made to work in these circumstances.

The usual solution to this problem<sup>(15,16)</sup> is to suppose that the pomeron does not contribute to these sum rules. This appears fairly reasonable, as the pomeron is clearly a different singularity from other Regge poles. It must also be pointed out that, as well as the pomeron on the right hand side of e.q.(1.30) we have omitted background terms on the left hand side. In refs.(15,16) it was suggested that these terms are dual to each other. A conjecture which is supported by the experimental observation that processes dominated by the pomeron at high energies appear to have a large amount of background in the resonance region, and vice versa.

We are then left with only known resonances on the left hand side of (1.30), and known trajectories on the right hand side.

With this provision, the sum rules imply very strong constraints on the Regge Pole parameters. Consider elastic K+p scattering, which as mentioned above, is exotic, that is it has no direct channel resonances that can be made from three quarks. The allowed t channel exchanges are  $\rho$ ,  $\omega$ ,  $f$ ,  $A_2$ , so substituting into e.q. (1.30) we obtain

$$\sum_{x=\rho, \omega, f, A_2} \frac{\delta_x(t) N^{\alpha_x(t)}}{\alpha_x(t) + n + 1} = 0 \quad (1.33)$$

Since, to have any significance at all, the Sum Rule cannot depend critically on N, we must have some of the  $\alpha$ 's equal. In fact, by consideration of other processes also, we can show that:

$$\alpha_\rho(t) = \alpha_\omega(t) = \alpha_f(t) = \alpha_{A_2}(t) \quad \text{for all } t \quad (1.34)$$

and also that

$$\delta_\rho(t) + \delta_\omega(t) = \delta_{A_2}(t) + \delta_f(t) \quad \text{for all } t.$$

These results are known collectively as Exchange Degeneracy. The

fact that the  $\rho$ ,  $\omega$ ,  $f$  and  $A_2$  particles all lie close to the same line

$$\alpha(t) \approx \frac{1}{2} + t \quad (1.35)$$

is a considerable success for this picture. The situation for the residues is less clear, as they cannot be extracted from data in a model independent way, and the matter is still a subject of controversy. The flatness of the  $pp$  and  $K+p$  total cross sections, however, suggests that Exchange degeneracy is at least approximately true at  $t = 0$ .

The status of Regge cuts in the Sum Rules is another problem. It has been shown <sup>(13,14)</sup> that most current cut models are difficult to accommodate in the Sum Rules. The equations are complicated and need to be calculated numerically, but it does seem that cut models are not easy to include.

1.4 Veneziano Model

Veneziano<sup>(17)</sup> constructed the following function:

$$V_{nmp}(s,t) = \frac{\Gamma(n-\alpha_s) \Gamma(m-\alpha_t)}{\Gamma(p-\alpha_s-\alpha_t)} \quad (1.36)$$

where  $n, m, p$  are integer constants, and  $\alpha_s(s), \alpha_t(t)$  are respectively  $s$  and  $t$  channel trajectory functions. If we take a sum of such terms:

$$V(s,t) = \sum_{n,m,p} C_{nmp} V_{nmp}(s,t) \quad (1.37)$$

with  $C_{nmp}$  constants, then amplitudes of the form

$$A(s,t,u) = V(s,t) + V(t,u) + V(s,u) \quad (1.38)$$

may be constructed, which have the correct crossing and asymptotic behaviour, and are explicit solutions of the Finite Energy Sum Rule.(1.29).

The drawback of this formula is that the resonance poles lie on the real axis and have zero width. This means that the amplitude cannot have Regge asymptotic behaviour on the real axis, and also that it violates unitarity. Attempts to construct simple unitarised Veneziano models<sup>(18)</sup> have usually caused the elegant duality properties of the amplitude to be lost.

A very attractive idea (for references see ref.(18)), is that the Veneziano model, or something like it, can be considered as the first term in a Born series, and that unitarity will be recovered when the whole series has been calculated. Unfortunately, progress on this front has been slow, and we confine ourselves to consideration of e.q.(1.38). We perform an asymptotic expansion of e.q.(1.36) along a line

$$\alpha_s = |\alpha_s| e^{i\epsilon} \quad ; \quad \epsilon > 0, \quad |\alpha_s| \rightarrow \infty \quad (1.39)$$

and hope that the resulting form is not altered too much by unitarisation.

For this purpose we use Stirling's formula

$$\Gamma(z) \underset{|z| \rightarrow \infty}{\sim} \sqrt{2\pi} e^{-z} z^{(z-\frac{1}{2})} \quad (1.40)$$

together with the well-known result

$$\Gamma(z) \Gamma(1-z) = \frac{\pi}{\sin \pi z} \quad (1.41)$$

and obtain

$$V_{nmp}(s,t) \underset{|s| \rightarrow \infty}{\sim} \frac{\pi(-)^{n-m-p-1}}{\Gamma(\alpha_t-m+1) \sin \pi \alpha_t} e^{-i\pi \alpha_t} [\alpha_s]^{\alpha_t-p+n} \quad (1.42)$$

In the case of a linear trajectory

$$\alpha_s(s) = \alpha_{s0} + \alpha'_s s \quad (1.43)$$

this becomes

$$V_{nmp}(s,t) \underset{|s| \rightarrow \infty}{\sim} \frac{\pi(-)^{n-m-p-1} e^{-i\pi \alpha_t}}{\Gamma(\alpha_t-m+1) \sin \pi \alpha_t} [\alpha'_s s]^{\alpha_t-p+n} \quad (1.44)$$

We now require that the leading asymptotic behaviour be

$$V_{nmp}(s,t) \sim s^{\alpha_t} \quad (1.45)$$

which gives the constraint

$$p \geq n. \quad (1.46)$$

In the case of the leading trajectory,  $p = n$  and we obtain

$$V_{\text{nmp}}(s,t) \underset{|s| \rightarrow \infty}{\sim} \frac{\pi(-)^{m+1} e^{-i\pi\alpha_t}}{\Gamma(\alpha_t - m + 1) \sin \pi\alpha_t} (\alpha'_s s)^{\alpha_t} \quad (1.47)$$

We see that this gives Regge behaviour with residue

$$\gamma_m(t) = \frac{\pi(-)^{m+1}}{\Gamma(\alpha_t - m + 1)} \quad (1.48)$$

and the additional result

$$s_0 = \frac{1}{\alpha'_s} \quad (1.49)$$

The integer  $m$  determines the mechanism, i.e. the behaviour of  $\gamma_m(t)$  at integer values of  $\alpha_t(t)$ .

### 1.5 Doubled Trajectory models

As may be seen from section (1.2) the main problems of Regge Pole theory arise through factorisation, namely the crossover zero and the pion conspiracy problem. Also, if one imposes duality, exchange degeneracy in  $\pi\pi \rightarrow \pi\pi$  constrains the  $\rho$  and  $f$  residues to be equal, which implies via factorisation that the  $\rho$  chooses nonsense at  $\alpha_\rho(t) = 0$  in  $\pi^-p \rightarrow \pi^0n$ , and therefore that the differential cross section for this process should vanish at  $t = -0.6 \text{ GeV}^2$ , instead of merely having the dip which is observed.

This evidence led Johnson and Squires<sup>(6)</sup> to question factorisation, and the observation of a split  $A_2$  meson provided a natural explanation of non-factorising residues. By invoking  $su$ <sup>(3)</sup> and exchange degeneracy in the  $K\bar{K}$  system, they were led to conclude that all other trajectories, and in particular the  $\rho$ , are also split. They were then able to formulate a model for  $\pi^-p \rightarrow \pi^0n$ , and confront it with the data.

The obvious objection to this model is that the  $\rho$  meson is not observed to be split, but Rittenberg and Rubinstein<sup>(7)</sup> showed in a  $6\pi$  Veneziano amplitude that doubled trajectories could occur, and that the doubling should not appear at the lowest particle on the trajectory.

Four benefits were immediately obtained from this model.

- (i) It was possible to have a non-zero amplitude in  $\pi^-p \rightarrow \pi^0n$  at  $\alpha_\rho(t) = 0$  without breaking Exchange Degeneracy in  $\pi\pi \rightarrow \pi\pi$ .
- (ii) The crossover zero was explained as a cancellation between the two components of the  $\rho$  meson. As the splitting of trajectories was small, this zero did not move significantly with energy.
- (iii) The polarisation was generated by interference between the two components.
- (iv) A more general benefit was that Johnson and Squires were able to use the simple Veneziano residues (see e.g. (1.48)) and still generate the considerable structure required by the data. That single Veneziano terms have insufficient structure to fit the data was shown, for example, by Berger and Fox<sup>(66)</sup>.

The model was thus qualitatively very successful, and succeeded in fitting the available data satisfactorily.

Of course, the  $A_2$  meson has since been shown not to be split, removing some of the justification for this model. The failure of cut models to explain the structure of the charge exchange polarisation, or to provide an elegant explanation of the energy-independent behaviour of dips and zeros in cross sections, however, suggests that the model is still worth considering.

In Chapter 2 we apply a modified version of the model to  $K^+p$  elastic scattering, where the crossover is particularly well defined. In this process many Regge poles can be exchanged, so that there is no need to split the trajectories to explain the polarisation, and indeed, since the  $A_2$  is no longer split, there is no justification for doing so.

### 1.6 Regge Cuts

Regge cuts, which have been mentioned several times in the preceding sections as a solution to the problems of Regge Pole theory, are generated by the simultaneous exchange of two or more trajectories. We shall consider only two-reggeon cuts, for which fig.(1.3a) is the general diagram. The contribution of this diagram may be evaluated by means of the Reggeon Calculus of Gribov<sup>(10)</sup>, and we shall later quote the result.

We consider first the box diagram in fig.(1.3c). This might be expected to be the simplest contribution to the two-reggeon cut amplitude, but in fact it does not contribute at all, and the reasons for this are important. (For a useful review of the situation see ref.(11)).

It is most convenient to transform the integral over the loop four-momentum in fig. (1.3c) into an integral over the invariants  $q_{\alpha 1}^2, q_{\alpha 2}^2, q_x^2, q_{x'}^2$ , where  $q_c$  is the four-momentum of particle (or reggeon) c. (This procedure was introduced by Rothe<sup>(62)</sup>). The transformation involves a Jacobian, J, given at large energies by

$$J = s^2 \lambda(t, t_1, t_2) \quad (1.50)$$

$$\text{where } \lambda = t^2 + t_1^2 + t_2^2 - 2(tt_1 + tt_2 + t_1t_2) \quad (1.51)$$

$$\text{and } t_1 = q_{\alpha 1}^2 \quad (1.52)$$

We assume for simplicity that the internal particles  $x, x'$  are identical spin-zero mesons of mass  $m$ . At the vertices of the diagram there are coupling functions  $g_i$ , which are related to the factorised Reggeon residues of e.g. (1.8) by

$$\gamma_{\alpha_i}^{a\bar{x}}(t_i) = g_i(t_i, m^2) \quad (1.53)$$

giving the contribution of the diagram as

$$A_{Box}^{ab \rightarrow a'b'} = i \int_{-\infty}^{\infty} \frac{dq_x^2 dq_{x'}^2}{(q_x^2 - m^2 + i\epsilon)(q_{x'}^2 - m^2 + i\epsilon)} \int dt_1 dt_2 \frac{\theta(\lambda)}{\sqrt{\lambda}} \times$$

$$\times S^{\alpha_1(t_1) + \alpha_2(t_2) - 1} g_1(t_1, q_x^2) g_1(t_1, q_{x'}^2) g_2(t_2, q_x^2) g_2(t_2, q_{x'}^2) \quad (1.54)$$

Consider, for example, the integral over  $q_x^2$ . As the coupling functions  $g_i$  have only a right-hand cut in the  $q_x^2$  plane, the integration passes above the pole in the propagator and above the cuts in the coupling functions which depend on  $q_x^2$ . Since the coupling functions are assumed to go to zero at large  $q_x^2$ , we may complete the contour in the upper half plane, and the integration therefore vanishes.

We see from this discussion that a necessary condition for a diagram to contribute is that it has both left-hand and right-hand cuts. This means that the bubbles at the top and bottom of fig.(1.3a) must have third double-spectral functions. The simplest contribution to the top bubble with this property is shown in fig.(1.3d).

The Reggeon calculus provides us with a general expression for fig.(1.3a). We merely quote the result, which is

$$A_{\alpha_1, \alpha_2}^{ab \rightarrow a'b'}(s, t) = \frac{i}{s} \int_{-\infty}^0 dt_1 dt_2 \frac{\theta(\lambda)}{\sqrt{\lambda}} N_{\alpha_1, \alpha_2}^{a\bar{a}'}(t, t_1, t_2) N_{\alpha_1, \alpha_2}^{b\bar{b}'}(t, t_1, t_2) \times$$

$$\times S_{\alpha_1}(t_1) S_{\alpha_2}(t_2) \left(\frac{s}{s_0}\right)^{\alpha_1(t_1) + \alpha_2(t_2)} \quad (1.55)$$

where  $S_{\alpha_1}, S_{\alpha_2}$  are, as usual, the signature factors of the exchanged reggeons.

The functions  $N_{\alpha_1, \alpha_2}^{a\bar{a}'}$  and  $N_{\alpha_1, \alpha_2}^{b\bar{b}'}$  are known as Gribov Vertices. They are obtained by integrals of the complete particle-reggeon scattering amplitudes at the vertices of fig.(1.3a), for example fig. (1.3b).

$$N_{\alpha_1, \alpha_2}^{a\bar{a}'}(t, t_1, t_2) = \int_C ds_1 A^{a\alpha_1 \rightarrow a'\alpha_2}(s_1, t; t_1, t_2) \quad (1.56)$$

with a similar expression at the lower vertex.  $C$  is the contour of fig.(1.4a), and  $N_{\alpha_1, \alpha_2}^{a\bar{a}'}$  is real for  $t$  below threshold.

If  $A^{a\alpha_1 \rightarrow a'\alpha_2}$  has no singularities in the lower half plane, the contour  $C$  may be distorted to enclose the right hand cut, becoming  $c'$  of fig.(1.4b). (This assumption is somewhat dubious - see ref. (11)). The vertex then becomes

$$N_{\alpha_1, \alpha_2}^{a\bar{a}'}(t, t_1, t_2) = 2i \int_{S_{TH}}^{\infty} ds_1 \text{Im} A^{a\alpha_1 \rightarrow a'\alpha_2}(s_1, t; t_1, t_2) \quad (1.57)$$

The Absorption Model

If we assume that e.q.(1.57) is correct, we can approximate the integration by a pole contribution. Calling the internal particle  $x$  (fig.1.3c) we obtain

$$N_{\alpha_1 \alpha_2}^{a\bar{a}'} = \gamma_{\alpha_1}^{a\bar{x}}(t_1) \gamma_{\alpha_2}^{x\bar{a}'}(t_2) \quad (1.58)$$

We see that this does not lead to a diagram like fig.(1.3e) since we have now put the internal particles on the mass shell. Such diagrams are used to represent the amplitude, but must not be interpreted as Feynman graphs.

The amplitudes resulting from (1.58) are known as the absorption model. An alternative approach is to sum over all allowed intermediate states  $x$ . This is known as the strong absorption model, but in practice it is usually approximated by multiplying the absorption model by a constant factor. The justification for this procedure is by no means obvious.

If we consider elastic scattering, and take  $x = a$ , we obtain, for identical trajectories

$$N_{\alpha\alpha}^{a\bar{a}} = \gamma_{\alpha}^{a\bar{a}}(t_1) \gamma_{\alpha}^{a\bar{a}}(t_2) \quad (1.59)$$

Taking a similar expression for the lower vertex, we obtain

$$A_{\alpha\alpha}^{ab \rightarrow ab}(s,t) = \frac{i}{s} \int_{-\infty}^0 dt_1 dt_2 \frac{\theta(\lambda)}{\sqrt{\lambda}} \gamma_{\alpha}^{ab \rightarrow ab}(t_1) \gamma_{\alpha}^{ab \rightarrow ab}(t_2) \times \\ \times \delta_{\alpha}(t_1) \delta_{\alpha}(t_2) s^{\alpha(t_1) + \alpha(t_2)} \quad (1.60)$$

where  $\delta_{\alpha}^{ab \rightarrow ab}$  is the residue function for ab elastic scattering. This result is identical to that of the eikonal model. (see ref.12 for a review).

The term Absorption Model comes from the impact parameter representation. This is obtained by the Hankel transform

$$\hat{A}(s,b) = \int_0^{\infty} d\sqrt{-t} \sqrt{-t} A(s,t) J_0(b\sqrt{-t}) \quad (1.61)$$

Pure Regge-poles are central in impact-parameter space

$$\hat{A}(s,b) \sim e^{-b^2/r_0^2} \quad (r_0 \text{ const.}) \quad (1.62)$$

but when cut corrections have been included, it is found that the central part has been "absorbed away" and contributions come only from the large - b "peripheral" amplitude. This is equivalent to the high partial waves, (1.61) being the high energy limit of the partial wave series.

Figures for Chapter 1

- 1.1 Exchange of the trajectory  $\alpha(t)$  in the process  $ab \rightarrow a'b'$ .
  
- 1.2 The integration contour for the derivation of the Finite Energy Sum Rule.
  
- 1.3
  - (a) Exchange of the two-reggeon cut, generated by the trajectories  $\alpha_1$  and  $\alpha_2$ , in the process  $ab \rightarrow a'b'$ .
  - (b) The particle-reggeon amplitude  $ax_1 \rightarrow a'\alpha_2$  used in the calculation of the upper vertex in fig.(1.3a).
  - (c) The pole contribution to fig.(1.3b), used in the derivation of the absorption model.
  - (d) The simplest contribution to the upper vertex in fig.(1.3a) which does not cause the cut amplitude to vanish.
  - (e) The box diagram which does not produce a Regge cut.
  
- 1.4
  - (a) The contour for the integration in the Gribov Vertex calculation.
  - (b) The contour of fig.(1.4a) after deformation as discussed in the text.

fig. (1.1)

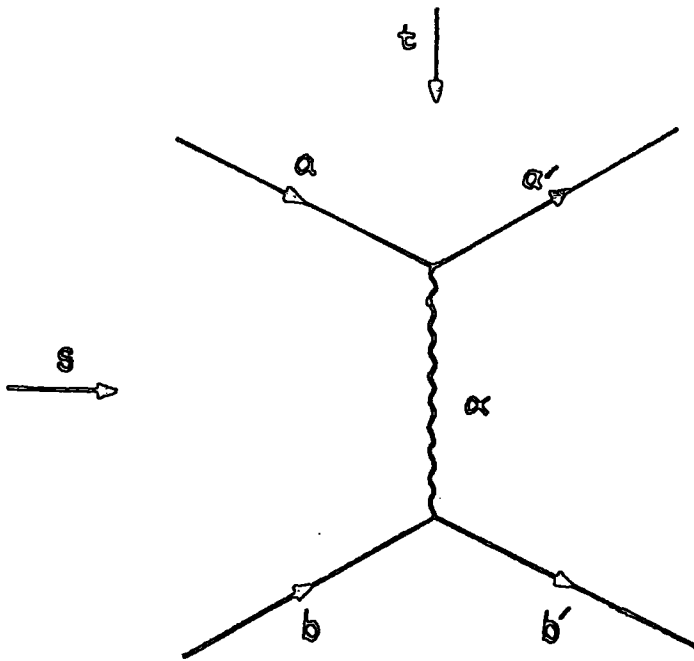


fig. (1.2)

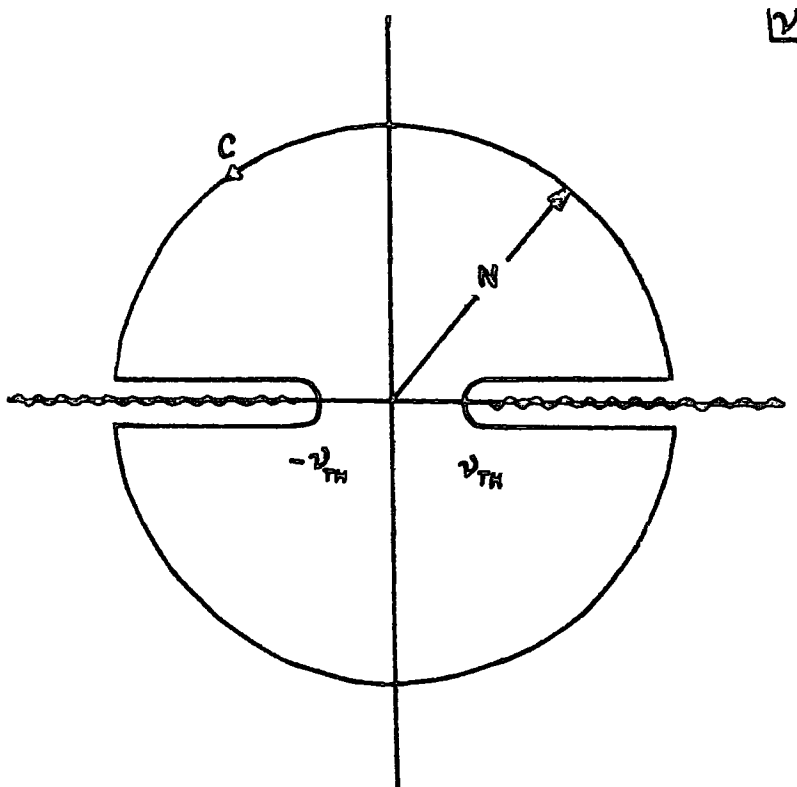
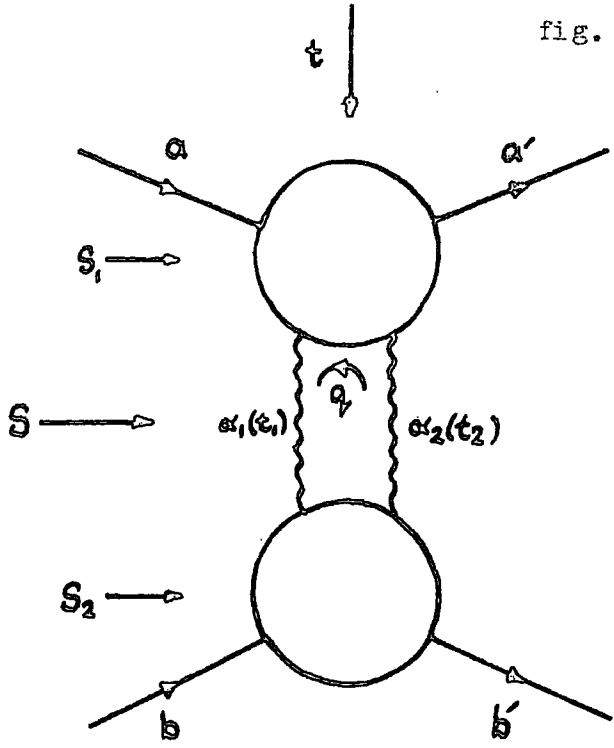
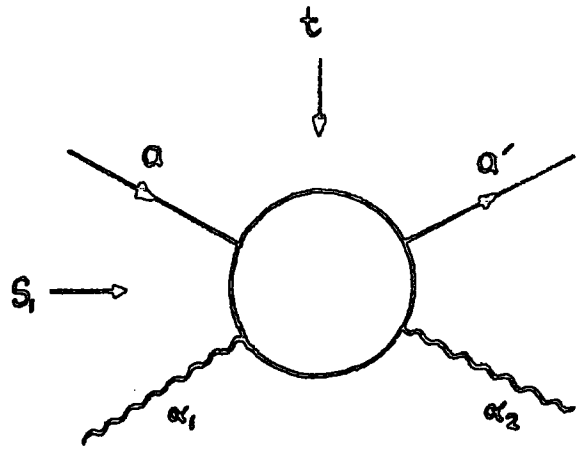


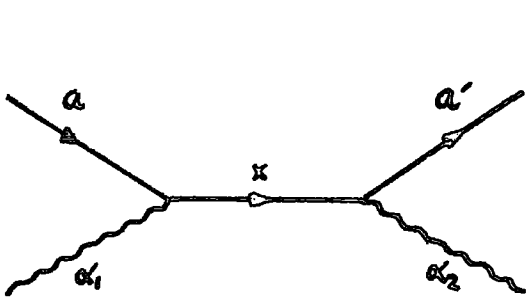
fig. (1.3)



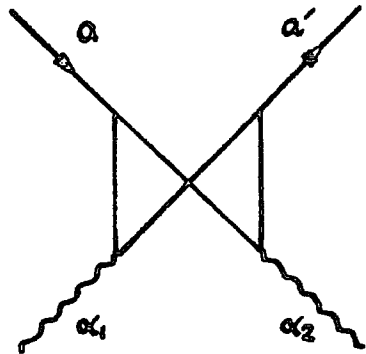
(a)



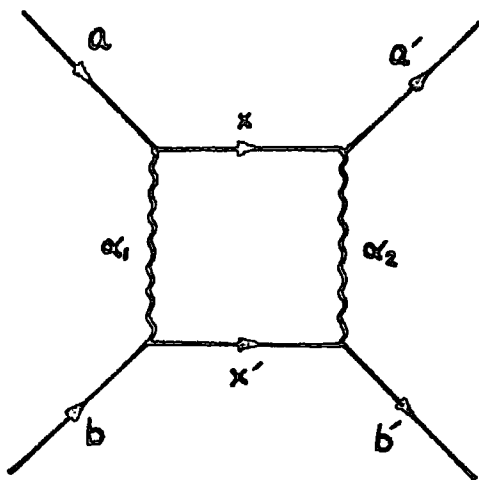
(b)



(c)

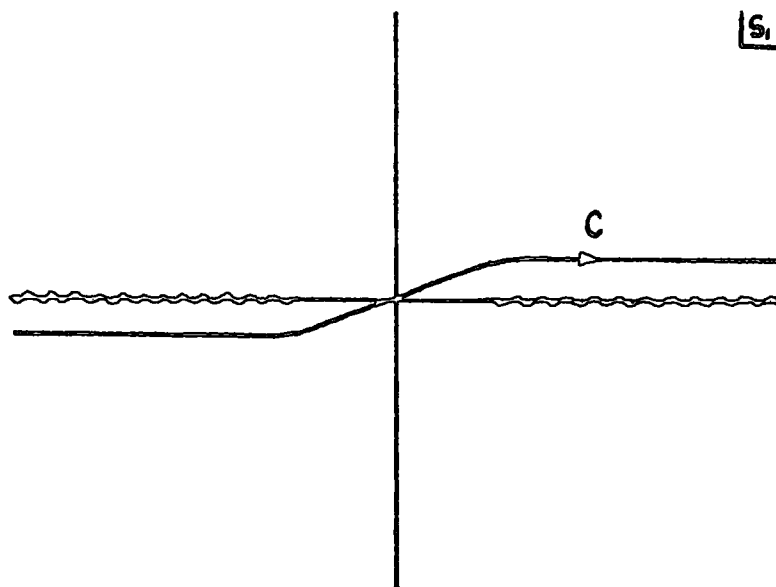


(d)

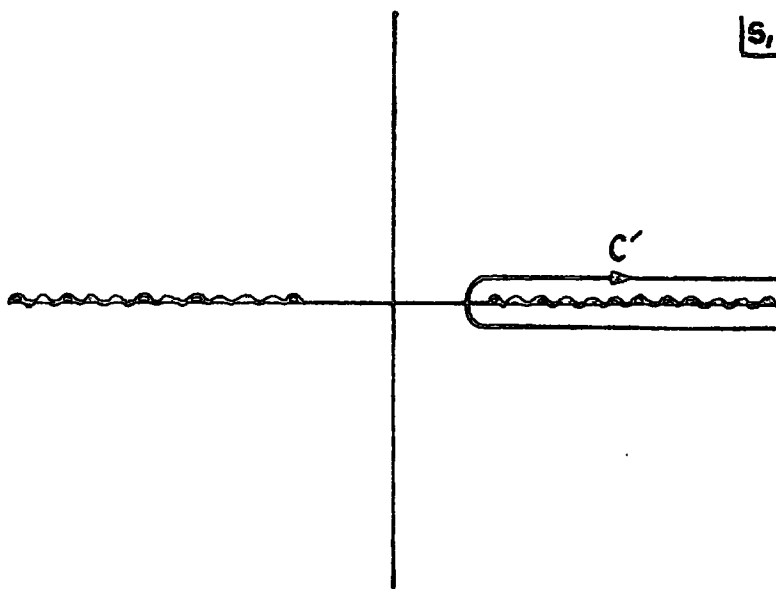


(e)

fig. (1.4)



(a)



(b)

## Chapter 2. DOUBLED TRAJECTORIES AND $K \rightarrow p$ ELASTIC SCATTERING

### Introduction

$K \rightarrow p$  scattering affords an opportunity to test the various assumptions and prejudices current in Regge theory. There is a very pronounced crossover (see section 1.2(11)), the  $K \rightarrow p$  channel is exotic, and there are good data on differential, total and polarised cross sections over a large energy range, while the spin structure is not so complicated as to render analysis impossible.

In section (2.1) we introduce the amplitudes and formalism to be used, and in section (2.2) we discuss the ambiguities involved in Regge parametrisations of these amplitudes. In section (2.3) we introduce a simple model with doubled trajectories and describe a fit to the data. In sections (2.4) and (2.5) we compare the amplitudes obtained in this way with the results of Heyot and Navelet<sup>(28)</sup> for  $K \rightarrow p$  at 10 GeV/c, and phase-shift analysis<sup>(29,30)</sup> for  $K \rightarrow p$  at 2.5 GeV/c. Conclusions are drawn in section (2.6).

### 2.1 Amplitudes and formalism

In  $K\bar{p}$  scattering there are two independent helicity amplitudes.

In the s channel we take these to be

$$f_{++}(s,t) = T_{0\frac{1}{2};0\frac{1}{2}}^s(s,t) \quad (2.1)$$

$$f_{+-}(s,t) = T_{0\frac{1}{2};0-\frac{1}{2}}^s(s,t) \quad (2.2)$$

The normalisation of these amplitudes is defined so that:

$$\frac{d\sigma}{d\Omega} = |f_{++}(s,t)|^2 + |f_{+-}(s,t)|^2 \quad (2.3)$$

$$P \frac{d\sigma}{d\Omega} = 2 \text{IM} [f_{++}(s,t) f_{+-}^*(s,t)] \quad (2.4)$$

$$\sigma_{\text{TOT}} = \frac{4\pi}{q} \text{IM} f_{++}(s,0) \quad (2.5)$$

We cannot insert Regge pole expressions into these amplitudes directly, because they contain kinematic singularities. If we remove these kinematic singularities, we are left with the invariant amplitudes  $A', B$  (5, 19) (Actually  $A'$  is singular at  $t = 4m^2$ , but this is so far from the s channel physical region that it does not affect the analysis). The advantage of these  $A', B$  amplitudes is that they are proportional to the t channel helicity non-flip and flip amplitudes respectively.

The relations between  $f_{++}, f_{+-}$  and  $A', B$  are

$$f_{++} = \frac{m}{4\pi\sqrt{s}} \cos\frac{1}{2}\theta \left[ A' - \frac{t}{4m^2} \frac{\sqrt{s}\sqrt{s}}{1-t/4m^2} B \right] \quad (2.6)$$

$$f_{+-} = \frac{m}{4\pi\sqrt{s}} \sin\frac{1}{2}\theta \left[ A' - \frac{\sqrt{s}q^2}{m^2} \frac{1+t/4q^2}{1-t/4m^2} B \right] \quad (2.7)$$

For the purposes of partial wave analysis, the scalar amplitudes  $f_1, f_2$  and  $f_{p,q}$  are usually used. These are related to  $f_{++}, f_{+-}$  by

$$f_{++} = (f_1 + f_2) \cos \frac{1}{2} \theta \quad (2.8)$$

$$f_{+-} = (f_1 - f_2) \sin \frac{1}{2} \theta \quad (2.9)$$

$$f = f_1 + f_2 \cos \theta \quad (2.10)$$

$$g = -f_2 \sin \theta \quad (2.11)$$

The reason for using these amplitudes is that they simplify the partial wave series. For  $P_{\mu\nu}$  ( $\mu, \nu = \pm$ ), this is

$$P_{\mu\nu}(s, t) = \sum_j (2j + 1) T_{\mu\nu}^j(s) d_{\mu\nu}^j(\theta) \quad (2.12)$$

but for  $f, g$  it may be written in terms of Legendre polynomials

$$f(s, t) = \sum_{l=0}^{\infty} [(1 + l) f_{10}(s) + l f_{1-}(s)] P_l(\cos \theta) \quad (2.13)$$

$$g(s, t) = \sum_{l=1}^{\infty} (f_{1+}(s) - f_{1-}(s)) P_l'(\cos \theta) \quad (2.14)$$

where  $f_{1\pm}(s) = T_{\pm\pm}^{1\pm} = T_{\pm-}^{1\pm}$  (2.15)

$$= \frac{1}{2iq} (\eta_{1\pm} e^{2i\delta_{1\pm}} - 1) \quad (2.16)$$

The partial waves  $f_{1\pm}(s)$  are most easily projected from  $f_1, f_2$

$$f_{1\pm}(s) = \frac{1}{2} \int_{-1}^1 d(\cos\theta) \left[ f_1(s, t) P_1(\cos\theta) \pm f_2(s, t) P_{1\pm 1}(\cos\theta) \right] \quad (2.17)$$

For completeness we also define the spin asymmetry and rotation parameters  $A, R$ . The usual definition of these is:

$$A = \frac{|f|^2 - |g|^2}{|f|^2 + |g|^2} \quad (2.18)$$

$$R = \frac{2\text{Re}(fg^*)}{|f|^2 + |g|^2} \quad (2.19)$$

Some authors use the following definitions, however:

$$A_{\text{HEL}} = \frac{|f_{++}|^2 - |f_{+-}|^2}{|f_{++}|^2 + |f_{+-}|^2} \quad (2.20)$$

$$R_{\text{HEL}} = \frac{2\text{Re}(f_{++}f_{+-}^*)}{|f_{++}|^2 + |f_{+-}|^2} \quad (2.21)$$

These definitions differ only by a rotation, since

$$A = A_{\text{HEL}} \cos\theta + R_{\text{HEL}} \sin\theta \quad (2.22)$$

$$R = -A_{\text{HEL}} \sin\theta + R_{\text{HEL}} \cos\theta \quad (2.23)$$

so that near the forward direction the definitions are equivalent.

## 2.2 Ambiguities in Regge Analysis

In processes, such as  $K^{\pm}p$ , where the data are insufficient to determine all the amplitudes, there are two possible procedures. Either we make some assumptions which determine the amplitudes in a particular model, or we consider only quantities which are not dependent on the ambiguity. In  $K^{\pm}p$  we find that there are two ambiguities. We shall eliminate one by the assumption of Regge theory, and discuss the other in more detail.

We have introduced the amplitudes  $A', B$ , which are complex, so that four real numbers at each value of  $s, t$  completely determine the system. The data, however provide only two numbers at each  $s, t$ , namely the differential cross section and polarisation. In the special case  $t = 0$ , we have also the total cross section, but since the polarisation vanishes identically because of angular momentum conservation, there are still only two real numbers determined by the data.

As we are going to work in the framework of Regge theory, we have, imposed upon us, the relation between the phase and energy dependence of each Regge pole, defined by the signature factor and  $(\frac{s}{s_0})^{\alpha}$ . This means that we have one ambiguity removed for us, leaving one remaining. This was elegantly isolated in ref.(24), where the following definitions were made:

$$a = A' \quad (2.24)$$

$$b = \frac{\sqrt{-t} P_L (1 + t/4q^2)^{\frac{1}{2}}}{2m (1 - t/4m^2)} B \quad (2.25)$$

These amplitudes  $a, b$  have the advantage that they appear symmetrically in the differential cross section. i.e.

$$\frac{d\sigma}{dt} = c (|a|^2 + |b|^2) \quad (2.26)$$

$$\text{also } p \frac{d\sigma}{dt} = 2c \text{Im}(ab^*) \quad (2.27)$$

$$\text{where } c = \frac{1 - t/4m^2}{16 \pi P_L^2} \quad (2.28)$$

This means that the differential cross section and polarisation are invariant under the transformation

$$a \rightarrow a \cos \chi + b \sin \chi \quad (2.29)$$

$$b \rightarrow -a \sin \chi + b \cos \chi \quad (2.30)$$

which is a rotation in the spin flip - non-flip plane.

An immediate advantage of this approach is that the constraint imposed by Regge theory is particularly simple, namely that  $\chi$  depends only on  $t$ . This is because it must not affect the  $(\frac{s}{s_0})^{\alpha}$  energy dependence of the amplitudes.

Analyticity implies further constraints. Because the amplitude  $a$  is analytic (except at  $t = 4m^2$ ), but  $b$  contains kinematic singularities, it is necessary that  $\chi$  cancel these in (2.29), that is we require  $b \sin \chi$  to be analytic, i.e..

$$b \frac{\sqrt{-t} p_L (1 + t/4q^2)^{\frac{1}{2}}}{2m (1 - t/4m^2)} \sin \chi \quad \text{analytic} \quad (2.31)$$

Hence we deduce that

$$\sin \chi \sim \frac{\sqrt{-t}}{2m} \quad \text{near } t = 0 \quad (2.32)$$

and

$$\sin \chi \sim (1 + t/4q^2)^{\frac{1}{2}} \quad \text{near } t = -4q^2 \quad (2.33)$$

(2.32) and (2.33) correspond to behaviour in the forward and backward directions respectively. Since our fit is to the forward direction, using  $t$  channel Regge poles, we applied only the constraint (2.32), by forcing

$$\chi(t) \sim \sqrt{-t} \quad \text{near } t = 0 \quad (2.34)$$

The backward direction should be sufficiently far from the region of interest for the behaviour (2.33) to have little effect.

The singularity at  $t = 4m^2$  in (2.31) is, of course, present in  $A'$  so does not have to be cancelled by  $\sin \chi$ .

We shall adopt a specific form for the meson residues, so there will be no room for arbitrary rotation angles there. It will be convenient to rotate the pomeron residue functions, since for them we have no theory. We may determine a starting-point for the rotation by the convention that  $\chi(t) = 0$  corresponds to  $t$  channel helicity conservation  $b_p(s,t) = 0$ .

It is also useful to determine the relation between  $s$  channel and  $t$  channel helicity conservation in terms of these variables. If we call  $P_{\leftrightarrow\leftrightarrow}^s, P_{\leftrightarrow\leftarrow}^s$  the pomeron contributions to the  $s$  channel helicity non-flip and flip amplitudes respectively, it is natural to define an  $S$  channel rotation angle  $\chi_s(s,t)$ , analogous to e.qs.(2.29, 2.30) by

$$\tan \chi_s(s,t) = \frac{P_{\leftrightarrow\leftarrow}^s(s,t)}{P_{\leftrightarrow\leftrightarrow}^s(s,t)} \quad (2.35)$$

so that  $\chi_s(s,t) = 0$  corresponds to  $s$  channel helicity conservation.

The relation between this and the  $t$  channel angle is

$$\tan \chi_s(s,t) = \frac{\rho \tan \frac{1}{2}\theta + \tan \chi_t(t)}{1 - \rho \tan \frac{1}{2}\theta \tan \chi_t(t)} \quad (2.36)$$

where  $\rho \equiv (1 + q^2/m^2)^{\frac{1}{2}} \quad (a.14)$

(see appendix)

We see that  $s$  and  $t$  channel helicity conservation are equivalent only in the forward direction, and since

$$\tan \frac{1}{2}\theta \sim \frac{\sqrt{-t}}{-t \rightarrow 0} \quad (2.37)$$

they quickly become different as  $|t|$  increases. For  $t$  channel helicity conservation, we see that

$$\tan \chi_s^{TCHC}(s,t) = \rho \tan \frac{1}{2}\theta \quad (2.38)$$

so that the two assumptions become further apart with increasing energy.

### 2.3 The Model

The trajectories which may be exchanged in  $K^{\pm}p$  elastic scattering are

$$K^{\pm}p \rightleftharpoons P \rightleftharpoons \rho \rightleftharpoons w \rightleftharpoons f_0 \rightleftharpoons A_2 \quad (2.39)$$

We have seen in Chapter 1 that there is evidence, both theoretical and experimental, that the meson trajectories are degenerate

$$\alpha_{\rho}(t) = \alpha_w(t) = \alpha_{A_2}(t) = \alpha_{f_0}(t) \equiv \alpha(t) \quad (2.40)$$

so we adopted this in our model.

Because our model was explicitly constructed with meson residues which do not factorise, we cannot use information from the charge exchange processes  $K^{\pm}p \rightarrow \bar{K}^0n$  or  $K^{\pm}n \rightarrow K^0p$  to separate the  $w$  contribution from the  $\rho$ , or the  $f_0$  from the  $A_2$ . We therefore worked only with the linear combinations

$$V \equiv \rho + w \quad (2.39)$$

$$T \equiv A_2 + f_0 \quad (2.40)$$

where  $V$  and  $T$  stand respectively for Vector and Tensor mesons.

We used the variable

$$v = \frac{s-u}{2S_0} \quad (1.26)$$

which produces a better low energy expansion than  $s$  (see ref.12), and

therefore parametrised the invariant amplitudes as

$$A'(v,t) = \sum_{i=P,V,T} \delta_i \gamma_i(t) v^{\alpha_i(t)} \quad (2.41)$$

$$B(v,t) = \sum_{i=P,V,T} \delta_i \gamma_i(t) v^{\alpha_i(t)-1} \quad (2.42)$$

As usual,  $\delta_i$  is the signature factor

$$\delta_i = \frac{e^{-i\pi\alpha_i} + \tau_i}{\sin \pi\alpha_i} \quad (2.43)$$

where, of course, the signatures of the trajectories are

$$\tau_p = \tau_f = 1 \quad (2.44)$$

$$\tau_v = -1 \quad (2.45)$$

In terms of this parametrisation the mechanism for the production of the crossover is extremely simple. The quantity  $\Delta \frac{d\sigma}{dt}$  defined in e.q. (1.20) is given by

$$\Delta \frac{d\sigma}{dt} = 4C (\gamma_p \gamma_v + E^2 \beta_p \beta_v) v^{\alpha + \alpha_p} \text{RE}(\delta_p^* \delta_v) \quad (2.46)$$

where C is defined in e.q. (2.28) and

$$E \equiv \frac{\sqrt{-t} P_L (1 + t/4q^2)^{\frac{1}{2}}}{2mv (1 - t/4m^2)} \quad (2.47)$$

Since the crossover occurs near the forward direction, the contribution of the second term in (2.46) is expected to be small so that the zero should be apparent in the first term. A zero in  $\gamma_p$  would produce a dip in the  $K^+\pi$  cross section which does not occur, so the conclusion is that  $\gamma_v(t)$  vanishes for  $t \approx -0.16 \text{ GeV}^2$ . In practice this zero will be shifted slightly by the presence of the second term, but because the quantity  $E^2$  necessarily vanishes like  $t$  in the forward direction, its effect at  $t \approx -0.16 \text{ GeV}^2$  is expected to be small.

The quantity  $\Delta \frac{d\sigma}{dt}$  enables us to check the validity of the simple pole model. If we plot  $\log(\Delta \frac{d\sigma}{dt})$  against  $\log(s)$  at fixed  $t$ , e.q. (2.46) predicts that we should see a straight line of slope  $\alpha + \alpha_p = 2$ . This has been done by Schmid<sup>(60)</sup>, and his results are shown in fig.(2.11). The data may be seen to be perfectly consistent with this simple power law from  $P_L = 1.5$  to  $15 \text{ GeV}/c$ . (the highest momentum for which sufficiently accurate data were available), and from  $t = 0$  to  $t = -1.0 \text{ GeV}^2$ . The curves for  $-0.6 \lesssim t \lesssim -0.4 \text{ GeV}^2$ , where the statistics are best, are in particularly good agreement.

It seems, therefore, that the data on differential cross sections are encouragingly suggestive of a simple pole model. Indeed, it is puzzling what has happened to the cut contribution, if it is a significant part of the amplitude. Unfortunately the polarisation data are not sufficiently accurate to apply a similar test to the tensor terms in any meaningful way, but it does appear that, in this process at least, cuts play a relatively minor role.

The Mesons

Our model has doubled trajectories, and the simplest way of achieving this is to make each meson residue a sum of two Veneziano terms of the form (see 1.48)

$$v(t) = \frac{c}{\Gamma(\alpha(t) - m + 1)} \quad (c = \text{constant}) \quad (2.48)$$

with  $s_0 = 1/\alpha'$

This form has zeros when

$$\alpha(t) = m - 1, m - 2, \dots \text{etc.} \quad (2.49)$$

which cancel the poles at alternate integers in the signature factor. The resulting amplitude thus has poles for positive integer  $\alpha(t)$ , starting at  $\alpha(t) = m$  or  $m + 1$  depending on the signature of the trajectory.

Since the lowest particle on each trajectory is not observed to be doubled we arranged that, of the two terms constituting each residue, one had the lowest particle and the other did not. We were thus led to the following forms for the residues

$$\delta_v(t) = \frac{\bar{\delta}_{v1}}{\Gamma(\alpha + 1)} + \frac{\bar{\delta}_{v2}}{\Gamma(\alpha - 1)} \quad (2.50)$$

$$\beta_v(t) = \frac{\bar{\beta}_{v1}}{\Gamma(\alpha)} + \frac{\bar{\beta}_{v2}}{\Gamma(\alpha - 1)} \quad (2.51)$$

$$\delta_T(t) = \frac{\bar{\delta}_{T1}}{\Gamma(\alpha)} + \frac{\bar{\delta}_{T2}}{\Gamma(\alpha - 1)} \quad (2.52)$$

$$\beta_T(t) = \frac{\bar{\beta}_{T1}}{\Gamma(\alpha)} + \frac{\bar{\beta}_{T2}}{\Gamma(\alpha - 1)} \quad (2.53)$$

The 8 parameters  $\{\bar{\delta}, \bar{\beta}\}$  are coupling constants, to be determined by fits to the data.

We fixed the meson trajectory at

$$\alpha(t) = 0.5 + 0.9 t \quad (2.54)$$

in accordance with exchange degeneracy (see e.g. 2.40).

As a preliminary step we fitted these forms to the residues from ref.(24), and were encouraged by the reasonable fits obtained, as these residues show considerable structure. This procedure was not entirely satisfactory, however, because the fitting procedure was not able to discriminate between regions where it was necessary to fit closely, such as for  $\gamma_V(t)$  near the crossover region, and regions where a rough approximation was adequate, such as for the  $\beta$  residues near the forward direction. Consequently we fitted the data directly, and for this it was necessary to construct a parametrisation for the pomeron.

The Pomeron

In accordance with the above discussion we made  $t$  channel helicity conservation for the pomeron correspond to  $\alpha(t) = 0$ . In terms of the residues, this gave

$$\gamma_p(t) = \gamma_p^0(t) \cos \alpha(t) \quad (2.55)$$

where  $\gamma_p^0(t)$  is the unrotated non flip residue. We parametrised it as

$$\gamma_p^0(t) = A c^{a_1 t + a_2 t^2} \quad (2.57)$$

This corresponds to the usual idea of a pomeron central in impact-parameter space.

We parametrised  $\alpha(t)$  as a polynomial, and included the kinematic  $\sqrt{-t}$  singularity mentioned in e.q. (2.34).

$$\alpha(t) = \sqrt{-t} (\alpha_1 + \alpha_2 t + \alpha_3 t^2) \quad (2.58)$$

We tried introducing a cubic term into this expression but found no improvement in the fit.

We used a linear trajectory

$$\alpha_p(t) = 1 + \alpha'_p t \quad (2.59)$$

allowing  $\alpha'_p$  to be a free parameter. Our pomeron parametrisation thus had 7 free parameters -  $A, a_1, a_2, \alpha_1, \alpha_2, \alpha_3, \alpha'_p$  - to be determined from the data.

It should be pointed out that the  $\alpha$  defined above is a rotation of the pomeron relative to the mesons, and is not the same as the  $\alpha$  defined on page 28, which cannot, of course, be determined by fits to the data.

Data

We fitted all available data in the range

$$2 \leq P_L \leq 16 \text{ GeV}/c$$

$$0 \geq t \geq -1.5 \text{ GeV}^2$$

The sources are listed in ref.26, and the numbers of experiments are summarised in Table (2.1).

Table 2.1

Data on  $K^+ p$  Elastic Scattering

Measurement	Number of Experiments	
	$K^+ p$	$K^- p$
$\sigma_{TOT}$	4	3
$\frac{d\sigma}{dt}$	9	5
$\rho$	3	2

In all there were 589 data points. Normalisation errors in the data, which reflect the difficulty of accurately counting the flux in the beam, were revealed by differences between experiments by different groups at similar energies. For example, there is a factor of about 1.3 between the  $K^+ p$  differential cross section data of deBaere et al, at  $P_L = 3.46 \text{ GeV}/c$  and that of Banaigs et al. at  $P_L = 3.55 \text{ GeV}/c$  (26). One possible way of dealing with these systematic errors is to assign each experiment an arbitrary normalisation parameter, to be determined by the fit. We did not use this procedure, since it possesses the inherent danger of allowing the model to introduce an altogether spurious energy dependence. We relied instead on fitting a large amount of data, and expected that the normalisation errors would to some extent average out.

### Fitting Procedure

We minimised  $\chi^2$ , defined by

$$\chi^2 = \sum_{s,t} \left[ \frac{\frac{d\sigma}{dt}(\text{calc}) - \frac{d\sigma}{dt}(\text{expt})}{\delta \frac{d\sigma}{dt}(\text{expt})} \right]^2 + \left[ \frac{P(\text{calc}) - P(\text{expt})}{\delta P(\text{expt})} \right]^2 + \sum_s \left[ \frac{\sigma_T(\text{calc}) - \sigma_T(\text{expt})}{\delta \sigma_T(\text{expt})} \right]^2 \quad (2.60)$$

We used the CERN minimisation program MINUIT, which is a combination of a random-search routine and a modified Rosenbrock co-ordinate variation program<sup>(61)</sup>. The action of MINUIT is summarised in the flow-diagram of fig.(2.12).

As starting-values for the parameters, we took the values obtained from fits to the residues from ref.(24). About 1000 iterations were required to reach a solution, and only one good fit was obtained.

Although the number of free parameters - 15 - was rather large, certain of them were determined in a straightforward way by the gross features of the data.

The pomeron parameter  $A$  was determined by the asymptotic  $K + p$  total cross section, since

$$\sigma_{\text{TOT}}^{K+p}(\infty) = \frac{MA}{2} \quad (2.61)$$

The forward direction vector meson residue was then determined by the difference between the  $K-p$  and  $K+p$  total cross sections

$$\begin{aligned} \sigma_{\text{TOT}}^{K-p} - \sigma_{\text{TOT}}^{K+p} &= m \gamma_V(0) \alpha(0)^{-1} \\ &= m v^{-\frac{1}{2}} (\bar{\gamma}_{V1} - \frac{1}{2} \bar{\gamma}_{V2}) \quad (2.62) \end{aligned}$$

As the errors on total cross sections are small the equations (2.61), (2.62) were well-determined. A further condition on  $\gamma_V$  was obtained from the crossover at  $t \approx -0.2 \text{ GeV}^2$ . This implies

$$\delta_v(t_c) = 0; \quad t_c \approx -0.2 \text{ GeV}^2$$

$$\text{or} \quad \bar{\delta}_{v1} + \alpha(\alpha-1) \bar{\delta}_{v2} = 0 \quad (2.63)$$

As was previously suggested, this zero was moved slightly by the presence of flip terms, but (2.63) represents a very useful constraint in restricting the movement of parameters.

With the non-flip pomeron and vector-meson parameters more or less fixed by the total cross section and crossover, constraints were imposed on the tensor meson residues by the value of the  $K + p$  total and forward  $K \rightleftharpoons p$  differential cross sections, effectively removing two more parameters.

Our fit thus had ten parameters with which to fit the polarisation data, and the angular structure of the differential cross section.

In addition to e.q.(2.46), three additional quantities may be defined:

$$\begin{aligned} \Sigma \frac{d\sigma}{dt} &\equiv \frac{d\sigma}{dt} (K-p) + \frac{d\sigma}{dt} (K^+p) \\ &= 2C \sum (\gamma_i^2 + E^2 \beta_i^2) |b_i|^2 v^{2\alpha_i} + 4C \text{Re}(\delta_p^* \delta_T) (\gamma_p \gamma_T + E^2 \beta_p \beta_T) \times \\ &\quad i = P, V, T \quad \times v^{\alpha + \alpha_p} \end{aligned} \quad (2.64)$$

$$\begin{aligned} \Sigma^P \frac{d\sigma}{dt} &\equiv P \frac{d\sigma}{dt} (K-p) + P \frac{d\sigma}{dt} (K+p) \\ &= 4CE (\gamma_p \beta_T - \gamma_T \beta_p) v^{\alpha + \alpha_p} \text{Im}(\delta_p^* \delta_T) \end{aligned} \quad (2.65)$$

$$\begin{aligned} \Delta^P \frac{d\sigma}{dt} &\equiv P \frac{d\sigma}{dt} (K-p) - P \frac{d\sigma}{dt} (K+p) \\ &= 4CE \left[ (\gamma_p \beta_v - \gamma_v \beta_p) v^{\alpha + \alpha_p} \text{Im}(\delta_p^* \delta_v) \right. \\ &\quad \left. + (\gamma_v \beta_T - \gamma_T \beta_v) v^{2\alpha} \text{Im}(\delta_v^* \delta_T) \right] \end{aligned} \quad (2.66)$$

where C and E are defined in (2.28) and (2.47) respectively.

Since the meson non flip residues are constrained as described in the previous discussion, they may be treated as known in the above three equations.

The pomeron parameters  $a_1, a_2, \alpha_1, \alpha_2, \alpha_3$  were determined largely by the differential cross section and polarisation data over the whole range of  $t$ , and the meson flip residue parameters mainly by the polarisation. It should be emphasised that, in a simple pole model, the pomeron is not predominantly a forward direction effect, and in fact because of its small slope, contributes more at large  $t$  relative to the mesons, than in the forward direction. (In cut models, of course, this is not true, since amplitudes generated by for example the absorption model fall off more slowly with  $t$  than the pole contributions).

## Results

The best least-squares fit to the data gave  $\chi^2 = 1.8$  per point and the following parameter values.

For the pomeron

$$\alpha'_p = 0.32$$

$$A = 9.1, a_1 = 2.3, a_2 = 0.2$$

$$\kappa_1 = -1. \times 10^{-2}, \kappa_2 = -0.2, \kappa_3 = 0.46$$

For the Vector meson

$$\bar{\delta}_{V1} = 10, \bar{\delta}_{V2} = 1.6$$

$$\bar{\beta}_{V1} = 23, \bar{\beta}_{V2} = 2.8$$

and for the tensor meson

$$\bar{\delta}_{T1} = 12, \bar{\delta}_{T2} = 5.3$$

$$\bar{\beta}_{T1} = 85, \bar{\beta}_{T2} = 45$$

Fits to differential cross section and polarisation at intermediate energies are shown in figs. (2.1, 2.2) and to the total cross sections in fig. (2.3). The model agreed well with the data over the whole range of energy considered. A large proportion of the  $\chi^2$  came from the normalisation errors mentioned above. We estimated that, if normalisation errors were taken into account, we would have  $\chi^2 \approx 1.2$  per point, which is a reasonable fit.

## The Meson Residues

In fig.(2.5) the meson residues are compared with those of the effective pole model of ref.(24). The agreement is seen to be good for the non-flip residues, especially near the forward direction. The flip residues are in poorer agreement. In general, as was mentioned above, they are less well determined than the non-flip residues, and near  $t = 0$  they are not determined at all, because their contribution to the observables vanishes kinematically.

It should be noted that these residues are not very compatible with exchange degeneracy. That the non flip residues are nearly equal at  $t = 0$  is not surprising, since that is necessary to ensure the flatness of the  $K^+ p$  total cross section. Our results at larger  $t$  support the assertion<sup>(27)</sup> that in a pure pole model exchange degeneracy cannot hold away from the forward direction.

### The Pomeron

The unrotated non flip residue  $\gamma_p^0(t)$  we obtained was the same as that of ref.(24). We tried a fit with  $a_2$  fixed equal to zero, but found that the fit was considerably worse.

The very small value ( $-1 \times 10^{-2}$ ) obtained for  $\alpha_1$  indicates support for t channel helicity conservation for  $|t| \lesssim 0.5 \text{ GeV}^2$ . This is illustrated in fig.(2.4), where the parameter  $\alpha_g(s,t)$ , which is defined in e.q.(2.35), is plotted at  $P_L = 10 \text{ GeV}/c$ . Also plotted is the t channel helicity conservation curve, defined in e.q. (2.38). It can be seen that our fit is even further from s channel helicity conservation ( $\alpha_g(s,t) = 0$ ) than is the T.C.H.C. curve. Some support for our  $\alpha(t)$  is obtained from consideration of the CERN  $\beta$  phase shift analysis, in section (2.4).

The pomeron slope  $\alpha'_p$  is simply related to the shrinkage of the forward peak in the  $K + p$  differential cross section. Since, in our model, the mesons are exchange degenerate at  $t = 0$ , we expect the pomeron to dominate there, so we can write

$$\frac{d\sigma}{dt} (K + p) \approx F(t) s^{2\alpha_p(t) - 2} \quad (2.67)$$

(where  $F(t)$  is a complicated function depending on  $\gamma_p^0(t)$ ,  $\alpha(t)$ , and kinematic factors). Putting in the linear form  $\alpha_p(t) = 1 + \alpha'_p t$  we obtain

$$\frac{d\sigma}{dt} = F(t) s^{2\alpha'_p t}$$

To obtain the slope of the forward peak we take logs, differentiate, and evaluate at  $t = 0$ , giving

$$b(s) \equiv \left. \frac{d}{dt} \left( \log \frac{d\sigma}{dt} \right) \right|_{t=0} = \frac{F'(0)}{F(0)} + 2\alpha'_p \log s \quad (2.68)$$

so that the rate of shrinkage of the forward peak is proportional to  $\alpha'_p$ . This means that the value of  $\alpha'_p$  obtained from the data is largely model-independent, and in fact any model assuming pomeron dominance of  $K + p$  will give the same result.

### Conclusions

We have formulated a simple model, involving doubled trajectories, which avoids the factorisation problems discussed in section (1.2). The model provides a satisfactory fit to  $K^+ p$  elastic scattering data in the range  $2 \lesssim P_L \lesssim 16$  GeV/c, and  $0 \lesssim |t| \lesssim 1.5$  GeV<sup>2</sup>.

Our parametrisation of the residues leads to a determination of  $\alpha(t)$  which supports  $t$  channel helicity conservation for the pomeron near the forward direction.

In the next two sections, we make use of the amplitudes obtained from this model. Although the fact that it fits the available data cannot be interpreted as convincing evidence for the physical reality of this model, it is useful because it provides a smooth parametrisation of the data in terms of Regge amplitudes, which can be used in testing general hypotheses (such as that of Zarmi<sup>(65)</sup>) or the assumptions made by amplitude analysts, such as Heyot and Navelet in the next section.

2.4 Comparison with the Amplitude Analysis of Heyot & Navelet

Heyot and Navelet<sup>(28)</sup> performed an amplitude analysis of the KN system at  $p_L = 10 \text{ GeV}/c$ . As there are data on an insufficient number of parameters to completely determine all the amplitudes, they were forced to make some assumptions.

They used amplitudes  $M_{\uparrow\uparrow}^I, M_{\uparrow\downarrow}^I$ , which are respectively s channel helicity non-flip and flip amplitudes of total isospin I in the t channel. If  $M_{\mu\nu}(K^-)$  is the amplitude for  $K - p \rightarrow K - p$ , and  $M_{\mu\nu}(\bar{K}^0)$  that for  $K - p \rightarrow \bar{K}^0 n$  ( $\mu, \nu = \uparrow, \downarrow$ ), then

$$M_{\mu\nu}(K^-) = \frac{1}{2} (M_{\mu\nu}^1 + M_{\mu\nu}^0) \tag{2.69}$$

$$M_{\mu\nu}(\bar{K}^0) = M_{\mu\nu}^1$$

These amplitudes are normalised such that

$$\frac{d\sigma}{dt} = |M_{\uparrow\uparrow}|^2 + |M_{\uparrow\downarrow}|^2 \tag{2.70}$$

$$p \frac{d\sigma}{dt} = 2 \text{Im} (M_{\uparrow\uparrow} M_{\uparrow\downarrow}^*) \tag{2.71}$$

The assumptions that they made were as follows:

- (i) In an amplitude analysis of the  $\bar{K}N$  system<sup>(28)</sup> the  $I = 1$  flip amplitude was found to have the behaviour expected of a simple Regge-pole. By analogy, assumption (i) is

$$M_{\uparrow\downarrow}^{-1} = |M_{\uparrow\downarrow}^{-1}| e^{-i\pi\alpha} \tag{i}$$

- (ii) The  $K - p \rightarrow \bar{K}^0 n$  differential cross section data has a forward dip, indicating a dominant flip amplitude, therefore

$$|M_{\uparrow\downarrow}^{-1}| \gg |M_{\uparrow\uparrow}^{-1}| \tag{ii}$$

(This can obviously not hold near  $t = 0$ , where  $M_{\uparrow\downarrow}^{-1}$  vanishes).

(iii) They assumed that the pomeron conserves a channel helicity, and that the pomeron is dominant at  $P_L = 10 \text{ GeV}/c$ , hence

$$|m_{++}^0| \gg |m_{+-}^0| \quad (iii)$$

(this assumption is certainly wrong for  $|t| \gtrsim 0.6$ )

They then wrote

$$m_{++}^0 = |m_{++}^0| e^{i\pi\beta}$$

and obtained the following formulae

$$|m_{++}^0| = 2 \sqrt{\frac{d\sigma}{dt}(K^-)}$$

$$|m_{+-}^1| = \sqrt{\frac{d\sigma}{dt}(K^0)}$$

and 
$$\sin \pi(\beta + \alpha) = P(K-p) \sqrt{\frac{d\sigma/dt(K^-)}{d\sigma/dt(R^0)}}$$

In fig. (2.6) we compare the results of this analysis with the  $K-p$  non flip amplitude in our model. It may be seen that for  $\text{Im } m_{++}^0(K-p)$  the agreement is good, whereas for  $\text{Re } m_{++}^0(K-p)$  the amplitudes do not agree. The reason for this is that Heyot and Navelet had no justification for neglecting  $m_{+-}^0$  compared with  $m_{+-}^1$ . If we write

$$m_{+-}^0 = |m_{+-}^0| e^{i\pi\psi}$$

we obtain for the  $K-p$  polarisation

$$P(K^-) = 2 \frac{|m_{+-}^1| \sin \pi(\beta + \alpha) + |m_{+-}^0| \sin \pi(\psi + \alpha)}{|m_{++}^0|} \quad (2.72)$$

This means that the result for the phase of  $m_{++}^0$  was incorrect, giving rise to a wrong real part. Because this amplitude is nearly purely imaginary, being pomeron dominated, this error did not significantly affect the imaginary part.

Heyot and Navelet also extracted what they called the "Regge Term", by assuming that the  $K+p$  differential cross section is given by the pomeron alone. This gave

$$\text{Im } M_{\leftrightarrow\leftrightarrow}^0 (\text{Regge}) = \frac{1}{2} \left[ \sqrt{\frac{d\sigma}{dt} (K - p)} - \sqrt{\frac{d\sigma}{dt} (K + p)} \right] \quad (2.73)$$

This, not surprisingly, has a zero at  $t = -0.16 \text{ GeV}^2$ , since the  $K + p$  and  $K - p$  differential cross sections are equal there. If we write

$$\sqrt{\frac{d\sigma}{dt} (K - p)} - \sqrt{\frac{d\sigma}{dt} (K + p)} = \frac{\frac{d\sigma}{dt} (K - p) - \frac{d\sigma}{dt} (K + p)}{\sqrt{\frac{d\sigma}{dt} (K - p)} + \sqrt{\frac{d\sigma}{dt} (K + p)}} \quad (2.74)$$

and approximate the denominator by the pomeron contribution, (assumed imaginary and conserving  $s$  channel helicity) we obtain

$$\text{Im } M_{\leftrightarrow\leftrightarrow}^0 (\text{Regge}) \approx \text{Im } V_{\leftrightarrow\leftrightarrow} \quad (2.75)$$

where  $V_{\leftrightarrow\leftrightarrow}$  is the vector meson contribution to the non-flip amplitude. Our Regge term contains also the tensor contribution, and does not have a zero at  $t = -0.16 \text{ GeV}^2$ . The Regge term in our model<sup>(1)</sup> and Heyot and Navelet's analysis<sup>(2)</sup> are compared in fig.(2.6).

The value of our smooth parametrisation in testing analyses of this kind is evident. As our amplitudes fit all the available data, they can only be excluded by an analysis whose physical assumptions are radically different from ours.

## 2.5 Comparison with K + p phase shift analysis

Since the K + p channel is exotic, smooth Regge-like behaviour of the cross sections has already set in for  $P_L \approx 2\text{GeV}/c$ , which was the lowest momentum we considered in our fit. There has also been much activity in the field of phase-shift analysis, where the search for exotic resonances such as the  $Z^*$ , has led to solutions being produced up to  $P_L = 2.5\text{ GeV}/c$  (29,30). We thus have an opportunity to compare the phase shifts directly with our results, without the need to invoke Finite Energy Sum Rules.

We considered projecting out the partial waves from our amplitudes, but since we had no model for backward scattering, we were unable to do this in a meaningful way. Instead we compared amplitudes directly.

This sort of comparison was performed by Daum et al (24) at  $P_L = 1.45\text{ GeV}/c$  with their effective pole model. Since then phase shift solutions have become available at higher energies, from which we expect more fruitful comparisons.

It is useful to compare quantities which are invariant under the rotation  $\chi$ . We therefore define  $\beta_s(s,t)$  by

$$\beta_s(s,t) = \frac{(\text{Re}f_{++})^2 + (\text{Re}f_{+-})^2}{(\text{Im}f_{++})^2 + (\text{Im}f_{+-})^2} \quad (2.76)$$

This may easily be seen to be independent of  $\chi_s(s,t)$ , defined in e.g. (2.35), and therefore cannot depend on  $\chi(t)$  either.

We first describe the phase shift solutions available at  $P_L \approx 2\text{ GeV}/c$ , and then compare them with our model. We cannot compare our model for  $\chi(t)$  with solutions which do not agree with our  $\beta_s(s,t)$ , so we made a direct comparison of the s channel amplitudes  $f_{++}(s,t)$ ,  $f_{+-}(s,t)$ .

## The Phase Shift Solutions

### (i) The CERN Solutions

Albrow et al<sup>(29)</sup> performed a conventional energy-independent phase-shift analysis of elastic  $K + p$  scattering from threshold up to  $P_L = 2.5$  GeV/c. They used data on unpolarised and polarised differential cross sections, total and elastic cross sections, and also real parts of the forward amplitude  $\text{Re} f_{\pm\pm}(s,0)$ , taken from the dispersion relation calculations of Martin and Perrin<sup>(33)</sup>.

In this type of analysis, the partial wave series (2.13, 2.14) is written down and truncated at some  $l = l_{\text{max}}$ . The resulting amplitudes are fitted to the data at each energy independently, using the partial waves  $f_{l\pm}(s)$  as parameters. The solution obtained in this way is by no means unique, in fact there are of the order of  $2^{2l_{\text{max}}+1}$  solutions at each energy<sup>(63)</sup>, and even these depend on the choice of  $l_{\text{max}}$ .

Albrow et al. included up to  $H$  ( $l_{\text{max}} = 5$ ) waves in their solution at the highest momenta considered. At each momentum they obtained 200 solutions, which they linked in energy by the "shortest path" method<sup>(31)</sup>, which selects solutions giving greatest continuity. Three distinct solutions were obtained, which the authors called  $\alpha, \beta, \gamma$ . Of these,  $\alpha$  and  $\gamma$  were nearly identical at the highest momenta, especially near the forward direction.

### (ii) The ACE solution

Miller et al<sup>(30)</sup> used the "Accelerated Convergence Expansion" of Cutkosky and Deo<sup>(32)</sup> to perform an analysis in the same energy range as the CERN group.

In this method the complex  $z$  plane is conformally mapped onto a plane in which the partial wave series is maximally convergent. This procedure has the advantage that much fewer partial waves (and therefore parameters) are required than in conventional methods, although it does have the serious drawback that the simplicity of the unitarity constraint  $\eta_{l\pm} \leq 1$  (see e.g. (2.16)) is lost in the process.

Miller et al. obtained a unique solution at each energy, which resembles the CERN  $\alpha$  and  $\beta$  solutions. In general the ACE solution gave a better fit to the data, particularly the polarisation near the forward direction, than the CERN solutions (see fig. (2.7)). When the partial waves were reconstructed from the ACE expansion, it was found that the series converged rather slowly, so that the CERN workers has apparently included too few terms in their fit.

### The Comparison

It is convenient first to compare quantities invariant under the rotation  $\chi_s(s,t)$ . Since the CERN  $\alpha$  and  $\beta$  and the ACE solutions resemble one another, we compare our solution with CERN  $\beta$  and ACE only. (These are labelled 'R', 'B', 'A' on the diagrams).

In fig. (2.9) we compare the quantity  $\beta_s(s,t)$ , defined in e.q. (2.76) at  $P_L = 2.5$  GeV/c. We see that our solution is in fairly good agreement with CERN  $\beta$ , but hopelessly different from ACE. (All solutions agree at  $t = 0$  because they fit total and forward differential cross sections with the two parameters  $\text{Re}f_{\leftrightarrow\leftrightarrow}$ ,  $\text{Im}f_{\leftrightarrow\leftrightarrow}$ , leaving no room for ambiguity). The fact that these results for  $\beta_s(s,t)$  are so different means that we cannot ascribe the differences in amplitudes to just s channel or t channel helicity conservation. To consider the subject in more detail we must look at the amplitudes directly.

In fig. (2.8) the s channel helicity amplitudes  $f_{\leftrightarrow\leftrightarrow}$ ,  $f_{\leftrightarrow-}$  are plotted at  $P_L = 2.5$  GeV/c. We see immediately that for the non flip amplitude there is no disagreement. It is particularly interesting that all solutions agree for  $\text{Re}f_{\leftrightarrow\leftrightarrow}(s,0)$ . Both phase-shift groups fitted dispersion relation real parts, although in KN these are somewhat dubious, since they depend on the parametrisation adopted for the unphysical region in the integration. In fact this ambiguity is the reason for the small difference between the ACE and CERN values for  $\text{Re}f_{\leftrightarrow\leftrightarrow}(s,0)$ , brought about by the fact that their input values were from different sources. Our value, which comes only from the total and forward differential cross sections, agrees with the CERN value<sup>(33)</sup>, indicating that dispersion relations provide no extra information in this problem.

It is in the flip amplitudes that the differences are really apparent. In the ACE solution  $\text{Im}f_{\leftrightarrow-}$  is very small for all t. This has been put forward as suggestive of s channel helicity conservation, both by the CERN group<sup>(29)</sup> and Cutkosky<sup>(34)</sup>. This interpretation runs into trouble, however, when we demand compatibility with K - p data, and

particularly the crossover zero at  $t \approx -0.16 \text{ GeV}^2$ . Since this zero must be present in the vector meson term, we would expect to see a dip in  $\text{Re}f_{\leftrightarrow}$  in this region (as the pomeron real component ought to be small near the forward direction). In our model, which does not have a channel helicity conservation, this problem does not arise.

The small  $\text{Im}f_{\leftrightarrow}$  in the ACE-type solutions has also been said to suggest exchange degeneracy<sup>(29)</sup>. Since, away from the forward direction, there are contributions to  $\text{Im}f_{\leftrightarrow}$  from both  $A'$  and  $B$  (see e.g. (2.7)), this degeneracy would be true for both  $\gamma$  and  $\beta$  residues, so that we would again expect to see a dip in the  $\text{Re}f_{\leftrightarrow}$  near the crossover point.

Another phenomenological point is worth mentioning. Davier and Harari<sup>(64)</sup> have shown that in impact parameter space the meson contribution to  $K^+ p$  appears to be peaked around  $b = 1f$ . In terms of partial wave this is, at  $P_L = 2.5 \text{ GeV}/c$ ,  $l_{\text{peak}} \approx 5$ . The CERN partial wave solutions, however, only go out to  $l_{\text{max}} = 5$ , so that they must miss a considerable part of the meson amplitude. It may be that all partial wave analysis which truncates the series at a fixed  $l$  has a built-in prejudice against such peripheral amplitudes.

These arguments have depended to some extent on the pomeron having a small real part. It is, of course, possible that the pomeron at low energies does not behave like an ordinary Regge-pole, that is, it does not have the usual Regge relationship between its phase and its energy dependence. If this were true, direct comparison of Regge fits with phase shift solutions would not be possible, at any rate until we have a more complete theory for the pomeron.

Some of the ambiguities that have been mentioned would be resolved by measurement of either the spin asymmetry parameter  $A$ , or the rotation parameter  $R$  (defined in e.g.s. (2.18, 2.19) respectively). Although measurement of these parameters is extremely difficult, as it requires a double-scattering experiment, it would be very worthwhile, because the predictions of the various solutions are wildly different.

As an example, in fig. (2.10) we show the predictions of all the amplitudes for the asymmetry  $A$  at  $P_L = 2.5 \text{ GeV}/c$ . It can be seen that even a very low-precision experiment would provide a means of distinguishing the two types of solution.

We conclude that our model agrees remarkably well with the CERN  $\rho$  solution. It differs from the ACE solution, and the CERN  $\alpha, \gamma$  solutions, largely in the phase of the flip amplitude. These last three solutions do not seem very compatible with simple Regge ideas.

## 2.6 Conclusions

- (i) Our simple model with non-factorising residues provides a satisfactory fit to  $K^+ p$  elastic scattering data. Our determination of  $\chi(t)$  supports  $t$  channel helicity conservation near the forward direction.
- (ii) Our model agrees with the results of Heyot and Navelet<sup>(28)</sup> for the Imaginary part of the  $K^+ p$  non-flip amplitude at  $P_L = 10 \text{ GeV}/c$ , but not for the real part of that amplitude. This has been traced to an erroneous assumption in ref.(28).
- (iii) The 'Regge Term' in ref.(28) is in fact just the vector meson contribution. It does not agree with the Regge term in our model, which also contains the tensor mesons.
- (iv) Our model agrees with all available phase shift solutions for the  $K^+ p$  non-flip amplitude at  $P_L = 2.5 \text{ GeV}/c$ . For the flip amplitude our model agrees with CERN  $\beta$ , but not with ACE or CERN  $\alpha, \delta$ . The last three solutions do not seem easily compatible with Regge theory, and in particular appear to require the pomeron to have a large real component.

Doubled trajectory models make the need for cuts less evident. They satisfactorily explain such features as the crossover zero and dips in cross sections in a way which allows these features quite naturally to be independent of energy - a phenomenon which cut models need to work hard to achieve.

That cuts must be present in Regge amplitudes, if only to shield wrong-signature fixed poles, is nevertheless now widely accepted.

The validity of currently available cut models, such as the absorption model, is, however, open to doubt, and the predictions of these models, particularly for the  $t$ -dependence of amplitudes, are somewhat suspect.

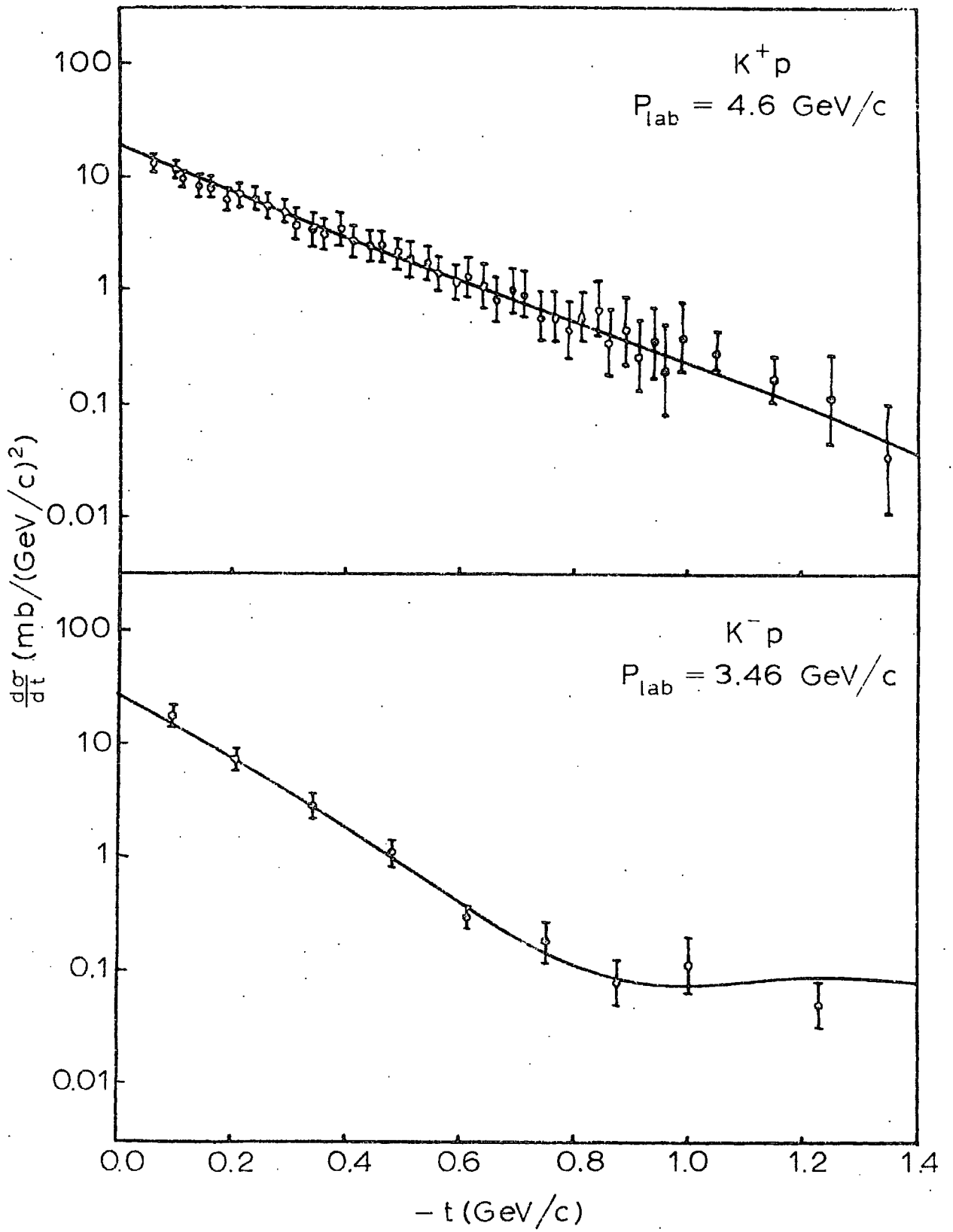
The one place where the effect of cuts ought to be unambiguous is in the energy dependence of amplitudes. The energy dependence produced by a cut is quite different from that produced by a pole, particularly if the cut discontinuity is not strongly peaked.

The best place to study energy dependences is where there are good data over a large range of energy. With the new data from Serpukov and ISR, pp elastic scattering now satisfies this criterion, and it is the subject of the next chapter.

Figures for Chapter 2

- 2.1 Comparison of our fit with  $K + p$  and  $K - p$  differential cross sections at  $P_L = 4.6$  and  $3.46$  GeV/c respectively.
- 2.2 Comparison of our fit with  $K + p$  and  $K - p$  polarisations at  $3.75$  and  $2.08$  GeV/c respectively.
- 2.3 Comparison of our fit with  $K + p$  and  $K - p$  total cross sections from  $P_L = 2$  to  $16$  GeV/c.
- 2.4 The parameter  $\chi_s(s,t)$ , defined in the text, at  $P_L = 10$  GeV/c. The solid line corresponds to our fit, and the broken line to  $t$  channel helicity conservation.
- 2.5 Comparison of the residues in our model with those of ref.(24). Continuous lines and dots are vector meson residues, broken lines and circles are tensor meson residues.
- 2.6 Comparison of the  $K - p$   $s$ -channel non flip amplitude in our model with the amplitude analysis of ref.(28). The solid lines are our model, broken lines and dots from ref.(28). Curves 1 and 2 are the meson contributions to the Imaginary part of the amplitude.
- 2.7 Comparison of fits to  $K + p$  polarisation at  $P_L = 2.5$  GeV/c. The curves shown are our model (labelled R), the ACE phase shift solution (labelled A) and the three CERN phase shift solutions (labelled  $\alpha$ ,  $\beta$ ,  $\gamma$ ).
- 2.8 Comparison of the  $s$  channel helicity amplitudes for  $K + p$  from our model with the ACE (labelled A) and CERN  $\beta$  (labelled  $\beta$ ) phase shift solutions.
- 2.9 Comparison of the predictions for the parameter  $\phi_s(s,t)$  defined in the text of our model with the ACE and CERN  $\beta$  phase shift solutions.
- 2.10 Comparison of the predictions for the asymmetry parameter A of our model with the ACE and CERN phase shift solutions.
- 2.11 The Simple-pole fits to  $\Delta \frac{d\sigma}{dt}$ , defined in the text, of ref.(60).
- 2.12 The flow-diagram for the CERN minimisation program MINUIT.

Fig. 11.11



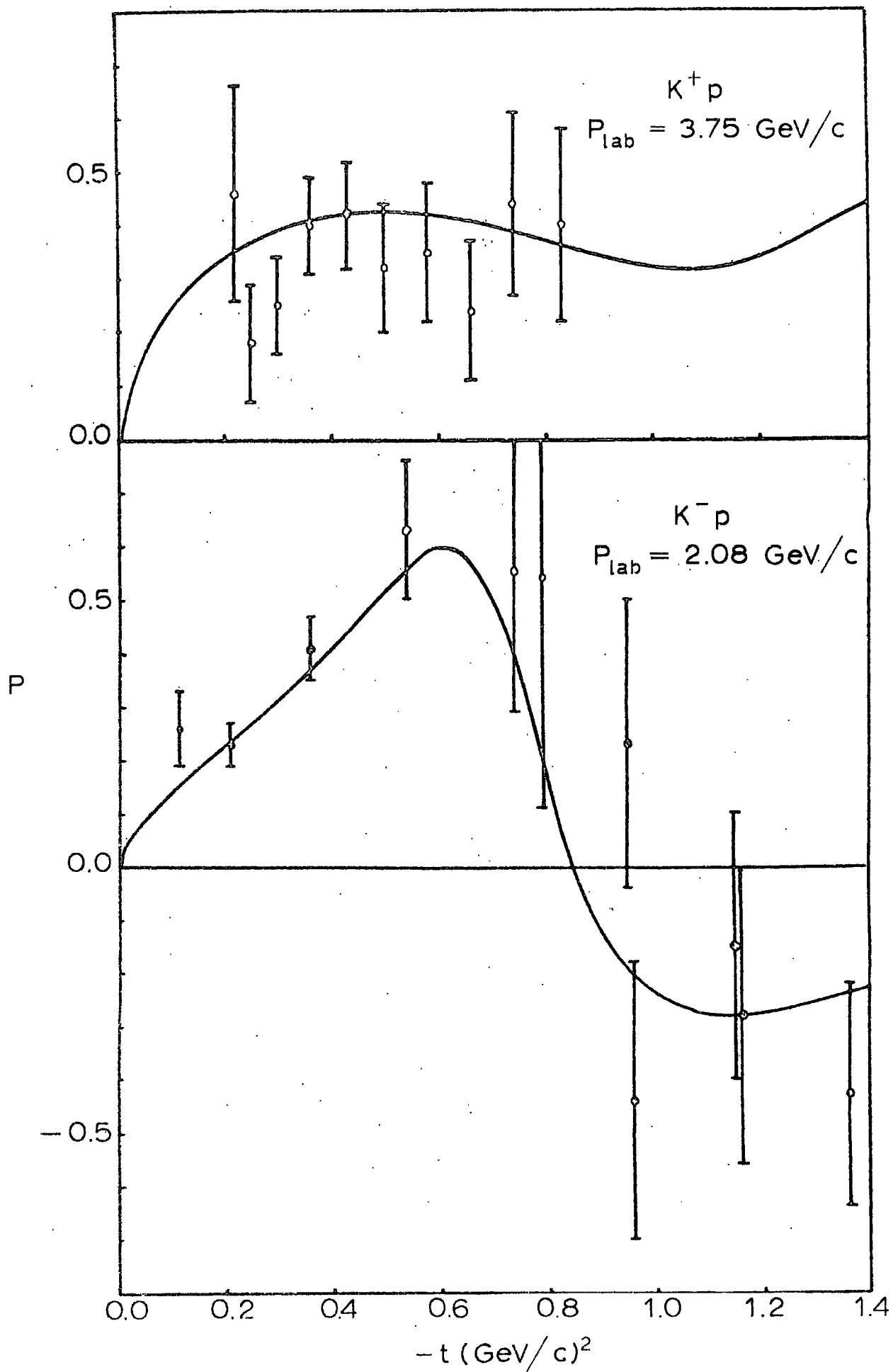


fig. (2.3)

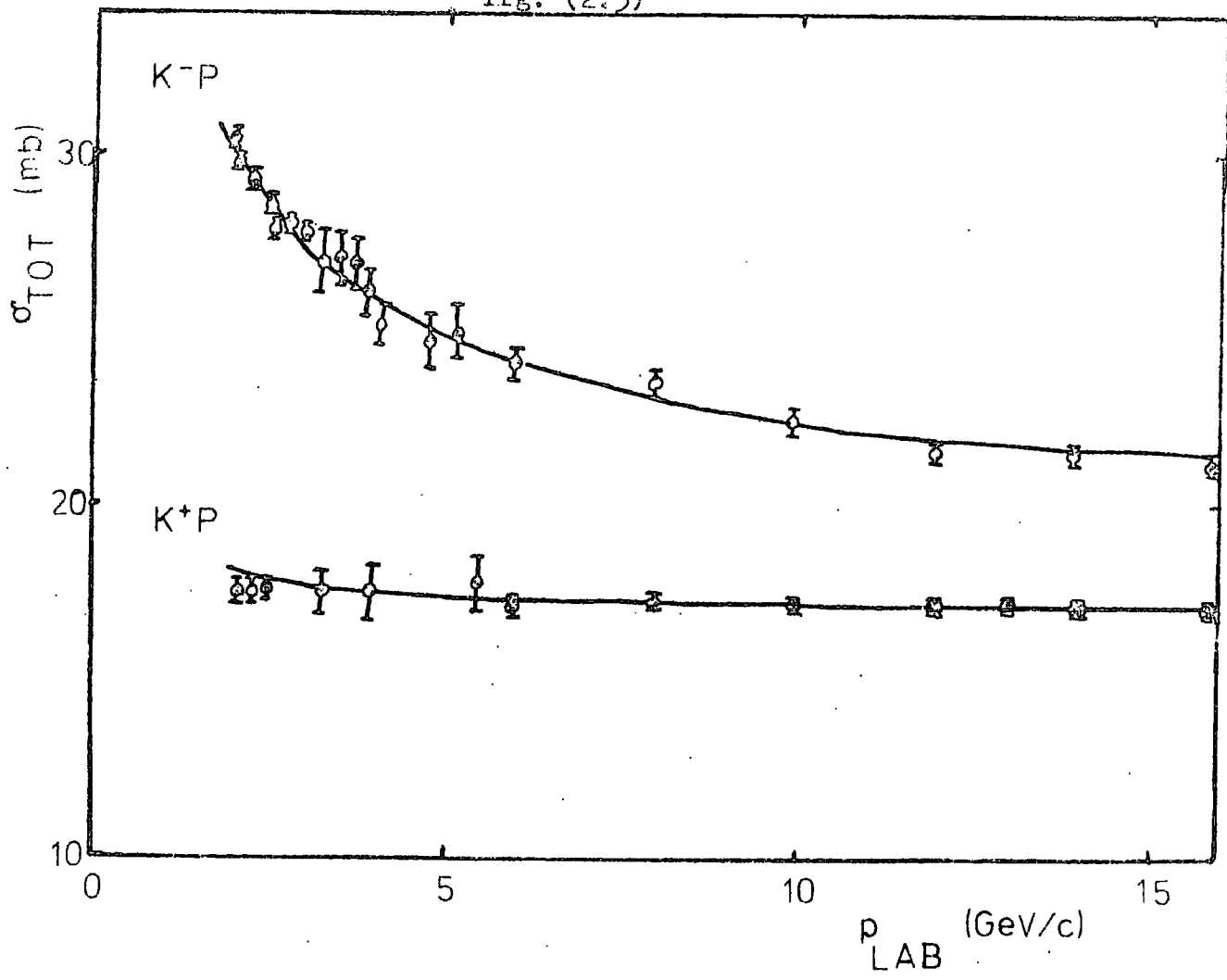


fig. (2.4)

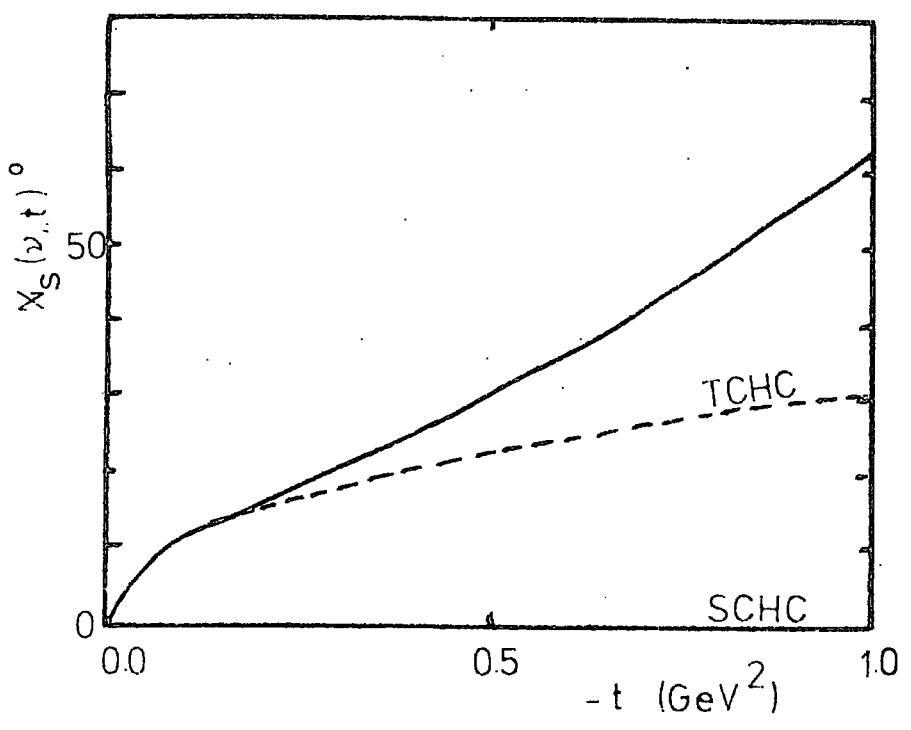


fig. (2.5)

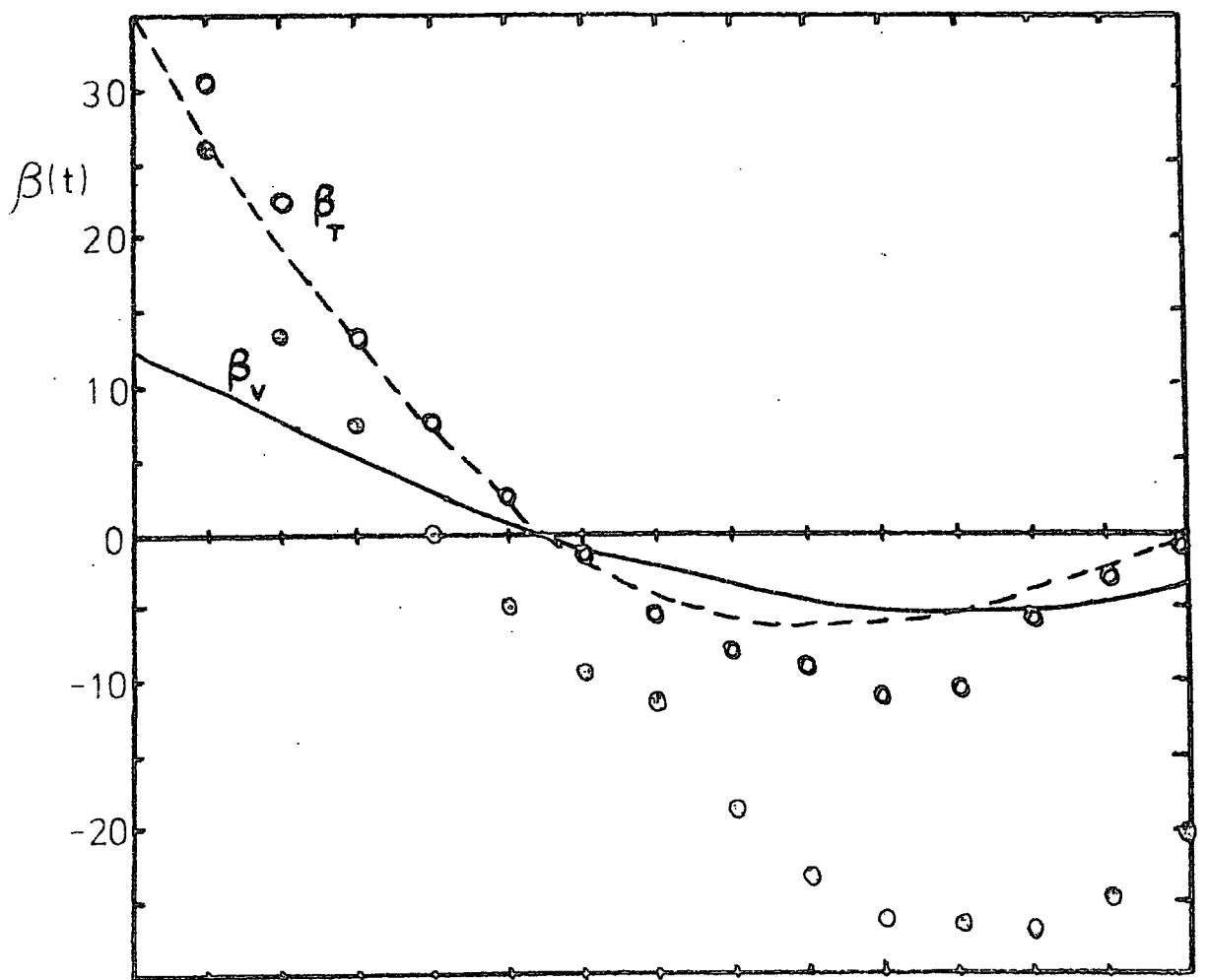
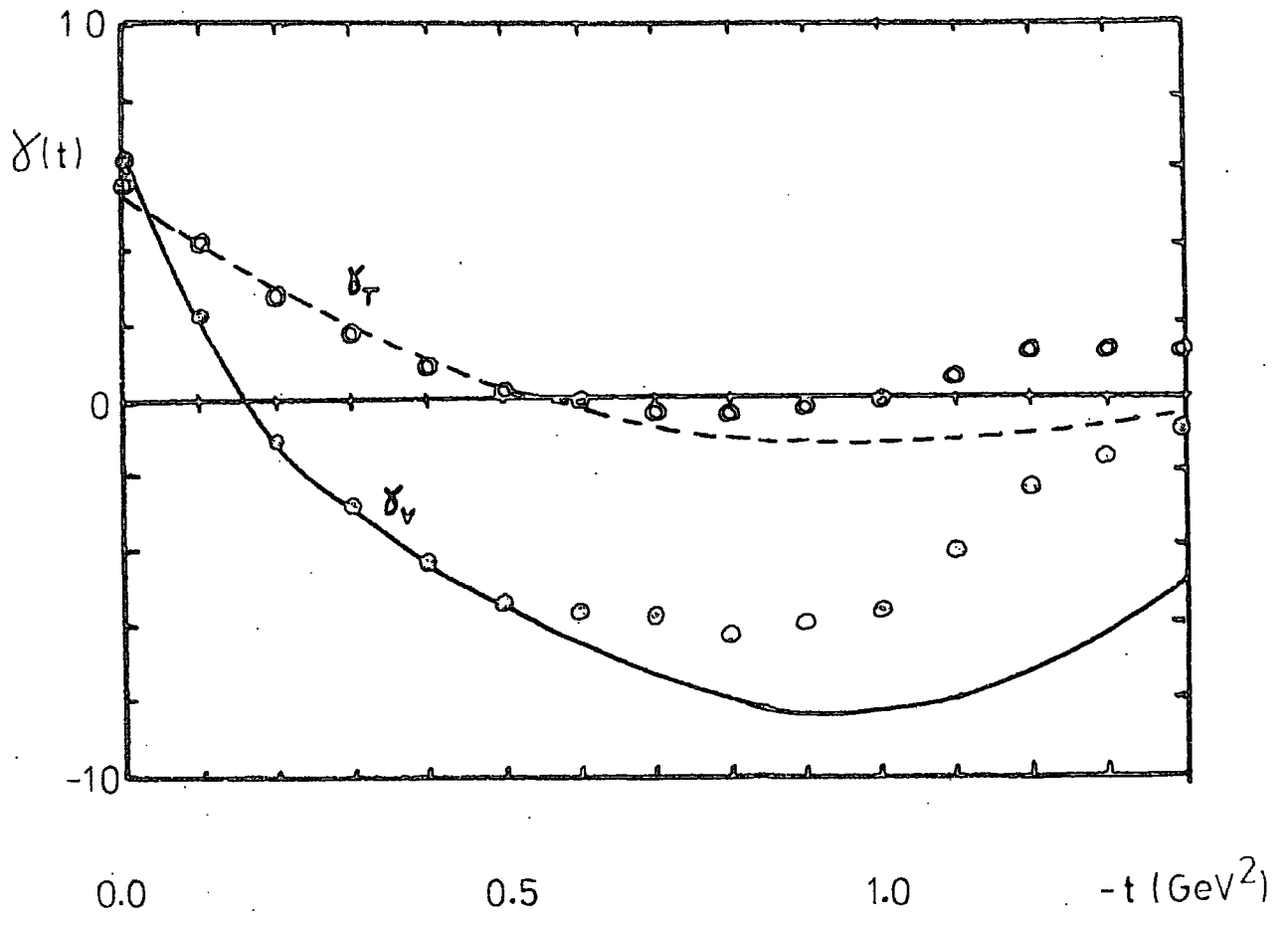


fig. (2.6)

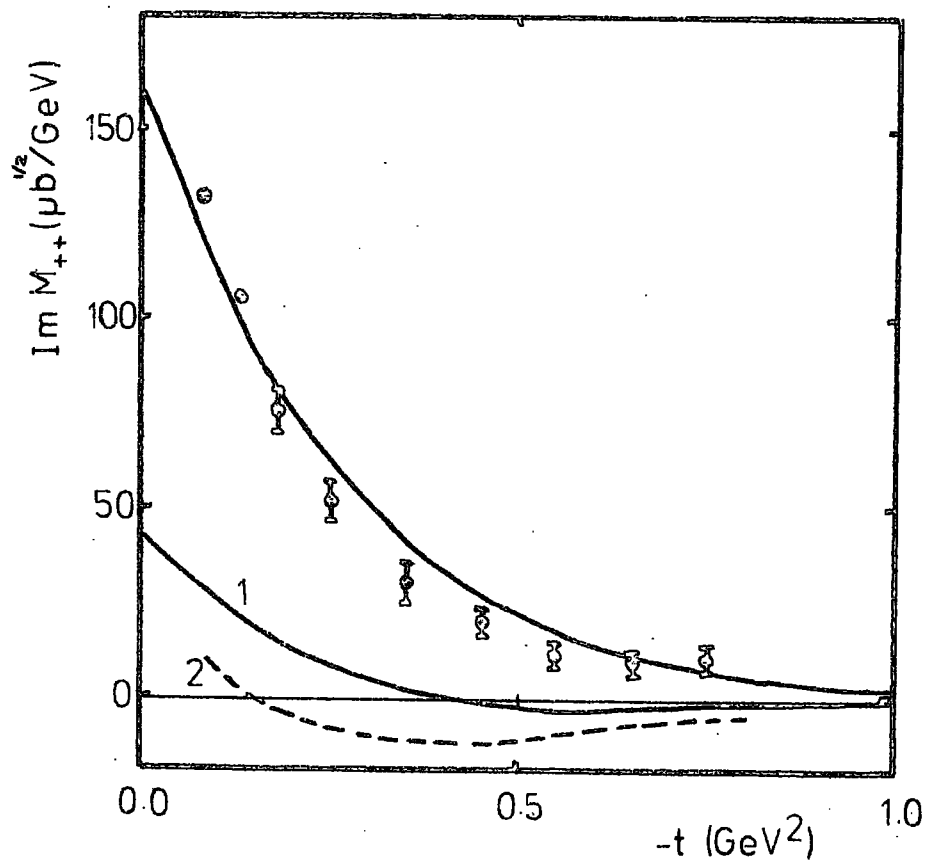
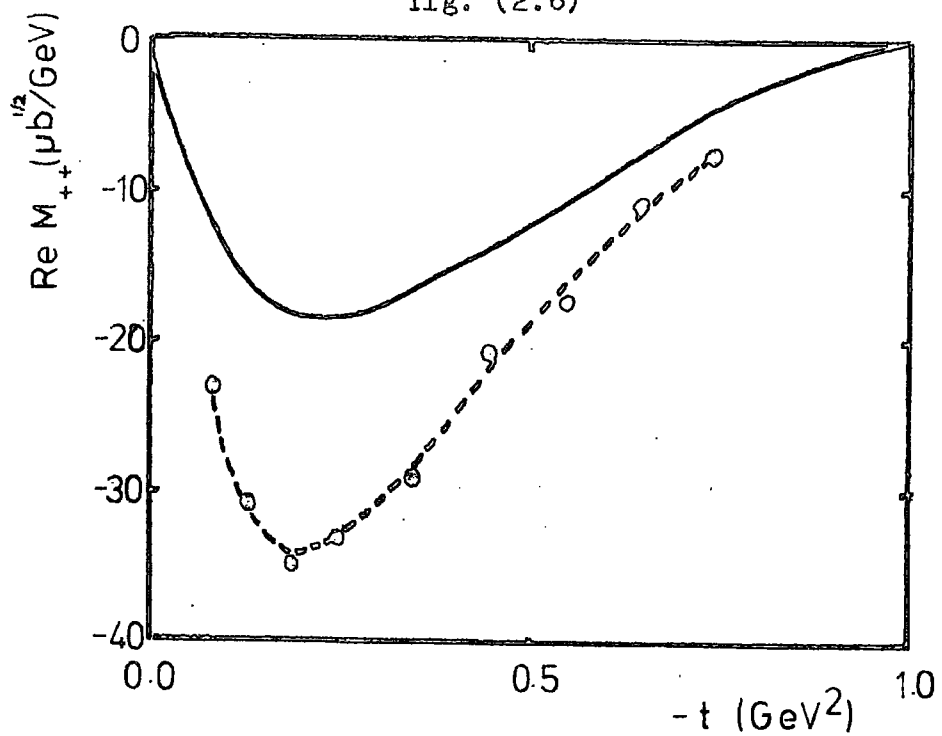


fig. (2.7)

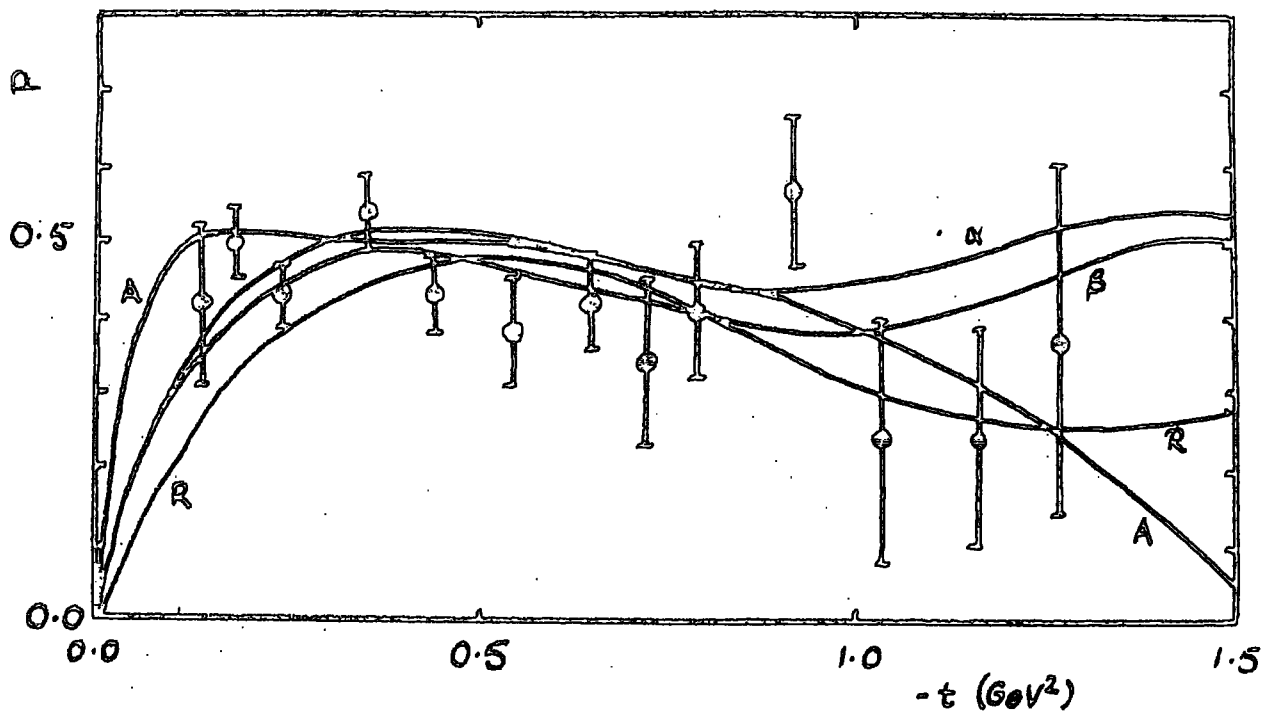


fig. (2.8)

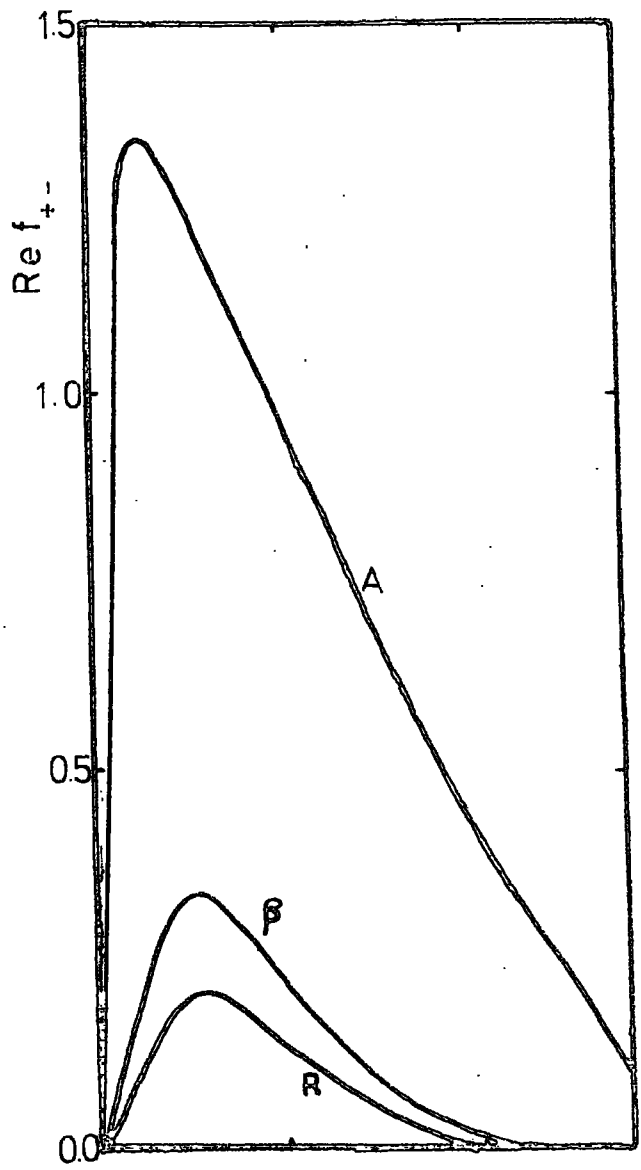
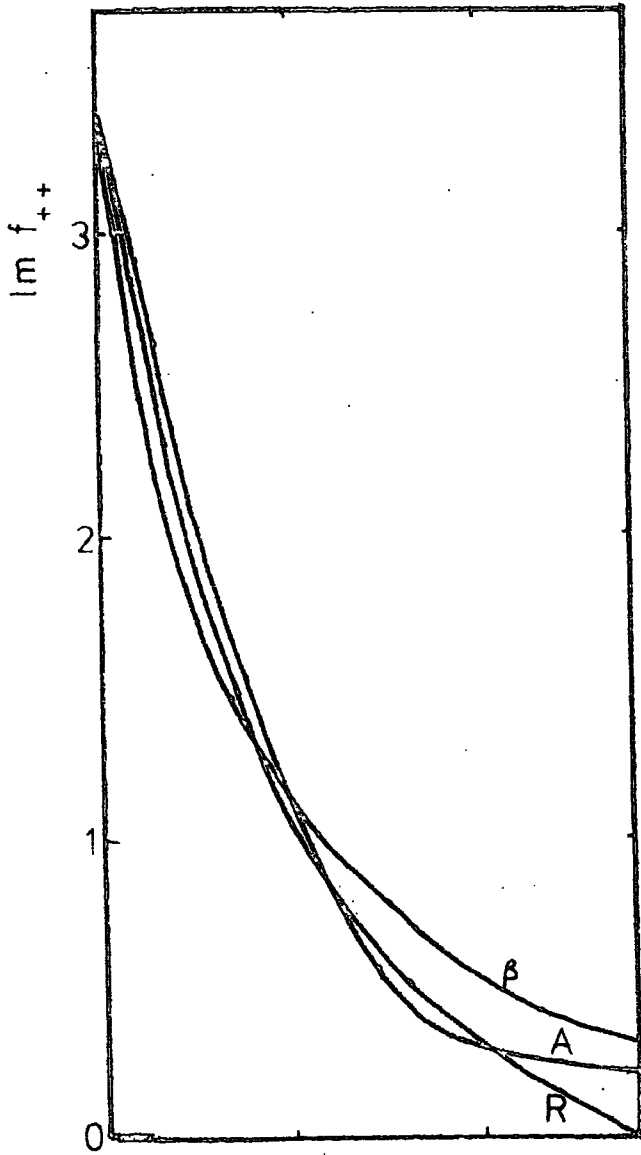
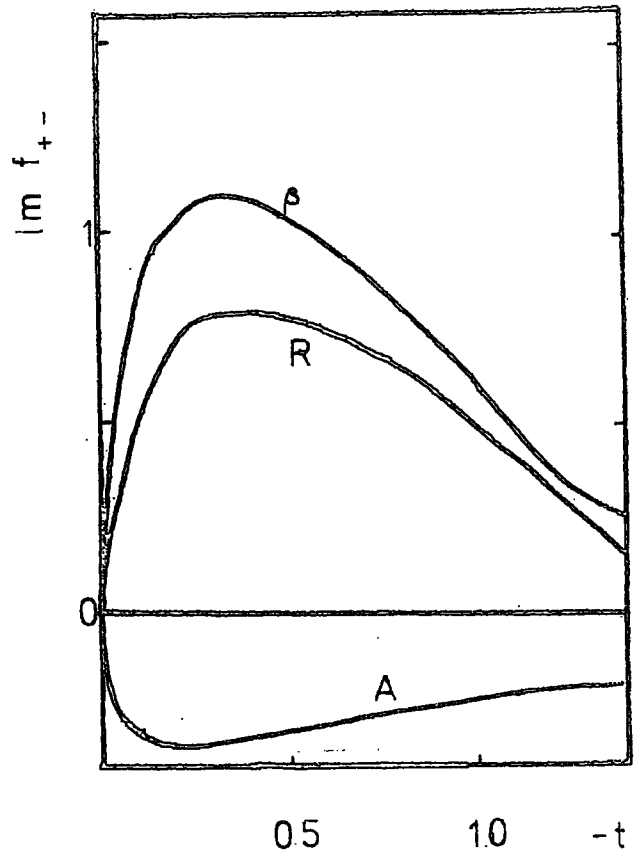
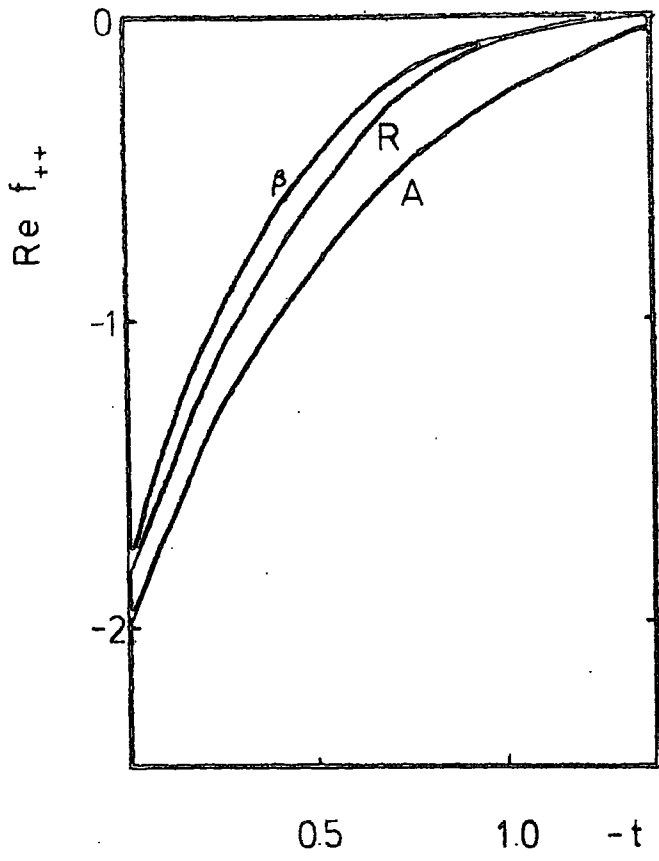


fig. (2.9)

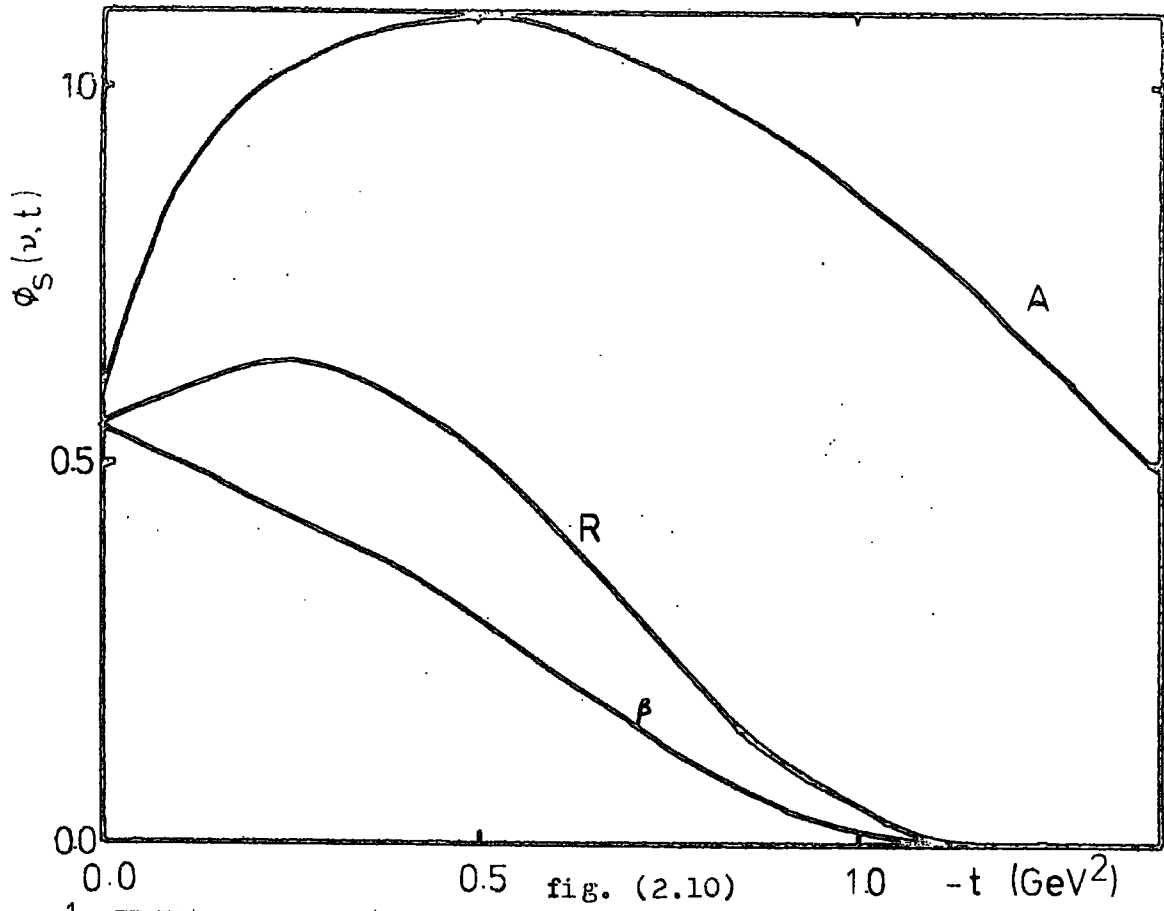


fig. (2.10)

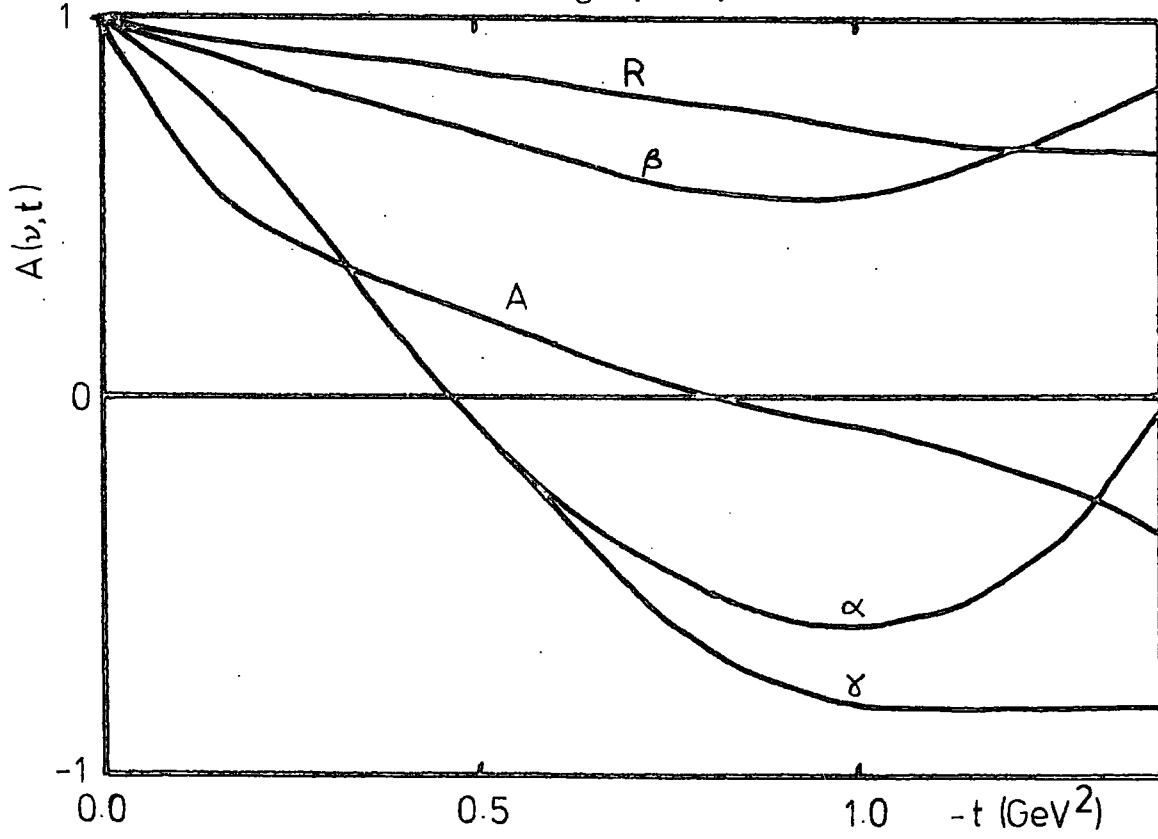


fig. (2.11)

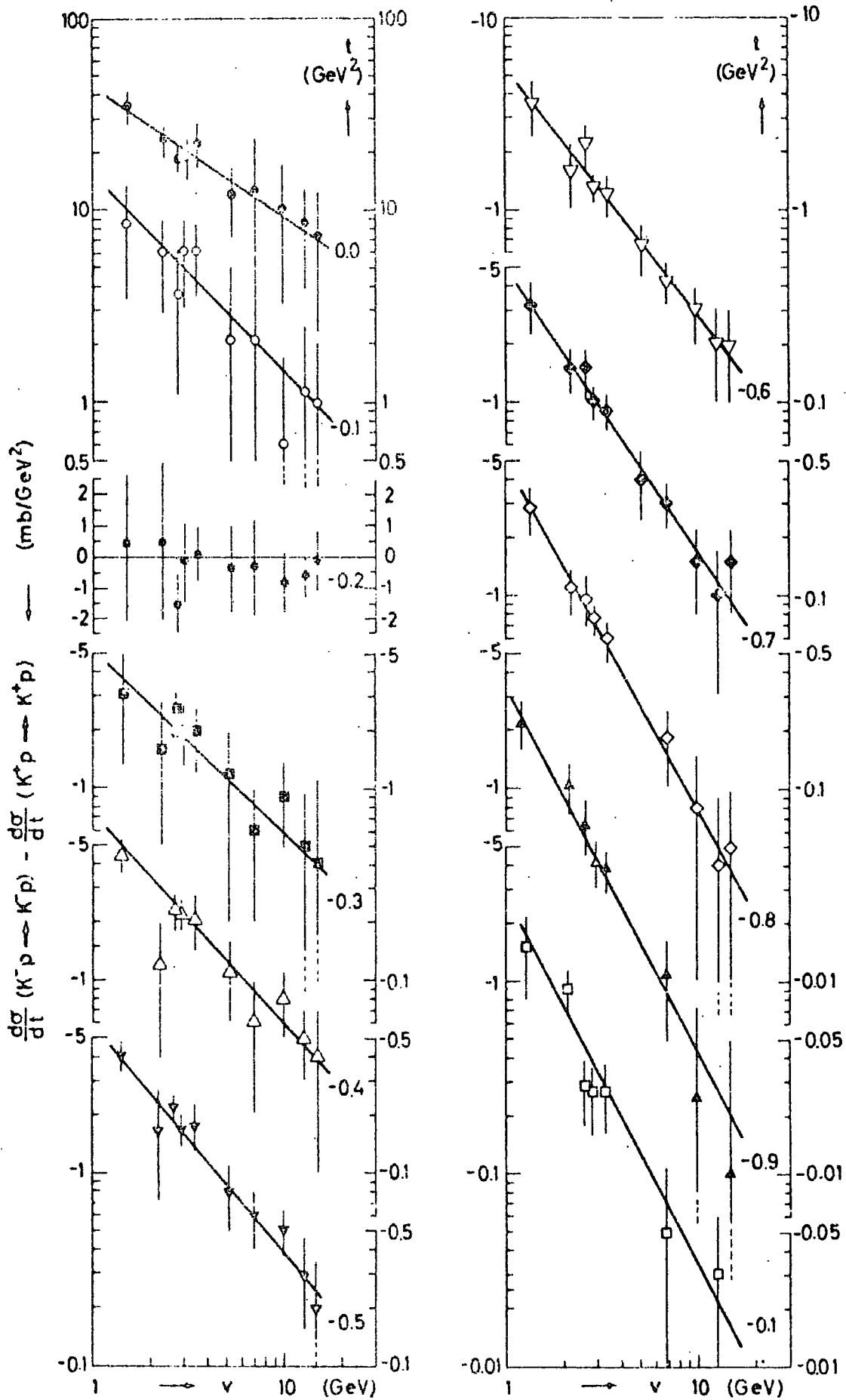
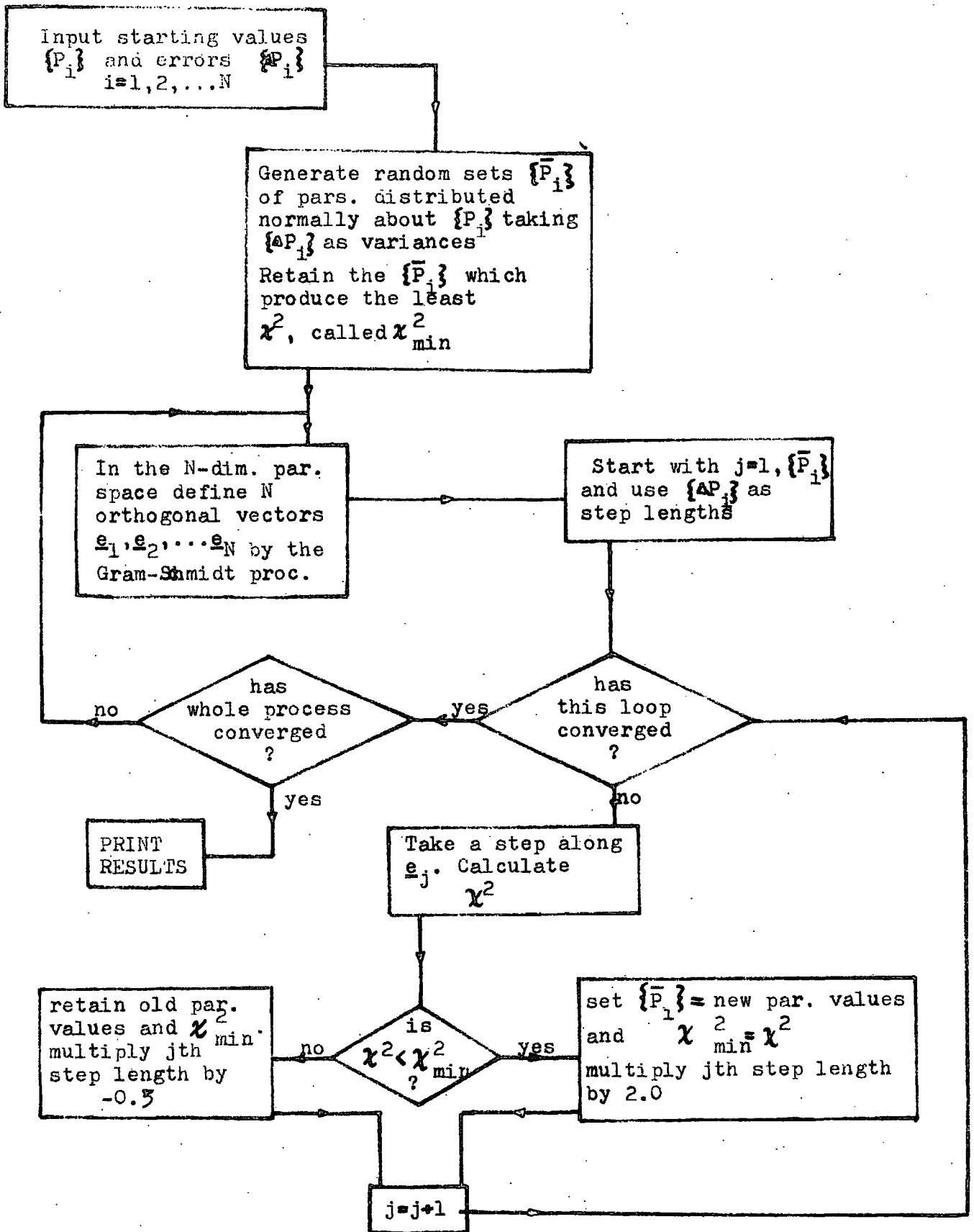


fig. (2.12)



### CHAPTER 3. J PLANE ANALYSIS OF PP ELASTIC SCATTERING

#### INTRODUCTION

The evidence for the existence of Regge Cuts is at best indirect, and comprises mainly the failure of the simple Regge Pole model to explain various features of the data, as discussed in section (1.2). Other explanations have, however, been put forward. (See, for example, section (1.2), Chapter 2, and ref.(67)). It is possible that cuts have a much smaller effect than is usually supposed, in which case their detection will be rather difficult.

Another difficulty with Regge Cuts is that we really do not have much idea how to calculate them. The absorption prescription, although precise, has a somewhat dubious derivation, and in any case does not provide quantitative fits to the data unless the cut amplitudes are multiplied by an arbitrary parameter. Such models then have great freedom and little predictive power, which is an entirely unsatisfactory situation. A remark, made by Lovelace<sup>(68)</sup> about the Michigan cut model, is worth quoting.

"The whole history of Physics tells us that a theory with few parameters which works only in simple situations, is more likely to be basically correct than a theory with many parameters which works only in complicated situations."

We are therefore led to search for cuts in situations where the theory is more substantial, and the data less ambiguous. Here we may take a lesson from Regge Pole theory, whose chief prediction is the energy dependence of cross sections, which on the whole is well supported by the data, whereas the  $t$ -dependence, which is largely arbitrary in the theory, has caused most of the problems. The situation is much the same for Regge Cuts. We do not know their prediction for  $t$ -dependence with any reliability, but, since the positions of cut branch points are known, we have much more information about their structure in energy.

It therefore makes sense to look for cuts in the energy dependence of cross sections. Of course, poles will still be present, and to unravel the cuts from the poles a considerable amount of good data, over a large energy range, is necessary. Although such an ideal situation is far from being realised, since the data from Serpukov, ISR and NAL have become available, the procedure is certainly worth trying for elastic pp scattering. This process has the additional advantage of being exotic, so that the contribution of the Regge Poles, especially to the total cross section, is expected from Exchange Degeneracy to be small. This means that cuts should be particularly easy to detect.

The main disadvantage of proton-proton scattering is that there are a large number of independent helicity amplitudes - five in the elastic process. Good data are available only on total and differential cross sections, so that it is not possible to determine all the amplitudes. This is not a serious drawback as far as this chapter is concerned, however, because poles and branch points in the  $j$ -plane have the same position in all amplitudes, and we are not concerned with  $t$ -dependences. (We shall show in the next chapter that, at energies where the pomeron can be considered to dominate, we can reduce the amplitudes to a single real number, although for this procedure some approximations must be made).

In section (3.1) we define the amplitudes and formalism that will be used. Sections (3.2, 3.3) deal with our analysis of the total and elastic differential cross sections respectively, and in section (3.4) the results are discussed and conclusions drawn.

### 3.1 Amplitudes and Formalism

There are five independent helicity amplitudes in elastic pp scattering. We take these to be  $T_{\uparrow\uparrow\uparrow\uparrow}$ ,  $T_{\uparrow\uparrow\downarrow\downarrow}$ ,  $T_{\uparrow\downarrow\downarrow\uparrow}$ ,  $T_{\downarrow\downarrow\downarrow\downarrow}$  and  $T_{\uparrow\downarrow\uparrow\downarrow}$  (in the s channel). The normalisation is chosen so that

$$\frac{d\sigma}{dt} = \frac{1}{16\pi q^2 s} \sum_{\mu, \nu, \lambda, \sigma} |T_{\mu\nu\lambda\sigma}(s, t)|^2 \quad (3.1)$$

$$\text{and } \sigma_T = \frac{1}{q \sqrt{s}} \sum_{\mu, \nu} \text{Im} [T_{\mu\nu\mu\nu}(s, 0)] \quad (3.2)$$

where  $\mu, \nu, \lambda, \sigma$  are helicity indices.

The contribution of a Regge trajectory  $\alpha$  to one of these amplitudes may be written as (see e.g. (1.1)).

$$T_{\mu\nu\lambda\sigma}^{\text{POLE}}(s, t) = \eta_{\mu\nu\lambda\sigma}^{\alpha}(t) s^{\alpha(t)} \quad (3.3)$$

and we write the contribution of a cut in the form of the integral of its discontinuity

$$T_{\mu\nu\lambda\sigma}^{\text{CUT}}(s, t) = \int_{-\infty}^{\alpha_{\text{CUT}}(t)} dj \beta_{\mu\nu\lambda\sigma}(j, t) s^j \quad (3.4)$$

(The functions  $\eta_{\mu\nu\lambda\sigma}$  and  $\beta_{\mu\nu\lambda\sigma}$  contain kinematic factors, which are not important in this discussion, as the s-dependence, in which we are interested, is displayed explicitly).

The amplitude will in general be a sum of terms like e.g.s.(3.3, 3.4). We combine both these forms by writing

$$T_{\mu\nu\lambda\sigma}(s, t) = \int_{-\infty}^{\alpha_{\text{max}}} dj s^j \tau_{\mu\nu\lambda\sigma}(j, t) \quad (3.5)$$

In this representation, poles appear as  $\delta$ -functions in  $\tau_{\mu\nu\lambda\sigma}$ , and cuts as continuous functions with  $\theta$ -functions at the branch points, i.e.

$$\tau_{\mu\nu\lambda\sigma}^{\text{POLE}}(j,t) = \tau_{\mu\nu\lambda\sigma}^{\alpha}(t) \delta(j - \alpha(t)) \quad (3.6)$$

$$\tau_{\mu\nu\lambda\sigma}^{\text{CUT}}(j,t) = \beta_{\mu\nu\lambda\sigma}(j,t) \theta(\alpha_{\text{CUT}}(t) - j) \quad (3.7)$$

Substituting e.q. (3.5) into e.qs.(3.1, 3.2) we obtain

$$\frac{d\sigma}{dt} = \frac{1}{s^2} \int_{-\infty}^{\alpha_{\text{max}}} \frac{d\alpha}{d\alpha} s^{2\alpha} \gamma(j,t) \quad (3.8)$$

$$\sigma_T = \frac{1}{s} \int_{-\infty}^{\alpha_{\text{max}}} \frac{d\alpha}{d\alpha} s^{\alpha} \beta(j) \quad (3.9)$$

where

$$\gamma(j,t) = \frac{1}{4\pi} \sum_{\mu,\nu,\lambda,\sigma} \int_{-(\alpha_{\text{max}}-j)}^{\alpha_{\text{max}}-j} d\alpha \tau_{\mu\nu\lambda\sigma}^*(j+1,t) \tau_{\mu\nu\lambda\sigma}(j-1,t) \quad (3.10)$$

and 
$$\beta(j) = \frac{1}{2} \sum_{\mu,\nu} \text{Im} [\tau_{\mu\nu\mu\nu}(j,0)] \quad (3.11)$$

and where we have used (from e.q.A.9))

$$q \underset{s \rightarrow \infty}{\sim} \frac{1}{2} \sqrt{s}. \quad (3.12)$$

Since a particular trajectory, such as the  $\rho$ , contributes in the same way to the  $j$ -dependence of all the amplitudes, the  $j$  dependence of  $\delta(j,t)$  and  $\beta(j)$  is expected to be rather simple, whereas the  $t$ -dependence is expected to be too complicated to yield much information.

It might be thought possible to invert e.qs. (3.8, 3.9) to obtain  $\delta(j,t)$ ,  $\beta(j)$  direct from the data. Unfortunately this is not so, for the following reason. If we put  $x = 2\log(s)$  and  $k = \alpha_{\max} - j$  in, for example, e.q. (3.8) we obtain

$$\frac{d\sigma}{dt} = e^{(\alpha_{\max}-1)x} \int_0^{\infty} dx e^{-kx} \gamma(2\alpha_{\max}-k, t) \quad (3.13)$$

The integral will be immediately recognised as the Laplace transform, of which the inverse is, of course, well known. We obtain

$$\delta(j,t) = \frac{1}{2\pi i} \int_{c-i\infty}^{c+i\infty} dx e^{-(j+1)x} \frac{d\sigma}{dt}(e^x, t) \quad (3.14)$$

and since neither the differential nor the total cross section is defined for complex  $\log(s)$ , this expression is of no use in determining  $\delta$ , and less direct methods need to be employed.

The method we shall use in the next two sections is to parametrise  $\delta$  and  $\beta$  in various ways, and determine the parameters by fitting e.qs. (3.8) and (3.9) to the data. We shall always use forms for  $\delta$  and  $\beta$  for which the integrals in e.qs. (3.8, 3.9) can be performed analytically, since this considerably simplifies the procedure.

### 3.2 The Total Cross Section

#### Data

Table (3.1) lists the sources and ranges of data used. The data are plotted in fig.(3.1). The circles are from ref.(36), black dots from ref.(37), and triangles from ref.(38). It may be seen that the Serpukov data of ref.(37) agree well with the older data of ref.(36) in the region  $30 < s < 51 \text{ GeV}^2$ , where there is considerable overlap. The data from ISR are somewhat isolated, and have such large errors that they cannot be expected to yield much information.

Since this work was finished, new data have become available from ISR<sup>(46)</sup> and NAL<sup>(47)</sup>. The present experimental situation at Serpukov energies and above is shown in fig.(3.8), and it may be seen that the very high energy data are by no means consistent. These data may affect our conclusions only for the pomeron, since by that energy the meson contributions have become negligible, but more likely they require a reappraisal when the very high energy data are known with more certainty. The methods are, in any case, still worthwhile.

Table 3.1

The PP Total Cross Section

MIN	$s$ ( $\text{GeV}^2$ )	MAX	Number of points	Reference
16.54		50.58	11	Foley (36)
29.96		114.4	10	Denisov (37) (Serpukov)
949.0		2808	3	Barbiellini (38) (I.S.R.)

Table 3.2The PP Elastic Differential Cross Section

MIN	$s$ (GeV <sup>2</sup> )	MAX	Number of points	Normalised ?	Reference
14.64		48.01	90	Yes	Foley (41)
28.47		46.80	35	Yes	Allaby (42)
102.0		131.2	-	No	Beznogikh (Serpukov) (43)
462.0		2808	-	No	Holder (I.S.R.) (44)

Models

In elastic pp scattering the allowed exchanges are

$$pp = P + f + A_2 - \rho - w \quad (3.15)$$

We have already discussed the idea that the meson trajectories are exchange degenerate, and under this assumption only two trajectories should contribute and it is logical first to consider the form

$$\sigma_T(s) = \frac{1}{s} (As^{\alpha_1} + Bs^{\alpha_2}) \quad (3.16)$$

We fitted this form to the data, and found the best-fit parameters to be

$$\begin{aligned} \alpha_1 &= 1.0 \pm 0.05 \\ \alpha_2 &= 0.0 \pm 0.1 \end{aligned} \quad (3.17)$$

These results are at first somewhat surprising. Although the first term is naturally associated with the pomeron, one would expect  $\alpha_2 \approx 0.5$  to correspond to the mesons.

Of course, exchange degeneracy predicts that the mesons should not contribute to the pp total cross section, since the pp channel is exotic, so perhaps this result is not so surprising. To verify it we tried a fit of the form

$$\sigma_T(s) = \frac{1}{s} (A s + B s^{0.5} + C) \quad (3.18)$$

The best fit had the following parameter values, and a mean  $\chi^2$  of 0.25 per point.

$$\begin{aligned} A &= 37.9 \pm 0.3 \text{ mb} \\ B &= 2.2 \pm 4.4 \text{ mb} \\ C &= 31.3 \pm 13.4 \text{ mb} \end{aligned} \quad (3.19)$$

This result confirms e.q. (3.17), in the sense that the parameter B, which represents the meson coupling, is entirely consistent with zero.

The fact that the pp total cross section is not entirely flat up to Serpukov energies has, in the past, usually been interpreted as evidence of a small amount of exchange degeneracy breaking. An example of this is the fit of Barger et al<sup>(35)</sup>, who parametrised both the pp and pp total cross sections as

$$\sigma_{TOT}(s) = A + B s^{-0.6} \quad (3.20)$$

and found for pp

$$\begin{aligned} A &= 37.3 \text{ mb} \\ B &= 15.6 \text{ mb} \end{aligned} \quad (3.21)$$

These fits are compared in fig.(3.1). Our fit, of e.qs. (3.18, 3.19) is labelled I, and that of Barger et al is labelled II. It may be seen that curve I is distinctly superior in its ability to fit both the low energy data and the high-energy end of the Serpukov data. These results indicate that the data prefer a singularity near  $j = 0$  to one near  $j = \frac{1}{2}$ .

We are left with the problem of identification of the  $j = 0$  singularity. The obvious candidate, the pion, cannot contribute because it has the wrong signature and parity.

To obtain more information we tried a continuum fit, using the form of e.q. (3.9) with  $\alpha_{\max} = 1$ , i.e.

$$\sigma_T(s) = \frac{1}{s} \int_{-\infty}^1 dj s^j \beta(j) \quad (3.22)$$

We parametrised  $\beta$  as a polynomial in  $(j - 1)$ :

$$\beta(j) = \sum_{k=0}^n b_k (j-1)^k \quad (3.23)$$

This parametrisation has the advantage that, when the integral has been performed, the expression for  $\sigma_T(s)$  is linear in the  $b$ 's. In fact

$$\sigma_T(s) = \sum_{k=0}^n b_k (-)^k k! \left[ \frac{1}{\log s} \right]^{k+1} \quad (3.24)$$

and the  $b$ 's can then be determined by a linear least squares fit. To maintain the same number of parameters as for the simple pole fit, we chose  $n = 3$ . The best fit is shown as curve III in fig. (3.1) and the best fit  $\beta(j)$  is shown in fig. (3.2).

As expected  $\beta(j)$  has a sharp peak at  $j = 1$ , which may be interpreted as an attempt to simulate the appearance of a  $\delta$ -function. There is, however, a broader peak in the region  $-1 \leq j \leq 0$ , which reproduces the same structure as the  $\delta$ -function at  $j = 0$  in the previous fit.

We see from fig. (3.1) that curve III provides as good a fit to the low-energy and Serpukov data as curve I, and that it is again superior to curve II in its ability to fit the high-energy Serpukov points, in the region of  $s \approx 100 \text{ GeV}^2$ . The fall in curve III at ISR energies is caused by the fact that  $\beta(j)$  is necessarily finite at  $j = 1$ , whereas the data require a  $\delta$ -function.

It is difficult to estimate whether the width of the peak at  $-1 \leq j \leq 0$  in  $\beta(j)$  is required by the data, or merely a consequence of the polynomial parametrisation. The latter explanation is probably more likely, because we have already shown that the data can be fitted with a  $\delta$ -function, but curve III shows that this is by no means necessary.

### 3.3 The Differential Cross Section

#### Data

The data used are summarised in table (3.2). The 'conventional' data, from refs. (41, 42) were in the form of points in the range  $0 > t > -0.6 \text{ GeV}^2$ , those from ref. (43) were slope parameters for data in the range  $0 > t > -0.13 \text{ GeV}^2$ , and those from ref. (44) were slope parameters in the ranges  $0 > t > -0.15 \text{ GeV}^2$  and  $-0.15 > t > -0.5 \text{ GeV}^2$ .

There is evidence for a systematic error in the data from ref.(43). In fig. (3.9) the slope parameter  $b$  is plotted, and it may be seen that the data of ref. (43) are too large by  $0.4 \text{ GeV}^{-2}$ . This is consistent with the possible systematic error of  $0.3 \text{ GeV}^{-2}$  quoted in that paper. Accordingly we adjusted the slope parameters from ref.(24) to bring them into line with the data from other sources.

#### Interpolation and normalisation of data

Data from refs. 41 and 42 were interpolated in  $t$  to obtain values from  $t = -0.05$  at intervals of  $0.05$  to  $t = -0.4 \text{ GeV}^2$ .

In the region  $0 > t > -0.4 \log d\sigma/dt$  is nearly linear in  $t$ , but it has been shown (45) that even at quite low energies (at least down to the lowest Serpukov energies, i.e.  $s \approx 30 \text{ GeV}^2$ )  $\log d\sigma/dt$  exhibits a change of slope near  $t = -0.15 \text{ GeV}^2$ . Consequently, we simultaneously smoothed and interpolated the data by fitting  $\log d\sigma/dt$  with cubic polynomials in  $t$ , i.e. we wrote

$$\log \frac{d\sigma}{dt} = \sum_{k=0}^3 a_k t^k \quad (3.25)$$

and determined the  $a$ 's by linear least squares. We used all the data for  $|t| < 0.4$ , plus that with the next largest value of  $t$ .

For data from ref.(41) a slight variation of this procedure was adopted. There are two sets of measurements by the same group at the same energies, but performed at different times, so that their normalisations are slightly different. One set deals with small  $t$  ( $|t| \lesssim 0.2$ ) and the other with larger  $t$  (although there is some overlap). In order to make best use of these data, we used both sets simultaneously, allowing a relative normalisation factor. We fitted the small  $t$  data with

$$\log \frac{d\sigma}{dt} = \sum_{k=0}^3 a_k t^k \quad (3.26)$$

and the large  $t$  data with

$$\log \frac{d\sigma}{dt} = N + \sum_{k=0}^3 a_k t^k \quad (3.27)$$

using the same  $a$ 's. The parameter  $N$  was thus determined to give the smoothest interpolation between the small and large  $t$  results. In some cases there was overlap between the two experiments, and the method could be tested by examination. In such cases it was found to be satisfactory.  $N$  was never as large as the published relative normalisation error.

Data from refs. (43, 44) were interpolated by means of the slope parameters, and normalised by the optical theorem to the total cross section fit I of fig. (3.1). Several considerations arose from this procedure.

The behaviour of a helicity amplitude near the physical region boundary  $t = 0$  is (39)

$$T_{\mu\nu\lambda\sigma}(s,t) \underset{t \sim 0}{\sim} (\sqrt{-t})^{|\alpha-\beta|} \quad (3.28)$$

where  $\alpha = \lambda - \sigma$  and  $\beta = \mu - \nu$ .

This means that, of the five independent amplitudes, three -  $T_{\leftrightarrow\leftrightarrow\leftrightarrow}$ ,  $T_{\leftrightarrow\leftrightarrow\leftarrow}$ , and  $T_{\leftrightarrow\leftarrow\leftarrow}$  - are finite at  $t = 0$ . Only the completely elastic amplitudes -  $T_{\leftrightarrow\leftrightarrow\leftrightarrow}$ ,  $T_{\leftrightarrow\leftrightarrow\leftarrow}$  - however, contribute to the optical theorem, i.e.

$$\frac{d\sigma}{dt}(s,0) = \frac{1}{16\pi q^2 s} \left[ |T_{\leftrightarrow\leftrightarrow\leftrightarrow}(s,0)|^2 + |T_{\leftrightarrow\leftrightarrow\leftarrow}(s,0)|^2 + |T_{\leftrightarrow\leftarrow\leftarrow}(s,0)|^2 \right] \quad (3.29)$$

and

$$\sigma_T(s) = \frac{1}{q\sqrt{s}} \text{Im} \left[ T_{\leftrightarrow\leftrightarrow\leftrightarrow}(s,0) + T_{\leftrightarrow\leftrightarrow\leftarrow}(s,0) \right] \quad (3.30)$$

Consequently, if we wish to use the total cross section for normalisation of differential cross section data, we are going to have to neglect not only  $\text{Re}T_{\leftrightarrow\leftrightarrow\leftrightarrow}$  and  $\text{Re}T_{\leftrightarrow\leftrightarrow\leftarrow}$ , but also  $\text{Re}T_{\leftrightarrow\leftarrow\leftarrow}$  and  $\text{Im}T_{\leftrightarrow\leftarrow\leftarrow}$ , compared with  $\text{Im}T_{\leftrightarrow\leftrightarrow\leftrightarrow}$  and  $\text{Im}T_{\leftrightarrow\leftrightarrow\leftarrow}$ .

It can be shown by dispersion relation calculations<sup>(40)</sup>, that this procedure is suspect for  $s \lesssim 70 \text{ GeV}^2$ , so we did not attempt to normalise any data for  $s < 100 \text{ GeV}^2$ . This meant that we did not use a considerable amount of the data from Serpukov, but there was no way we could use these data without the danger of introducing a spurious dip into the differential cross section at  $s \approx 60 \text{ GeV}^2$ .

Serpukov data were used only at  $t = -0.05 \text{ GeV}^2$  and  $t = 0.1 \text{ GeV}^2$ , since the experiments did not extend beyond  $t = -0.13 \text{ GeV}^2$ . The extent of the ISR data varied with energy, being at the least out to  $t = -0.25 \text{ GeV}^2$ , and at most to the largest  $|t|$  considered. No extrapolated data were used, since, even near  $t = 0$  there is no way of doing this consistently.

### Fitting Procedure

We worked at fixed  $t$ , fitting the interpolated data with functions continuous in  $s$ . This meant that at each  $t$  we obtained parameter values, and were thus able to determine our parameters as functions of  $t$ . The remarkable continuity of these parameters (see, for example, figs. (3.4, 3.5)) is encouraging evidence of the consistency of our interpolation procedures.

Because our interpolation was in  $t$ , and our fits were in  $s$ , there was necessarily a large scatter in the data points (see figs. (3.3, 3.6)), which was especially troublesome at small  $t$ , where there were fewest points. We were therefore forced to keep the numbers of our parameters to a minimum so as to reproduce the broad features of the data, without fitting the statistical fluctuations. Consequently we rejected parametrisations which fitted so well that the mean  $\chi^2$  was very much less than unity.

### Models

#### (i) Pole Models

In the same way as for the total cross section, the natural model to try first is a sum of poles. For each amplitude we used a two-pole model

$$T_{\mu\nu\lambda\sigma}(s,t) = a_{\mu\nu\lambda\sigma}(t) s^{\alpha_1(t)} + b_{\mu\nu\lambda\sigma}(t) s^{\alpha_2(t)} \quad (3.31)$$

Here  $a_{\mu\nu\lambda\sigma}(t)$ ,  $b_{\mu\nu\lambda\sigma}(t)$  are complex functions of  $t$  containing kinematic factors as well as the Regge residues and signature factors.

This gives, for the differential cross section (by e.q. (3.1))

$$\frac{d\sigma}{dt} = \frac{1}{s^2} \left[ A_{11}(t) s^{2\alpha_1(t)} + A_{12}(t) s^{\alpha_1(t) + \alpha_2(t)} + A_{22}(t) s^{2\alpha_2(t)} \right] \quad (3.32)$$

where, using e.q. (3.12)

$$A_{11}(t) = \frac{1}{4\pi} \sum_{\mu\nu\lambda\sigma} |a_{\mu\nu\lambda\sigma}(t)|^2 \quad (3.33)$$

$$A_{22}(t) = \frac{1}{4\pi} \sum_{\mu\nu\lambda\sigma} |b_{\mu\nu\lambda\sigma}(t)|^2 \quad (3.34)$$

$$\text{and } A_{12}(t) = \frac{1}{2\pi} \sum_{\mu\nu\lambda\sigma} \text{Re} [a_{\mu\nu\lambda\sigma}(t) b_{\mu\nu\lambda\sigma}^*(t)] \quad (3.35)$$

If  $\alpha_1(t)$  is the leading trajectory, at high enough energies the third term in e.q. (3.32) will become negligible, so that only a two-term fit to the differential cross section will be appropriate.

Accordingly we tried various two and three term fits, and found in all cases that the leading trajectory  $\alpha_1(t)$  was well fitted by a straight line of intercept 1.0 and slope 0.15, and we maintained this form in subsequent fits.

Using the information gained from the total cross section, we were led to try a fit with e.q. (3.32), where as mentioned above

$$\alpha_1(t) = 1.0 + 0.15t \quad (3.36)$$

and we used the usual meson trajectory

$$\alpha_2(t) = 0.5 + 0.9t \quad (3.37)$$

The first term of e.q. (3.32) then corresponds to the (pomeron)<sup>2</sup> term, the second to pomeron x meson interference, and the third to the (meson)<sup>2</sup> term. If the  $j = 0$  singularity discovered in the total cross section is also included, then its interference with the pomeron will contribute to the third term, and it will also generate a term like

$s^{-1.5}$  by interference with the mesons, and a term like  $s^{-2}$  by itself, both of which should be negligible.

The resulting best fit had a mean  $\chi^2$  of 1.5 per point, and is compared to the data in fig. (3.3). The parameters are plotted as functions of  $t$  in fig. (3.4). The fit is quite satisfactory, but as we shall show, there are certain constraints which the parameters ought to obey, but which are violated for some values of  $t$ .

The first two constraints which may be obtained from e.qs. (3.32 - 3.35) are trivial

$$A_{11}(t) \geq 0 \quad (3.38)$$

$$A_{22}(t) \geq 0 \quad (3.39)$$

and it may be seen from fig.(3.4a) that they are easily satisfied.

It is possible, however, to deduce a third, less trivial constraint as follows.

We write for brevity

$$H \equiv (\mu, \nu, \lambda, \sigma) \quad (3.40)$$

and we define the phases of the functions  $a_{\mu\nu\lambda\sigma}$ ,  $b_{\mu\nu\lambda\sigma}$  in e.qs.(3.33, 3.34) by

$$a_H(t) \equiv |a_H(t)| e^{i\theta_H(t)} \quad (3.41)$$

$$b_H(t) \equiv |b_H(t)| e^{i\phi_H(t)} \quad (3.42)$$

With these definitions we obtain

$$A_{12}(t) = \frac{1}{2\pi} \sum_H |a_H| |b_H| \cos(\theta_H - \phi_H) \quad (3.43)$$

from which we may deduce that

$$A_{12}^2 - 4 A_{11} A_{22} = \frac{1}{4R^2} \sum_{H, H'} \left[ |a_H| |b_H| |a_{H'}| |b_{H'}| \cos(\theta_H - \beta_H) \cos(\theta_{H'} - \beta_{H'}) - |a_H|^2 |b_{H'}|^2 \right] \quad (3.44)$$

hence, using trigonometry

$$A_{12}^2 - 4A_{11}A_{22} \leq \frac{1}{4R^2} \sum_{H, H'} \left[ |a_H| |b_H| |a_{H'}| |b_{H'}| - |a_H|^2 |b_{H'}|^2 \right] \quad (3.45)$$

since the right hand side of e.q. (3.45) is symmetric in H and H' we can interchange them without altering the result, i.e.

$$A_{12}^2 - 4A_{11}A_{22} \leq \frac{1}{4R^2} \sum_{H, H'} \left[ |a_{H'}| |b_{H'}| |a_H| |b_H| - |a_{H'}|^2 |b_H|^2 \right] \quad (3.46)$$

Averaging e.qs. (3.45) and (3.46) then gives

$$A_{12}^2 - 4A_{11}A_{22} \leq - \frac{1}{8R^2} \sum_{H, H} \left( |a_H| |b_{H'}| - |a_{H'}| |b_H| \right)^2 \leq 0 \quad (3.47)$$

$$\Rightarrow A_{12}^2 \leq 4 A_{11} A_{22} \quad (3.48)$$

which is the required constraint.

The equality in e.q. (3.48) holds only under the following unlikely conditions

(i)  $\theta_H = \beta_H$  for all H. This is in direct conflict with Regge Theory, and the interpretation of the terms as a pomeron and a meson

(ii)  $\left| \frac{a_H}{a_{H'}} \right| = \left| \frac{b_H}{b_{H'}} \right|$  for all H, H'

The  $j = 0$  singularity contributes to the total cross section with the same sign as the pomeron, so that its imaginary part is positive. Since the pomeron contribution ought to be nearly purely imaginary, the  $j = 0$  singularity should have a positive interference with the pomeron, reinforcing the inequality in e.q. (3.48).

In fig. (3.5) we have plotted the ratio  $A_{12} / 2(A_{11}A_{22})^{\frac{1}{2}}$ , which should be less than unity by e.q. (3.48). It may be seen that the constraint is violated at  $t = -0.2 \text{ GeV}^2$ , and only just satisfied for  $-0.15 \geq t \geq -0.3 \text{ GeV}^2$ .

To investigate the significance of this result we tried to fit the data with the constraint (3.48) satisfied. There were several ways we might have attempted this, but since the tendency to break it seemed to come from the dip in  $A_{22}(t)$  near  $t = -0.2 \text{ GeV}^2$  (see fig. 3.4a) we fitted the data with  $A_{22}(t)$  fixed as the best linear fit to  $\log A_{22}$  through the first two and last two points, shown as the solid line in fig. (3.4a). The equation of this line is

$$A_{22}(t) = 729 \exp(3.9 t) \quad (3.49)$$

We found that  $A_{12}(t)$  was now much smaller, and it is shown as black dots in fig. (3.5). The fit, however, was considerably worse, especially for the data at lower energies. The two fits are compared at  $t = -0.2 \text{ GeV}^2$  in fig. (3.6), and it may be seen that improved data in the low energy region, or any data at all in the Serpukov region, would distinguish between them.

This discussion illustrates the importance of accurate data at lower energies in making full use of the new very high-energy data. It is an unfortunate reflection of the present system of priorities that the most useful experiments at energies below Serpukov were performed in 1963 and 1965<sup>(41)</sup>.

(ii) Continuum Models

We performed a fit with the form of e.q. (3.8) using

$$\alpha_{\max} = 1, \text{ i.e.}$$

$$\frac{d\sigma}{dt} = \int_{-\infty}^1 dj \gamma(j, t) s^{2j-2} \quad (3.50)$$

In the same way as for the total cross section, we parametrised  $\gamma(j, t)$  as a polynomial in  $(j - 1)$ :

$$\gamma(j, t) = \sum_{k=0}^n c_k(t) (j - 1)^k \quad (3.51)$$

which gave in an analogous way to e.q. (3.24)

$$\frac{d\sigma}{dt} = \sum_{k=0}^n \frac{(-)^k k!}{2^{k+1}} c_k(t) \left[ \frac{1}{\log s} \right]^{k+1} \quad (3.52)$$

and we fitted this form to the data as before. Taking a cubic ( $n = 3$ ) form for  $\gamma$  we obtained a fit whose mean  $\chi^2$  was 1.1 per point. The best fit  $\gamma(j, t)$  is shown in fig. (3.7) at  $t = -0.1$  and  $t = -0.25 \text{ GeV}^2$ . It may be seen that there is a distinct tendency to peak at  $j = 1$  and  $j \approx 0.5$ , in agreement with the pole models previously discussed.

We also tried a fit with a quartic form for  $\gamma$ . Although, as one might expect with five parameters at each value of  $t$ , the parameters were somewhat poorly determined, the peak at  $j = 1$  did show a distinct tendency to move out with  $t$ , and in fact the position of the peak closely obeyed the relation

$$j_{\text{PEAK}}(t) = 1 + 0.2 t \quad (3.53)$$

Of course, the cubic  $\gamma$  could not exhibit this behaviour, because a cubic is only allowed two peaks if one of them is at the extreme end of the integration region.

We were again faced with the question of whether the width of the peaks in  $\delta(j, t)$  was a consequence of the data or of the parametrisation. We therefore tried a fit with a sum of terms of the gaussian form

$$\delta_i(j, t) = \frac{c_i(t)}{\Delta_i \sqrt{\pi}} e^{-((j - j_i(t))/\Delta_i)^2} \quad (3.54)$$

where

$$\delta(j, t) = \sum_{i=1}^m \delta_i(j, t) \quad (3.55)$$

This form has the property that

$$\delta_i(j, t) \xrightarrow{\Delta_i \rightarrow 0} c_i(t) \delta(j - j_i(t)). \quad (3.56)$$

With this form, the expression for the differential cross section is somewhat more complicated

$$\frac{d\sigma}{dt} = \frac{1}{2} \sum_{i=1}^m c_i(t) e^{(\Delta_i \log s)^2 + 2(j_i(t) - 1) \log s} \text{Erfc} \left( \Delta_i \log s + \frac{j_i(t) - 1}{\Delta_i} \right) \quad (3.57)$$

This has more (3) parameters per term than the previous models used, so we tried a two-term fit with  $\Delta_1$  fixed equal to zero for all  $t$ . This gave 5 parameters:  $c_1, j_1, c_2, j_2, \Delta_2$  at each value of  $t$ , and in each case we found  $\Delta_2 = 0$  and the same solution as for previous two-pole fits.

### 3.4 Conclusions

(i) The curvature of the pp total cross section is better fitted by a pole at  $j = 0$  than at  $j = \frac{1}{2}$ . A broader peak in the region  $-1 \leq j \leq 0$  also provides a good fit. This indicates that exchange degeneracy may not be broken in pp scattering in the forward direction, but lower-lying singularities may be important.

(ii) Simple Regge poles cannot explain the differential cross section data at the larger values of  $t$ . Inclusion of the lower-lying singularities discussed above only make matters worse.

(iii) We found no evidence that the differential cross section data require a continuous  $j$  - plane structure, i.e. the singularities look more like poles than cuts.

(iv) Improved accuracy of data at presently-accessible energies would make much more conclusive statements possible.

In the next chapter we consider the  $j$  - plane structure to be expected in pp scattering, and compare it with the results of this analysis.

Figures for Chapter 3

- 3.1 The pp total cross section. Curve I is the three-parameter fit of e.q. (3.18), curve II is the fit of Barger et al and curve III is the continuum fit of e.qs. (3.22, 3.23).
- 3.2 The function  $\beta(j)$  for the total cross section fit of e.qs. (3.22, 3.23).
- 3.3 The three-term fit of e.q. (3.32) to the pp differential cross section.
- 3.4 The parameters of the three-term fit to the differential cross section.
  - (a) The parameters  $A_{11}(t)$  and  $A_{22}(t)$ .
  - (b) The parameter  $A_{12}(t)$ .
- 3.5 The ratio  $A_{12} / 2 (A_{11} A_{22})^{\frac{1}{2}}$  for the three-term fit of e.q. (3.32) and for the similar fit when  $A_{22}$  is constrained as described in the text.
- 3.6 A comparison of the unconstrained and constrained fit to the differential cross section at  $t = -0.2 \text{ GeV}^2$ .
- 3.7 The form of  $\mathcal{G}(j, t)$  for the differential cross section fit of e.qs. (3.50, 3.51) at  $t = -0.1 \text{ GeV}^2$  and  $t = -0.25 \text{ GeV}^2$ .
- 3.8 The pp and  $\bar{p}p$  total cross sections at Serpukov energies and above.
- 3.9 The data on the pp slope parameter b. Figure from ref. (44).

fig. (3.1)

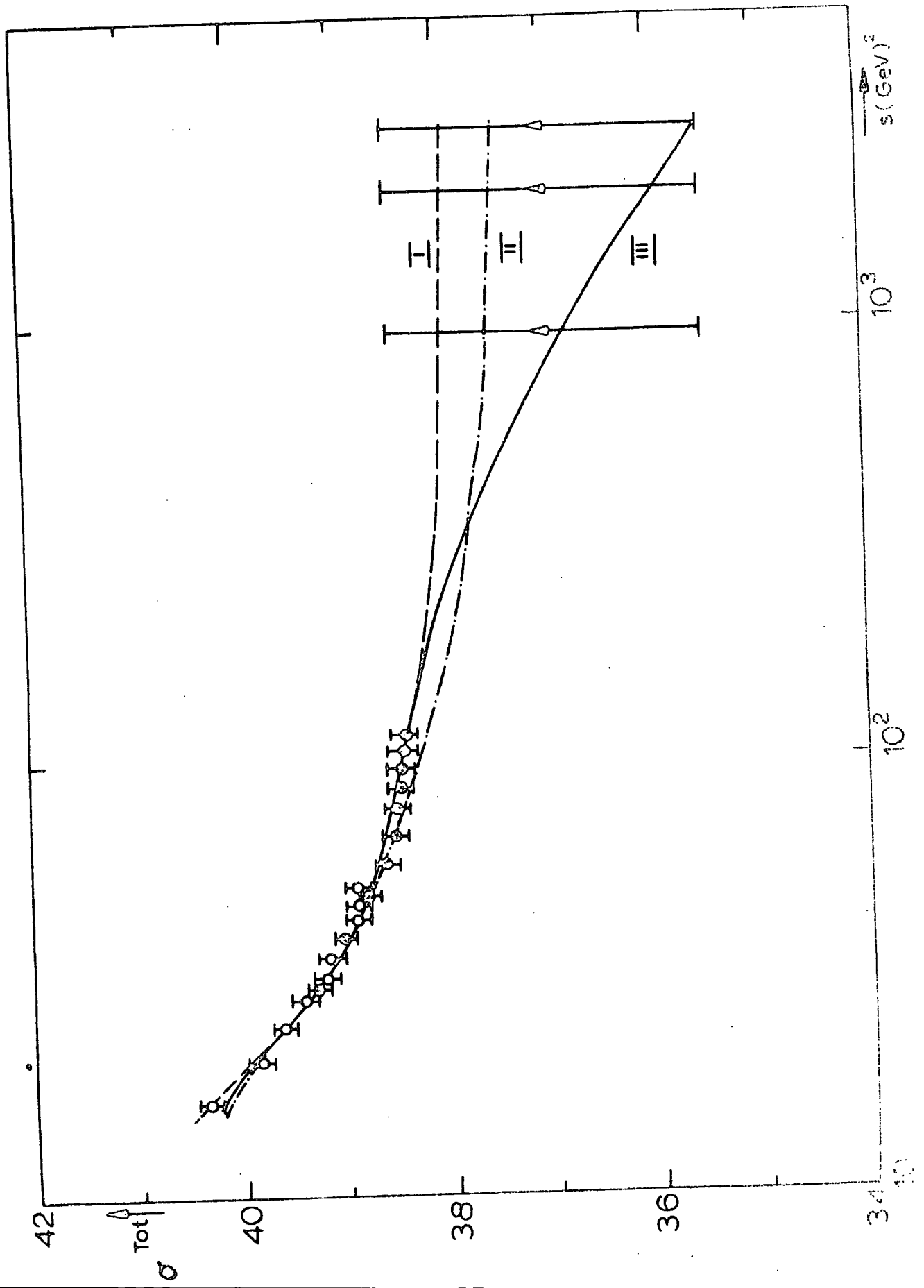


fig. (3.2)

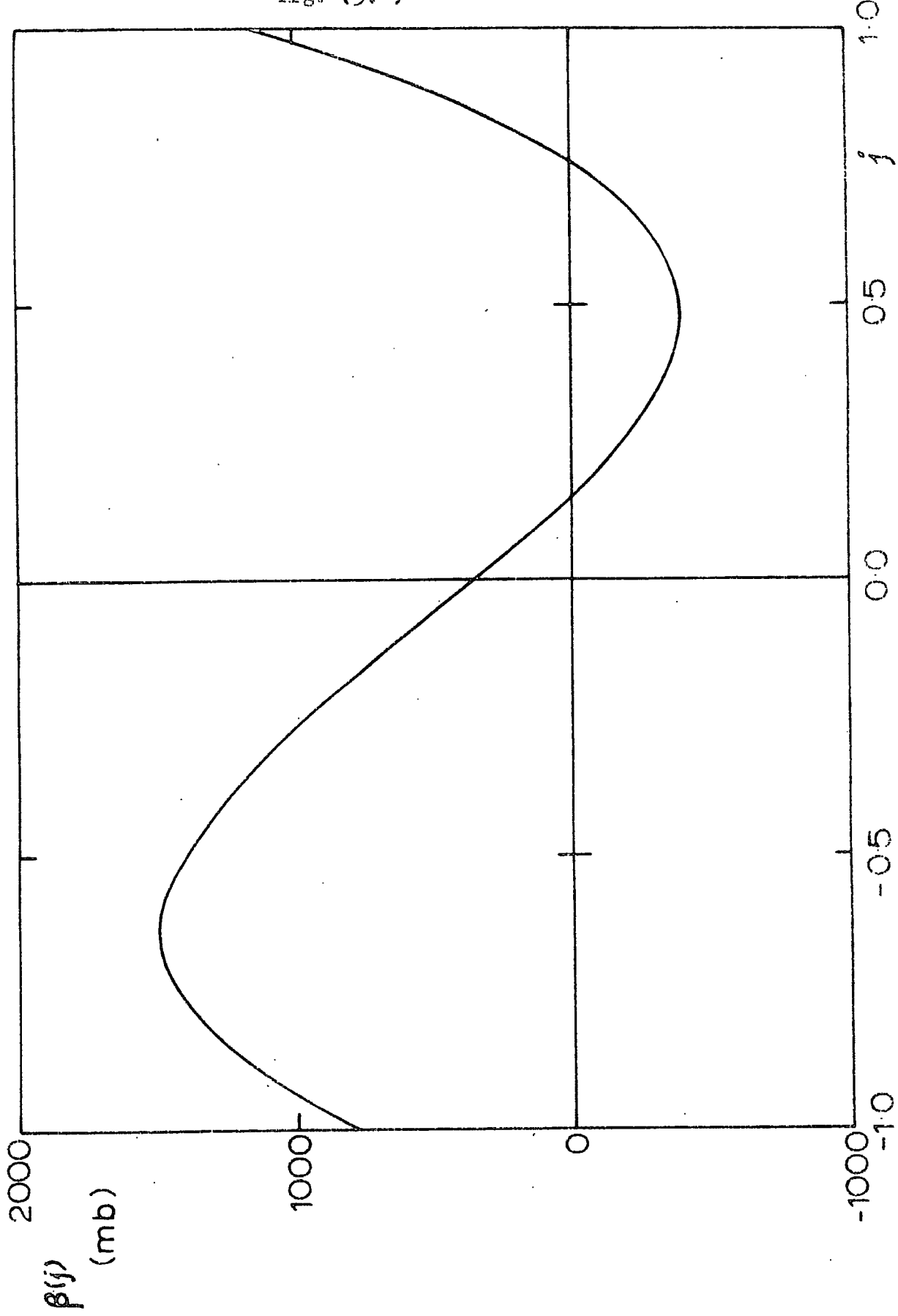


fig. (3.3)

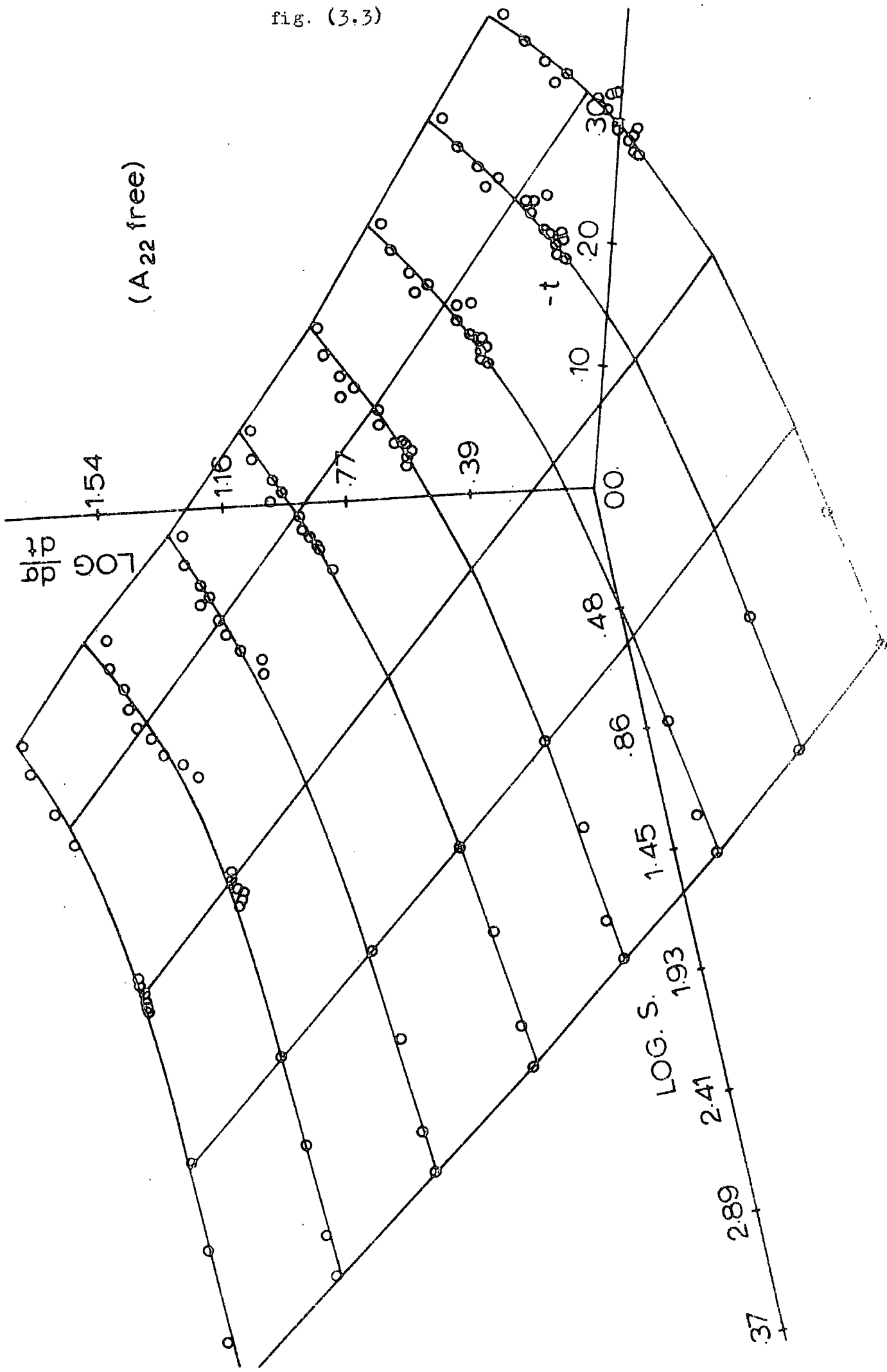


fig. (3.4a)

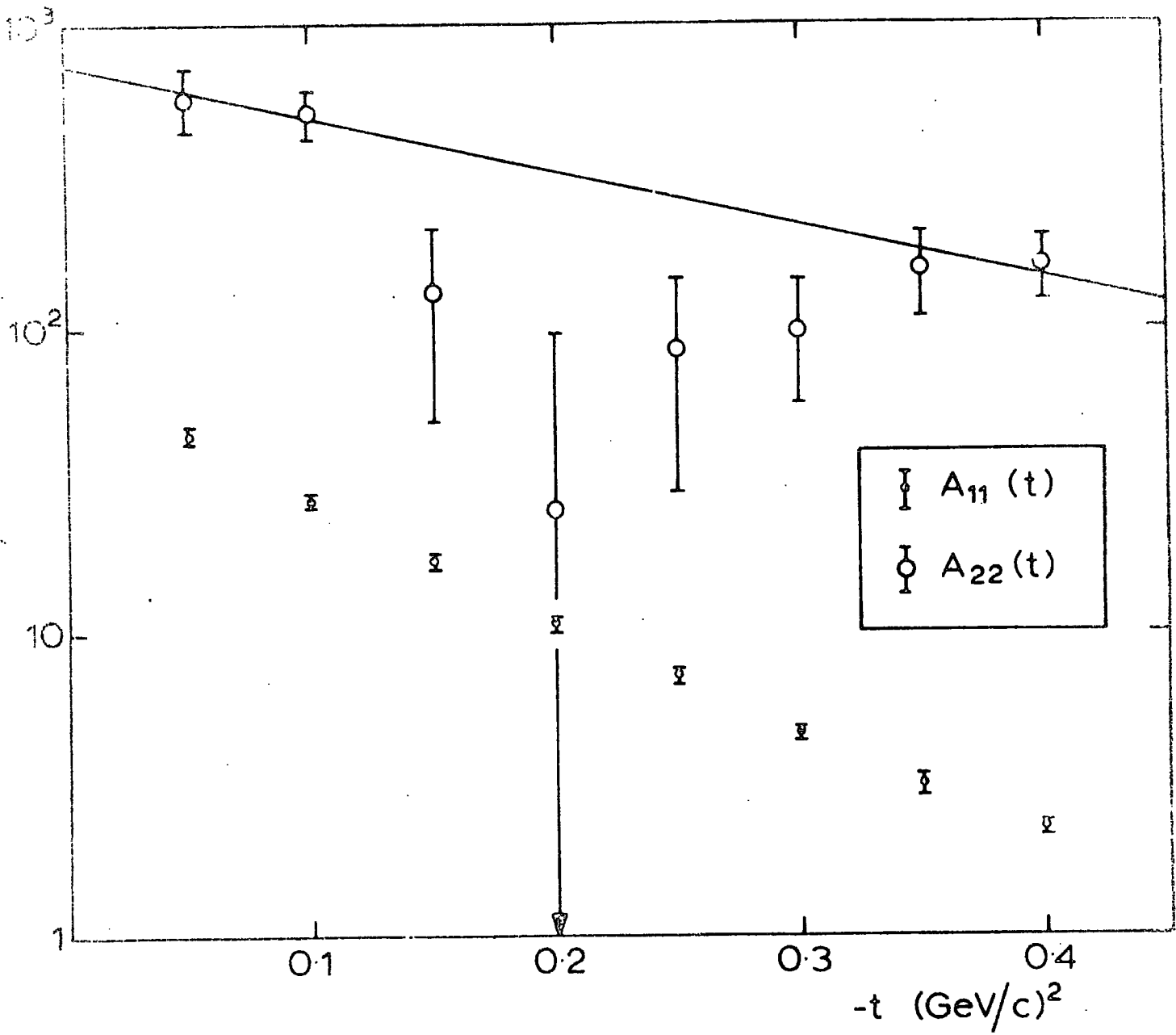


fig. (3.4b)

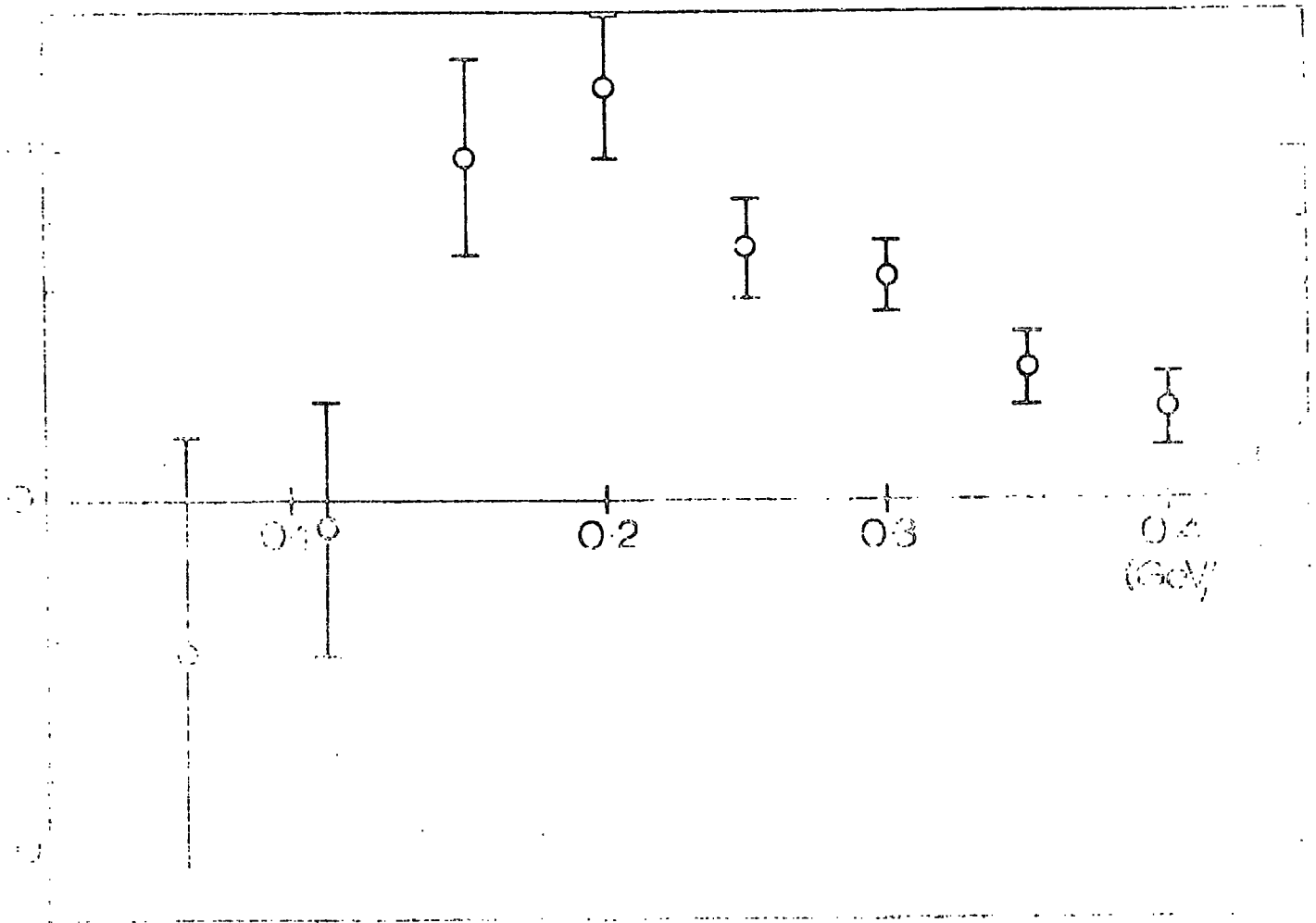


fig. (3.5)

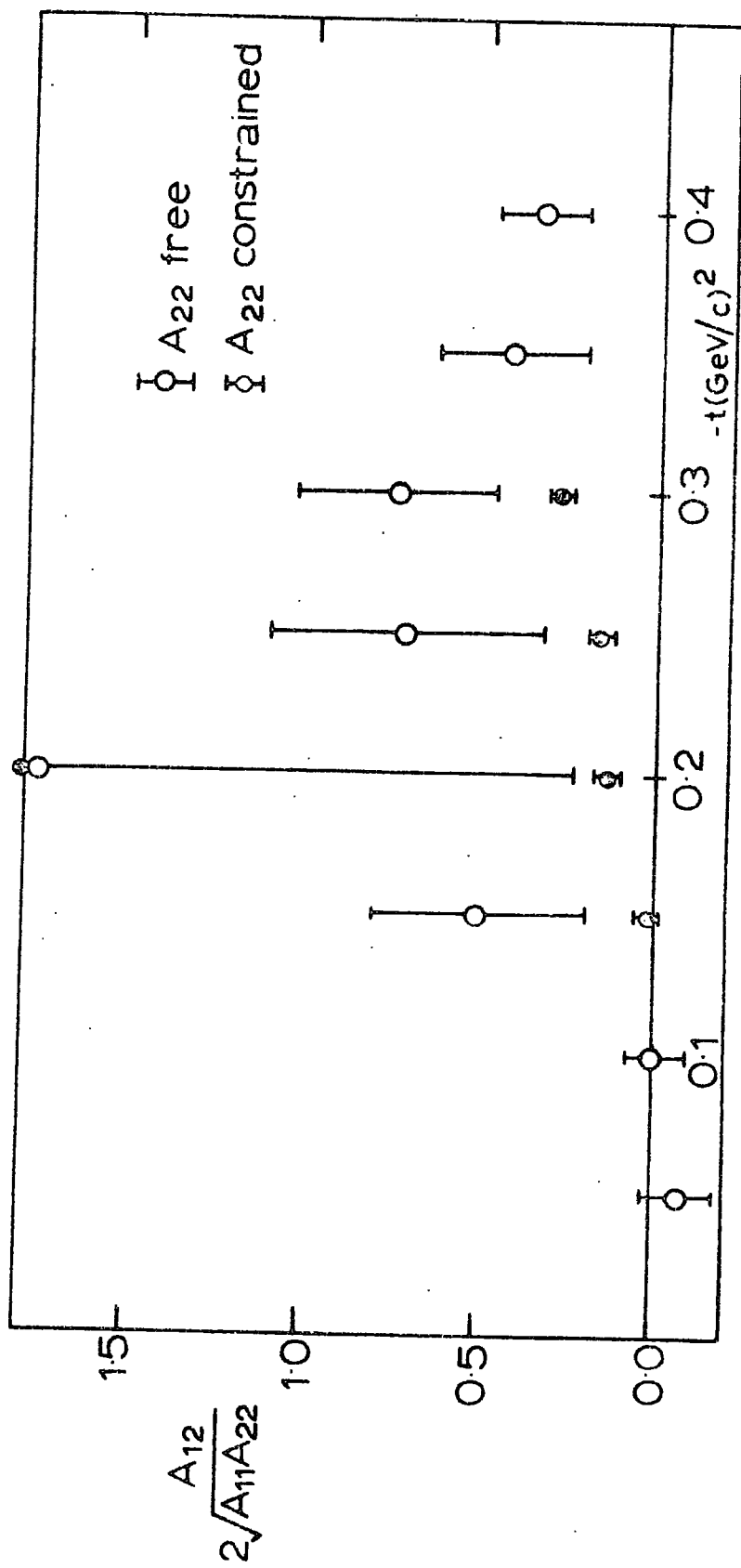


fig. (3.6)

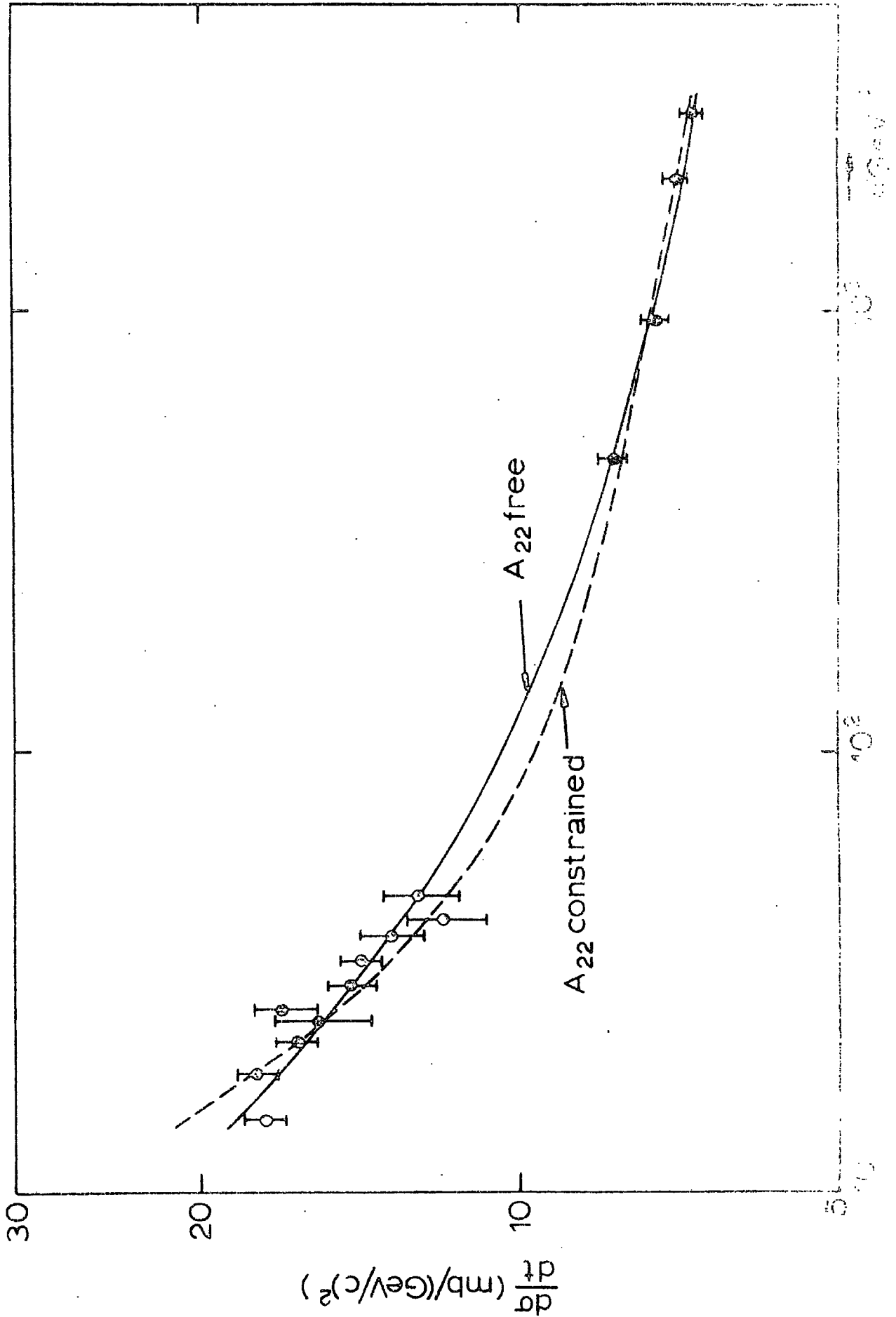


fig. (3.7)

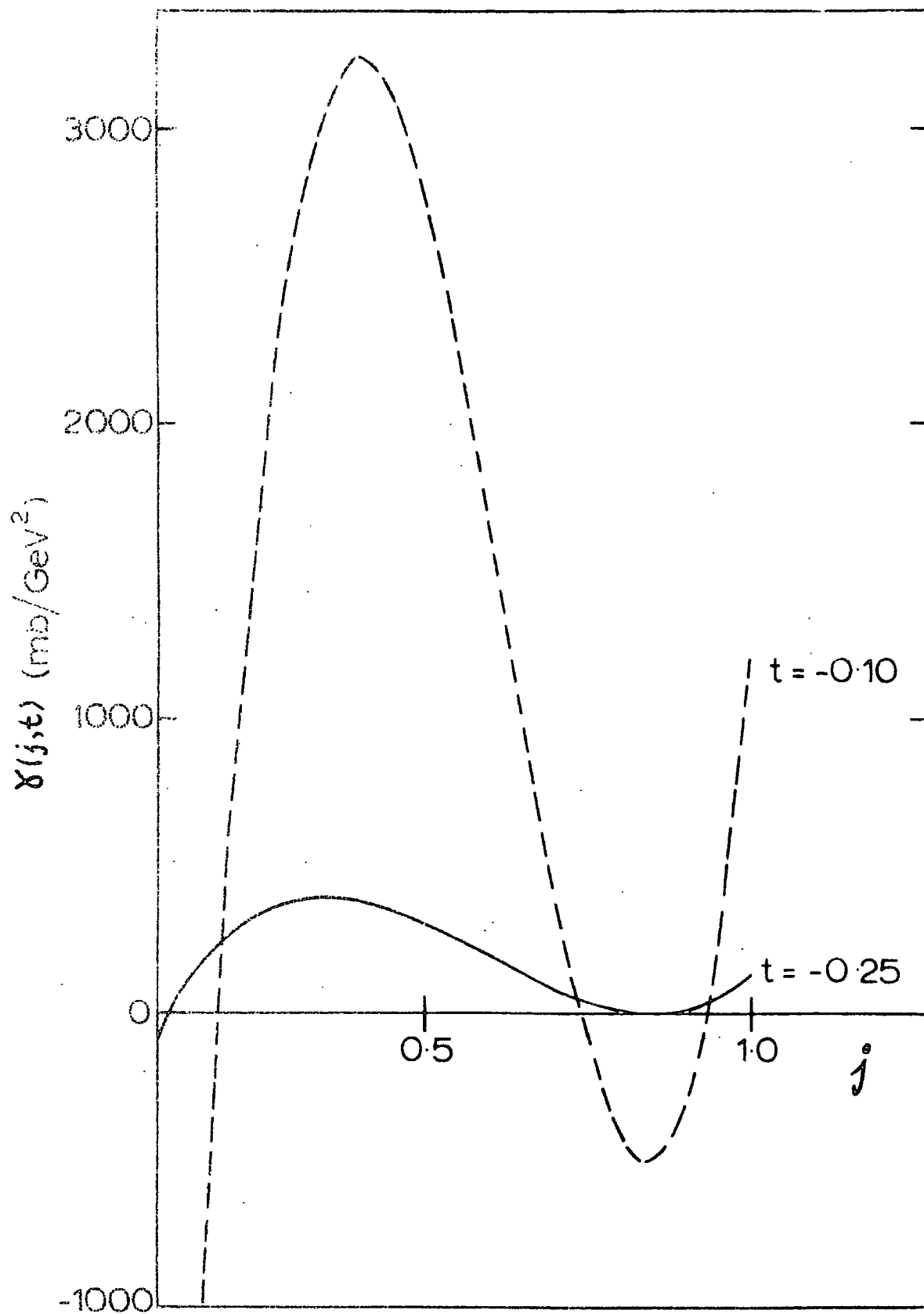


fig. (3.8)

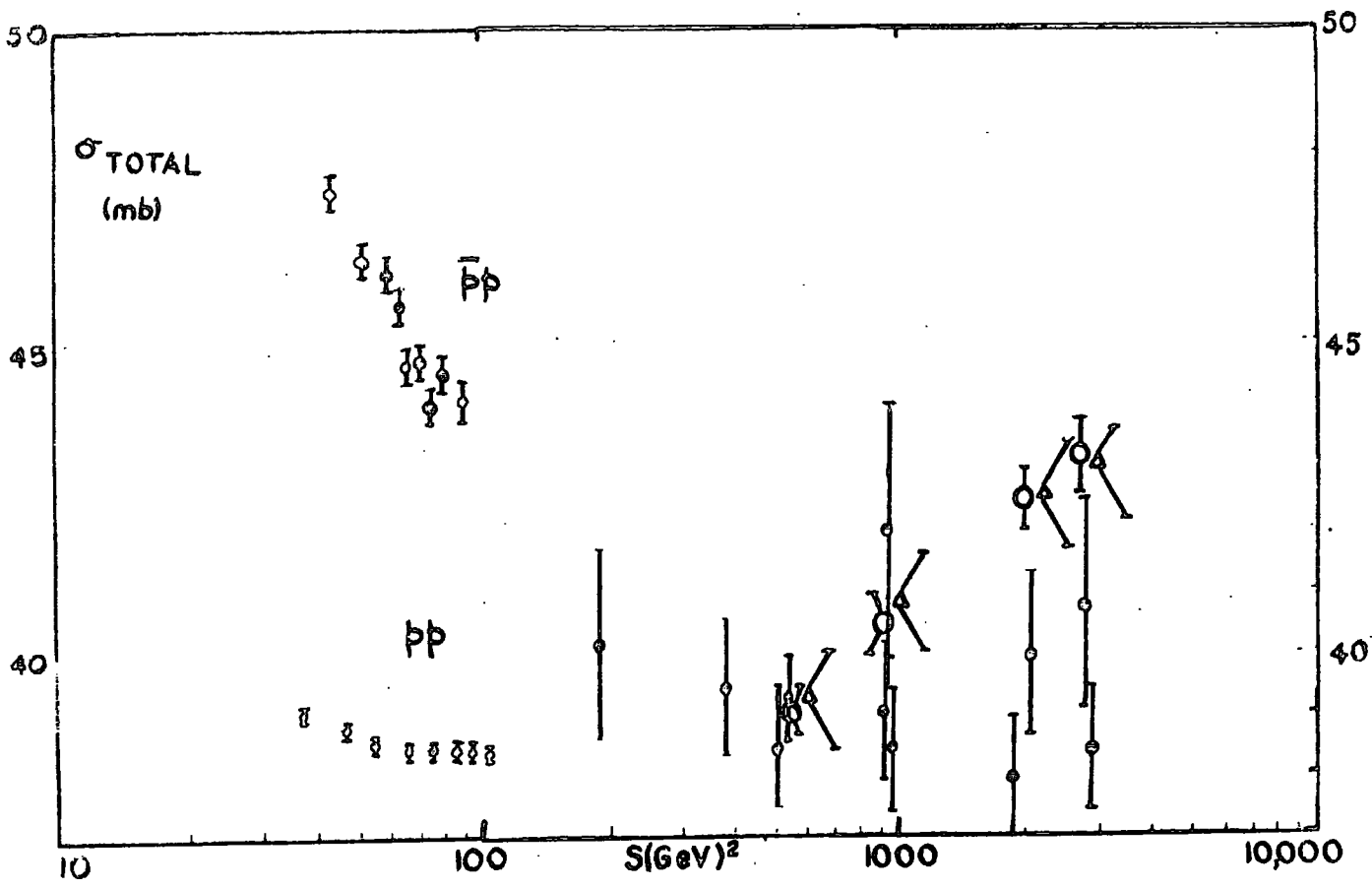
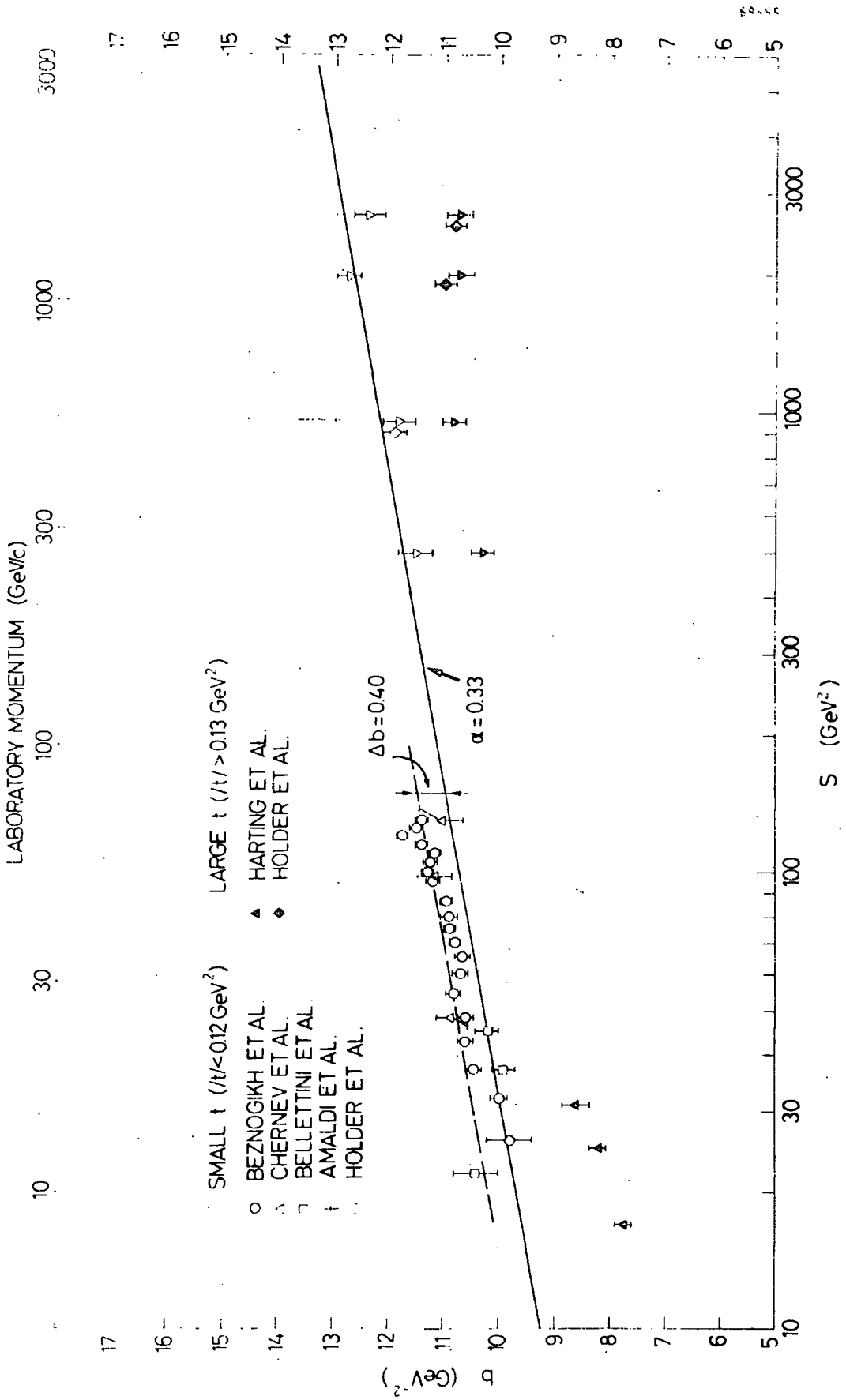


fig. (3.9)



CHAPTER 4. THE J-PLANE STRUCTURE OF PP ELASTIC SCATTERING IN THE  
ABSORPTION MODEL

INTRODUCTION

In the previous chapter we obtained information from the data about the  $j$ -plane singularities which are important in  $pp$  elastic scattering. In particular we found that the data were not consistent with simple poles corresponding to the exchange of the known mesons and the pomeron. The discontinuities found, however, were strongly peaked and looked more like poles than cuts.

Despite its drawbacks, (see section 1.2)), we expect that the absorption model, derived in section (1.6), will supply some information about the  $j$ -plane structure of Regge Cuts. Of course, because the absorption model does not provide detailed fits to the data unless multiplied by arbitrary factors, we know that it cannot be the whole answer, but we hope that it will at least provide some clues.

That the absorption model should not be interpreted as anything other than a very crude first approximation is illustrated by Bronzan and Jones condition<sup>(69)</sup>, obtained from unitarity, that the two-reggeon cut discontinuity must vanish and be singular at the branch point. In the absorption model, as we shall show, the discontinuity is both finite and non-singular. White<sup>(70)</sup> has shown that unitarity is recovered when one considers the two-reggeon cut in the two particle - two reggeon amplitude and in the four reggeon amplitude, as well as in the four particle amplitude. This means, for example, that the cut must contribute to the Gribov Vertex in e.g. (1.56).

In this chapter we investigate the  $j$ -plane structure of  $pp$  elastic scattering generated by the pomeron and meson poles and the corresponding cuts. We expect that the absorption model will throw some light on the form of the cut discontinuities, without making detailed numerical calculations.

In section (4.1) we define the quantities and introduce the formalism with which we are going to work. In section (4.2) we propose a simple model and use it to calculate cut discontinuities. We compare the results from this model with our previous deductions about the j-plane structure in section (4.3), and in section (4.4) we discuss the results and draw some conclusions.

#### 4.1 Formalism and Definitions

From e.q. (1.1) we write the contribution of a Regge Pole  $\alpha_k$  to an elastic pp non-flip amplitude as

$$A_k(s, t) = \int_{\alpha_k} \gamma_{\alpha_k}^{pp} s^{k(t)} \quad (4.1)$$

(The reason we only consider non-flip amplitudes will become apparent in the next section).

In the absorption model, the contribution of the cut generated by the trajectories  $\alpha_1$  and  $\alpha_2$  to the same amplitude is, from e.qs.

(1.55, 1.59)

$$A_{12}^C(s, t) = \frac{1}{16\pi^2} \int_{-\infty}^0 dt_1 dt_2 \frac{\Theta(\lambda)}{\sqrt{\lambda}} \delta_{\alpha_1}(t_1) \delta_{\alpha_2}(t_2) \gamma_{\alpha_1}^{pp}(t_1) \gamma_{\alpha_2}^{pp}(t_2) s^{\alpha_1(t_1) + \alpha_2(t_2) - 1} \quad (4.2)$$

where  $\lambda(t, t_1, t_2)$  is defined in e.q. (1.51).

The position of the branch point is

$$\alpha_{CUR}(t) = \max(\alpha_1(t_1) + \alpha_2(t_2) - 1) \quad (4.3)$$

under the condition

$$\lambda(t, t_1, t_2) = 0 \quad (4.4)$$

To obtain the discontinuity form of e.q. (3.4) it is necessary to change variables from  $t_1, t_2$  in e.q. (4.2) to

$$j = \alpha_1(t_1) + \alpha_2(t_2) - 1 \quad (4.5)$$

$$k = \alpha_1(t_1) - \alpha_2(t_2) \quad (4.6)$$

We know that we can do this because the trajectories are Herlotz functions of  $t$ , as we discussed in section (1.1 (vi)).

The Jacobian for the transformation is

$$\left| \frac{\partial (l, k)}{\partial (t_1, t_2)} \right| = 2\alpha'_1 \alpha'_2 \quad (4.7)$$

and, if we define for convenience

$$g_k(\alpha_k) = \oint_{\alpha_k} (t_k) \gamma_{\alpha_k}^{pp}(t_k) \quad (4.8)$$

we can write that

$$A_{12}^C(s, t) = \int_{-\infty}^{\alpha_{CUT}(t)} dj s^j \bar{c}_{12}(j, t) \quad (4.9)$$

with

$$\bar{c}_{12}(j, t) = \frac{1}{32\pi^2} \int_{j-1}^{1-j} dk \frac{g_1(\frac{1}{2}(j+k+1)) g_2(\frac{1}{2}(j-k+1))}{\alpha'_1 \alpha'_2 \sqrt{\lambda}} \quad (4.10)$$

If the trajectories are linear

$$\alpha_k(t) = \alpha_{k0} + \alpha'_k t \quad (4.11)$$

we find from e.g.s. (4.3, 4.4) that the branch point for the (1,2) cut is

$$\alpha_{12}(t) = \alpha_{10} + \alpha_{20} - 1 + \frac{\alpha'_1 \alpha'_2}{\alpha'_1 + \alpha'_2} t \quad (4.12)$$

which reduces in the special case of identical trajectories to

$$\alpha_{11}(t) = 2\alpha_{10} - 1 + \frac{1}{2} \alpha'_1 t \quad (4.13)$$

## 4.2 The Model

Since we are not interested in elaborate quantitative fits to the data it is sensible to choose the model to be the simplest possible. We did this as follows:

(i) In the previous chapter we found evidence that the pomeron slope is rather small, so that the pomeron ought to be purely imaginary, at least near the forward direction. Consequently we parametrised the pomeron contribution to an s channel non-flip amplitude as

$$g_p(\alpha_p) = i \bar{\gamma}_p e^{b_p(\alpha_p - 1)} \quad (4.14)$$

(with  $\bar{\gamma}_p, b_p$  real constants)

(ii) We assumed that the pomeron conserves s channel helicity, this ought to be fairly reasonable near the forward direction.

(iii) We chose the pomeron trajectory to have the linear form

$$\alpha_p(t) = 1 + 0.15 t \quad (4.15)$$

(iv) We assumed exchange degeneracy for the mesons, with a linear trajectory, which we took as

$$\alpha_M(t) = 0.5 + 0.9 t \quad (4.16)$$

In Chapter 3 we saw that the data show no evidence of exchange degeneracy breaking in the forward direction, so we chose the meson contribution to the non-flip amplitude to be

$$g_M(\alpha_M) = -\bar{\gamma}_M e^{b_M(\alpha_M - \frac{1}{2})} \quad (4.17)$$

(with  $\bar{\gamma}_M, b_M$  real constants)

(v) we considered only the non-flip meson contributions. This should not affect the total cross section, but it means that, in the differential cross section, we have neglected (meson)<sup>2</sup> terms, so that our model cannot be reliable at low energies.

We can immediately calculate the positions of the branch points from e.qs. (4.15, 4.16, 4.12, 4.13). They are

$$\alpha_{pp}(t) = 1 + 0.07 t \quad (4.18)$$

$$\alpha_{pM}(t) = 0.5 + 0.13 t \quad (4.19)$$

$$\alpha_{MM}(t) = 0.45 t \quad (4.20)$$

We did not calculate the effects of cuts generated by three or more trajectories. The cut generated by  $n$  identical reggeons with trajectory  $\alpha$  has branch point <sup>(11)</sup>

$$\alpha_n(t) = n\alpha(t/n^2) - n + 1 \quad (4.21)$$

which, for linear trajectories, reduces to

$$\alpha_n(t) = n(\alpha_0 - 1) + 1 + \frac{\alpha'}{n} t \quad (4.22)$$

We see that for multi-pomeron cuts

$$\alpha_{nP}(t) = 1 + \frac{\alpha'_P}{n} t \quad (4.23)$$

whereas for multi-meson cuts

$$\alpha_{nM}(t) = 1 - \frac{n}{2} + \frac{\alpha'_M}{n} t \quad (4.24)$$

so that multi-pomeron cuts condense on  $j = 1$  and may well be important, whereas multi-meson cuts are low-lying and should be insignificant. Multi-reggeon cuts can be calculated in the eikonal model, where it can be shown <sup>(12)</sup> that the contribution of the  $n$ -pomeron cut decreases rapidly with  $n$ . It seems fairly reasonable, therefore, to assume that the major contribution to the discontinuity structure comes from two-reggeon cuts.

In this model the discontinuities can be calculated analytically. In practice, e.g. (4.10) is not the easiest way to proceed, but it is more straightforward to use the representation

$$\frac{\Theta(\lambda)}{\sqrt{\lambda}} = \frac{\pi}{2} \int_0^{\infty} b db J_0(b\sqrt{-t}) J_0(b\sqrt{-t_1}) J_0(b\sqrt{-t_2}) \quad (4.25)$$

in e.g. (4.2), then perform the  $t_1$  and  $t_2$  integrations explicitly.

The results are as follows:

For the two-pomeron cut

$$\tau_{pp}(j, t) = -i \frac{\bar{\gamma}_p^2}{32\pi \alpha'_p} e^{b_p(j-1)} \quad (4.26)$$

For the pomeron-meson cut

$$\tau_{pM}(j, t) = \frac{\bar{\gamma}_p \bar{\gamma}_M}{16\pi (\alpha'_p + \alpha'_M)} e^{-c \frac{\alpha'_p - \alpha'_M}{\alpha'_p + \alpha'_M} t} \exp \left[ \frac{b_p \alpha'_M + b_M \alpha'_p}{\alpha'_p + \alpha'_M} (j - \frac{1}{2}) \right] \times$$

$$\times J_0 \left( 2 |c| \sqrt{\frac{t}{\alpha'_p + \alpha'_M}} (j - \alpha_{pp}(t)) \right) \quad (4.27)$$

$$\text{with } c = (b_p - b_M) \frac{\alpha'_p \alpha'_M}{\alpha'_p + \alpha'_M}$$

And for the two-meson cut

$$\tau_{MM}(j, t) = i \frac{\bar{\gamma}_M^2}{32\pi \alpha'_M} e^{b_M j} \quad (4.28)$$

We note that although the discontinuities of the identical-particle cuts are independent of  $t$ , their contributions to the amplitude will depend on  $t$ , since the integrations in e.g. (4.9) run up to  $\alpha_{\text{CUT}}(t)$ . We see also that the Bronzan and Jones condition is indeed violated, as mentioned in the introduction to this chapter.

### 4.3 Comparison with the Data Analysis of Chapter 3

#### (1) The Total Cross Section

If we write the total cross section in the form of e.q. (3.9), we obtain from e.qs. (4.26 - 4.29) the following prediction for  $\beta(j)$ :

$$\beta(j) = \bar{\sigma}_p \mathcal{S}(j-1) = \frac{\bar{\sigma}_p^2}{32\pi\alpha'_p} e^{b_p(j-1)} \Theta(1-j) + \frac{\bar{\sigma}_m^2}{32\pi\alpha'_m} e^{b_m j} \Theta(-j) \quad (4.30)$$

We see that the cut contributions are peaks of width

$$\Delta_i = 1/b_i \quad (i = p, m) \quad (4.31)$$

at  $j = 1$  and  $j = 0$ . There is no meson contribution because of exchange degeneracy, and the pomeron-meson cut is absent for the same reason. We see that the singularities are in just the right places to explain the structure found in section (3.2).

To investigate the widths of the peaks, we adopted the parameter values found in section (3.3). We used exponential fits to the parameters  $A_{11}(t)$ ,  $A_{22}(t)$  (defined in e.q. (3.32)), and obtained

$$A_{11}(t) = 68 \exp(8.9 t) \quad (4.32)$$

$$A_{22}(t) = 730 \exp(3.9 t) \quad (4.33)$$

This gave in e.qs. (4.14, 4.17)

$$b_p \approx 30 \quad (4.34)$$

$$b_m \approx 2 \quad (4.35)$$

or, for the widths of the peaks in  $\beta(j)$

$$\Delta_p \approx 0.03 \quad (4.36)$$

$$\Delta_m \approx 0.5 \quad (4.37)$$

The narrowness of the peak at  $j = 1$  implies that, in a fit of the form of, for example e.q. (3.23), the cut term would be impossible to distinguish from the pole, and we would just see a peak of reduced height.

Our model therefore predicts precisely the  $j$ -plane structure found for the total cross section in chapter 3, in particular a very narrow peak at  $j = 1$  and a broader structure for  $j \leq 0$ , with nothing in between.

The model has a further feature, however, which is that the negative sign of the second term in e.q. (4.30) provides a natural mechanism for the recently-measured rising total cross section. Indeed, if  $b_p$  and  $b_M$  are fixed at the values in e.qs. (4.34, 4.35), there are only two parameters in e.q. (4.30) -  $\bar{\gamma}_p$  and  $\bar{\gamma}_M$  - which may be determined from low-energy data alone.

As we have mentioned previously, this model is too crude to make detailed fits worthwhile, so we just constrained the model to fit the data at  $s = 20$  and  $s = 100 \text{ GeV}^2$ . On integration, e.q.(4.30) gives

$$\sigma_T(s) = \bar{\gamma}_p - \frac{\bar{\gamma}_p^2}{32\pi \alpha'_p} (b_p + \log s)^{-1} + \frac{\bar{\gamma}_M^2}{32\pi \alpha'_M} s^{-1} (b_M + \log s)^{-1} \quad (4.38)$$

By evaluating this equation at the two values of  $s$  we obtained

$$\bar{\gamma}_p = 131 \quad (4.39)$$

$$\bar{\gamma}_M = 218 \quad (4.40)$$

which means that

$$\sigma_T(\infty) = 51 \text{ mb.} \quad (4.41)$$

This fit is compared with the data in fig. (4.1), where we have also shown curve I from chapter 3 for comparison. We see that, by fitting the low energy data alone, our model predicts a rising total cross section at ISR energies. That it does not rise as fast as the latest data indicates the limitations of the model, although, as may be seen from the figure, the experimental situation is not yet by any means resolved. The function  $\beta(j)$  corresponding to this curve is shown in fig. (4.2). (The arrow at  $j = 1$  indicates the position of the  $\delta$ -function due to the pomeron pole).

(ii) The Differential Cross Section

As discussed in section (4.2 (v)), our model cannot be correct at low energies, because we have neglected most of the (meson)<sup>2</sup> terms. The singularities will still be in the right places, of course, but will have the wrong magnitudes. The effects of the various interference terms are somewhat complicated, but can be calculated from e.q. (3.10). Because of the strongly peaked nature of the pomeron-meson cut in e.q. (4.27), - if  $b_p = 30$  and  $b_m = 2$  then  $\tau_{pm} \sim e^{26(j-1)}$  - it is reasonable to neglect the Bessel function. This means that we can write the contributions of a pole and a general two-reggeon cut to the function  $\mathcal{U}(j, t)$  as, respectively

$$\mathcal{U}_n(j, t) = \gamma_n \delta(j - \alpha_n(t)) e^{b_n \alpha'_n t} \quad (4.42)$$

where  $n = P$  or  $M$ , and

$$\mathcal{U}_{nm}(j, t) = Q_{nm} e^{b_{nm}(j - \alpha_{nm}(0))} \Theta(\alpha_{nm}(t) - j) \quad (4.43)$$

where  $n, m = P$  or  $M$  and  $\gamma_n, Q_{nm}$  are complex constants.

Substituting these forms into e.q. (3.10) we obtain the following formulae (dropping the  $1/4\pi$  for convenience):

For the interference between the  $n$  and  $m$  poles

$$\gamma_{n \times m}(j, t) = \text{Re}(\gamma_n^* \gamma_m) e^{(b_n \alpha'_n + b_m \alpha'_m)t} \Theta(2j - \alpha_n - \alpha_m) \quad (4.44)$$

(this is of course just the ordinary 2-pole interference)

For the interference between the  $n$  pole and the  $m$ -pole cut

$$\gamma_{n \times mp}(j, t) = \text{Re}(Q_{mp}^* \gamma_n) e^{b_{mp}(2j - \alpha_n - \alpha_{mp}(0))} e^{b_n \alpha'_n t} \Theta(\alpha_n(t) + \alpha_{mp}(t) - 2j) \quad (4.45)$$

And for the interference between the  $k=n$  cut and the  $m=p$  cut

(where  $\alpha_{kn} > \alpha_{mp}$ )

$$\begin{aligned} \delta_{knxmp}(j, t) = \operatorname{Re}(Q_{kn}^* Q_{mp}) e^{(b_{kn} + b_{mp})j - (b_{kn} \alpha_{kn}(0) + b_{mp} \alpha_{mp}(0))} \\ (e^{(b_{kn} - b_{mp})(\alpha_{kn} - j)} - e^{(b_{mp} - b_{kn})(\alpha_{mp} - j)}) \Theta(\alpha_{kn} + \alpha_{mp} - 2j) \end{aligned}$$

(4.46)

These functions are again peaked, and the positions of the peaks are given by the  $\delta$  and  $\Theta$  functions. Because of exchange degeneracy and the Imaginary pomeron, we have the following expressions:

$$\delta_P = i |\delta_P|$$

$$\delta_M = -i |\delta_M|$$

$$Q_{PP} = -i |Q_{PP}|$$

$$Q_{PM} = i |Q_{PM}|$$

$$Q_{MM} = i |Q_{MM}|$$

from which we may deduce that

$$\begin{aligned} \operatorname{Re}(\delta_P^* \delta_M) &= \operatorname{Re}(\delta_P^* Q_{PM}) = \operatorname{Re}(\delta_M^* Q_{PP}) \\ &= \operatorname{Re}(\delta_M^* Q_{MM}) = \operatorname{Re}(Q_{PP}^* Q_{MM}) = \operatorname{Re}(Q_{MM}^* Q_{PM}) \\ &= 0 \end{aligned} \tag{4.47}$$

and hence that

$$\begin{aligned} \delta_{PXm}(j, t) &= \delta_{PXPM}(j, t) = \delta_{MXPM}(j, t) \\ &= \delta_{MXMM}(j, t) = \delta_{PPXPM}(j, t) = \delta_{MMXPM}(j, t) \\ &= 0 \end{aligned} \tag{4.48}$$

In table (4.1) those terms which do not vanish, with the positions and signs of their peaks, are listed.

TABLE 4.1

Non-Vanishing Terms in the PP Differential Cross Section

Term	Peak	Sign
P x P	$j = \alpha_P(t)$	+
M x M	$j = \alpha_M(t)$	+
PP x PP	$j = \alpha_{PP}(t)$	+
MM x MM	$j = \alpha_{MM}(t)$	+
PM x PM	$j = \alpha_{PM}(t)$	+
P x PP	$j = \frac{1}{2}(\alpha_P(t) + \alpha_{PP}(t))$	-
P x MM	$j = \frac{1}{2}(\alpha_P(t) + \alpha_{MM}(t))$	+
M x PM	$j = \frac{1}{2}(\alpha_M(t) + \alpha_{PM}(t))$	-
PP x MM	$j = \frac{1}{2}(\alpha_{PP}(t) + \alpha_{MM}(t))$	-

These singularities are displayed in fig. (4.3). The location of the pomeron-meson pole interference term, which vanishes in this model, is also included, as the dot-dash line.

We can now interpret the three-pole fit of e.q. (3.32) in terms of this model. The fact that  $A_{12}(t)$  is consistent with zero for small  $t$  is explained by the fact that there is no singularity near  $j = 0.75$  in fig. (4.3). At larger  $t$ ,  $A_{12}(t)$  is built up from the effects of several terms close together. Similarly  $A_{11}(t)$  has three contributory terms. In this model, of course, there is no reason for e.q. (3.48) to apply.

#### 4.4 Conclusions and Discussion

We have formulated a very simple model, which satisfactorily explains the  $j$ -plane structure found in chapter 3, both for the total and differential cross sections.

- (i) For the total cross section, the  $j \approx 0$  singularity discovered in chapter 3 is identified with a meson-meson cut.
- (ii) When constrained to fit data at energies at and below Serpukov, the model predicts that the total cross section should rise at ISR energies, as has been recently observed.
- (iii) The constraint of e.q. (3.48), which caused trouble for a simple pole interpretation of the fit of e.q. (3.32), does not apply to this model. Both  $A_{11}(t)$  and  $A_{12}(t)$  are built from a number of closely-situated terms.
- (iv) The small value of  $A_{12}(t)$  near  $t = 0$  is explained because the model has no singularity near  $j = 0.75$ .
- (v) All cut discontinuities except the meson-meson cut, are strongly peaked at their branch points, thus explaining the pole-like structure found in chapter 3. This property of the model implies that, if it is correct, the methods of chapter 3 will have trouble obtaining definite results, since in any continuous parametrisation the leading cuts will look like poles.

Whilst we must admit that this model is by no means the only possible explanation of these effects, the ease with which it accounts for them is nonetheless remarkable.

Figures for Chapter 4

- 4.1 Comparison of the model of e.q. (4.38) for the total cross section (curve C) with the data. Curve I from chapter 3 is also shown.
- 4.2 The function  $\beta(j)$  for the curve C of fig. (4.1).
- 4.3 The  $j$ -plane structure of the differential cross section. Solid lines are positive contributions, broken lines are negative. The dot-dash line is the location of the pomeron-meson interference term, if it were present.

fig. (4.1)

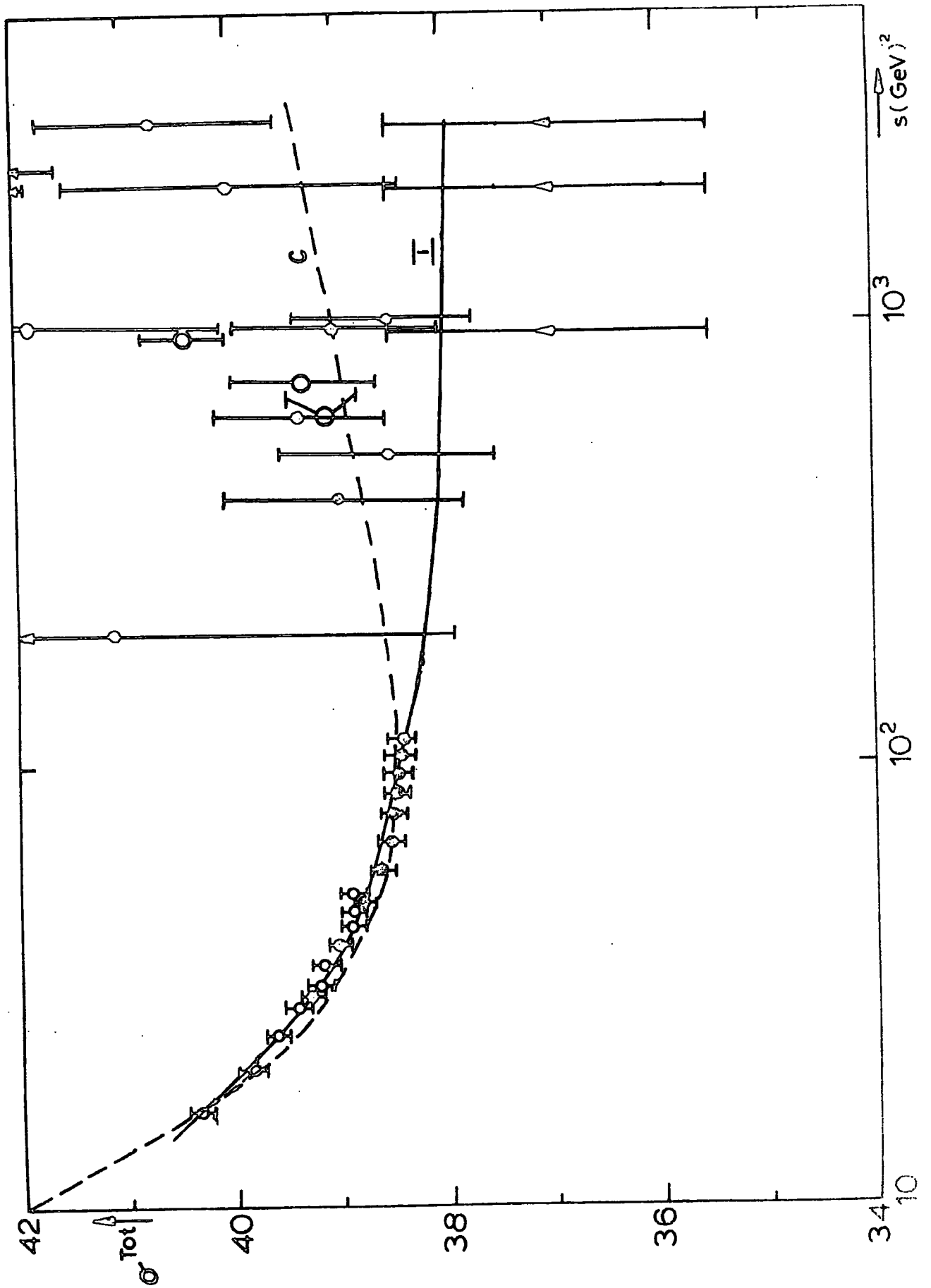


fig. (4.2)

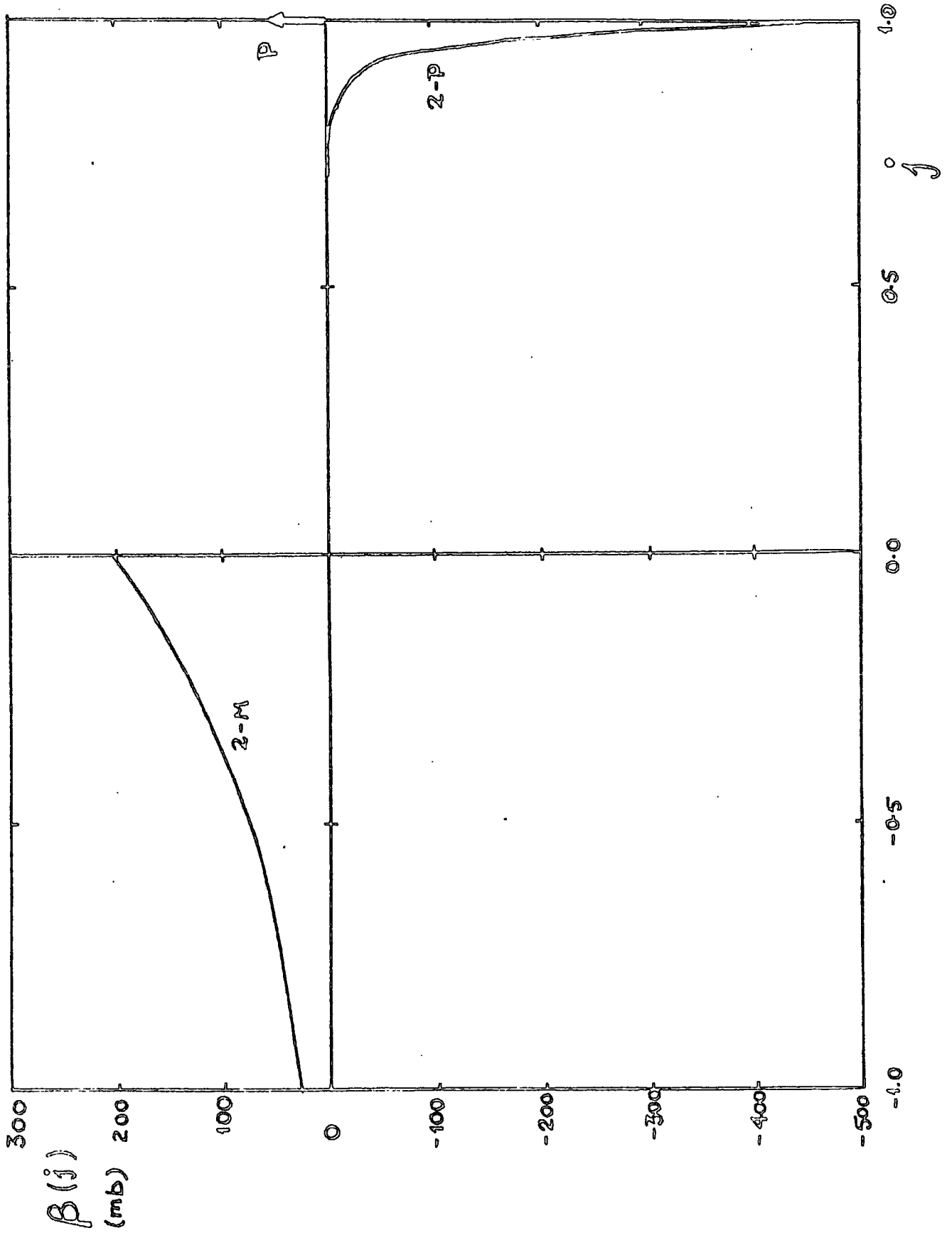
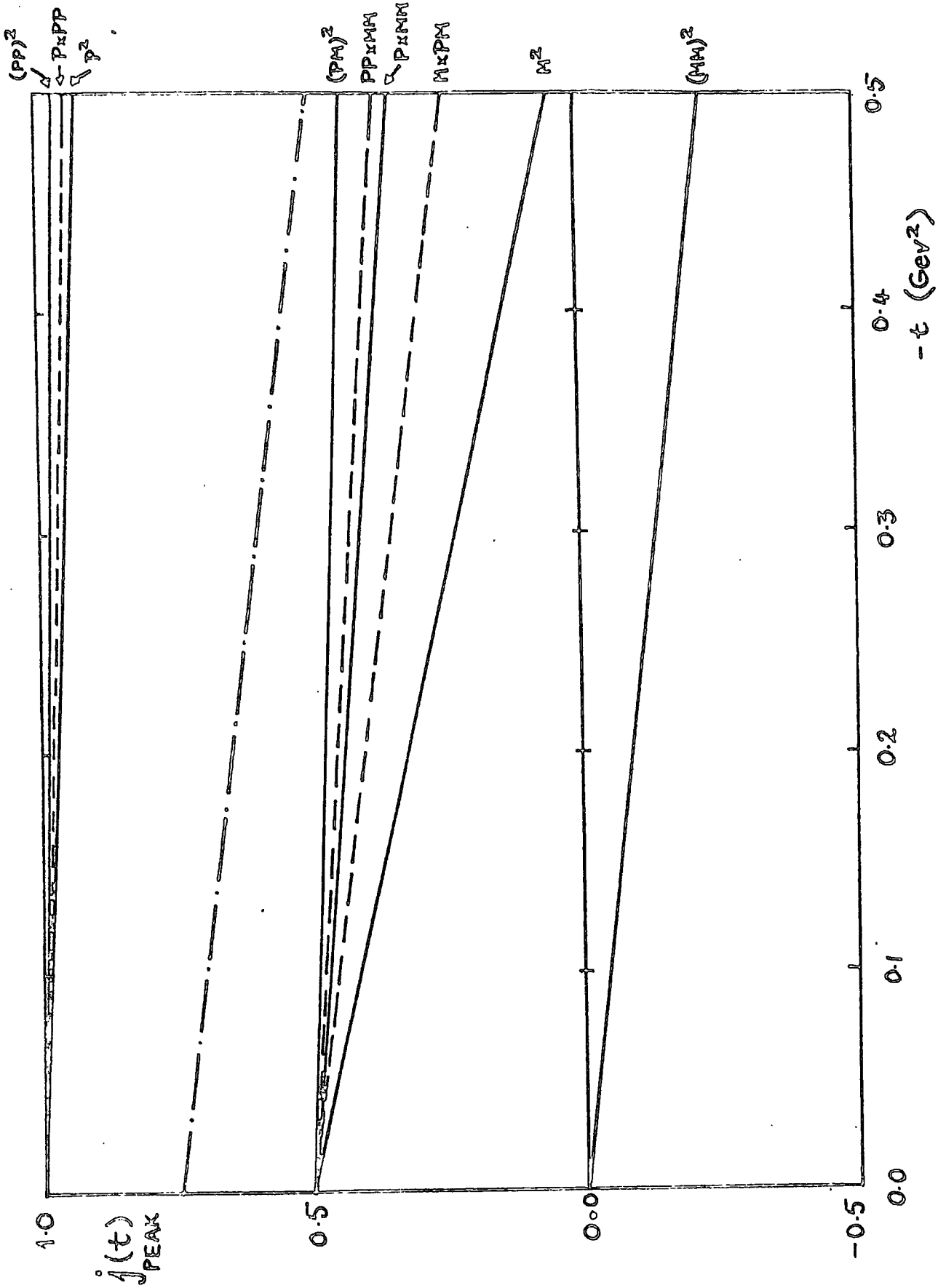


fig. (4.3)



CHAPTER 5. THE PP DATA AT VERY HIGH ENERGIES AND CONCLUDING REMARKS

INTRODUCTION

The recent experiments at the CERN intersecting storage rings<sup>(46,73,74)</sup> have caused a great deal of theoretical and phenomenological activity. In this chapter we discuss some of the explanations that have been proposed, and consider the present state of the situation.

Perhaps the most unexpected of the results is the apparent sharp rise in the total cross section above  $s \approx 500 \text{ GeV}^2$ . The rise appears to have the form

$$\sigma_T \sim (\log s)^2 \quad (5.1)$$

$$s \rightarrow \infty$$

and the models that we shall discuss may be divided into two groups - those that retain this property as  $s$  goes to infinity, and those for which  $\sigma_T$  flattens off and tends to a constant from below.

In section (5.1) we review the experimental situation, and list the important features of the data. The various models are described in sections (5.2 - 5.4), and section (5.5) is a general discussion.

### 5.1 The Experimental Situation

The prominent features of the data are as follows:

- (i) The total cross section rises by about 4 mb between  $s = 548 \text{ GeV}^2$  and  $s = 2776 \text{ GeV}^2$ . (see fig. (5.1)).
  - (ii) The differential cross section is approximately exponential in  $t$  for seven orders of magnitude. (see fig. (5.2)).
  - (iii) There is a break in the slope of the differential cross section which remains constant in position at  $t \approx -0.15 \text{ GeV}^2$  for all energies.
  - (iv) The mean differential cross section slope for  $|t| < 0.15 \text{ GeV}^2$  varies from  $11.8 \text{ GeV}^{-2}$  to  $13.1 \text{ GeV}^{-2}$  between  $s = 548 \text{ GeV}^2$  and  $s = 2776 \text{ GeV}^2$ , whereas that for  $|t| > 0.15 \text{ GeV}^2$  is approximately constant at  $10.8 \text{ GeV}^{-2}$  in this energy range.
  - (v) The differential cross section shows a dip-bump structure for large  $|t|$ . The position of the dip is constant at  $t = -1.3 \text{ GeV}^2$ , but the height of the bump decreases with energy. (see fig. (5.2)).
- Leader and Maor<sup>(52)</sup> analysed the total cross section. They found that, above  $s \approx 20 \text{ GeV}^2$ , the data are well described by

$$\sigma_T(s) \approx C + D (\log(s/s_0))^2 \quad (5.2)$$

where

$$\begin{aligned} C &= 38.4 \text{ mb} \\ D &= 0.49 \text{ mb} \\ s_0 &= 122 \text{ GeV}^2 \end{aligned} \quad (5.3)$$

They also pointed out that, if we define the differential cross section slope by

$$b(s,t) \equiv \frac{d}{dt} \left( \log \frac{d\sigma}{dt} \right) \quad (5.4)$$

then if e.q. (5.2) is true, it can be shown<sup>(54)</sup> that

$$b(s,0) \underset{s \rightarrow \infty}{\sim} (\log s)^2 \quad (5.5)$$

Now in point (iv) above we mentioned that  $b(s,t)$  is approximately

independent of  $s$  for larger  $|t|$ . This means that, as energy increases, a slope break at small  $|t|$  will develop. Thus there is a correlation between the slope break and the rising total cross section.

## 5.2 Field Theoretical Models

The model of Cheng, Walker and Wu<sup>(55)</sup> deserves to be mentioned first, since it was proposed before the new data became available<sup>(75)</sup>. It is based on the impact picture of high energy scattering derived from quantum field theory.

The model is supposed to apply to all hadrons at sufficiently high energies. In a particular scattering process, each hadron is considered as a superposition of virtual states with short lifetime. In the rest-frame of the other hadron, however, the lifetimes of the virtual states are appreciable. Lorentz contraction deforms each virtual state into a thin pancake, which can be separated into an absorbing core of radius  $R \sim R_0 \log s$ , ( $R_0$  constant), and a partially absorbing fringe whose width is constant at about 1 f. The predictions of this model at very high energies are as follows.

- (i) Total cross sections for all hadron-hadron scattering processes become equal at infinite energy.
- (ii) All total cross sections rise like  $(\log s)^2$  with energy.
- (iii) Elastic cross sections approach one half of total cross sections, i.e.

$$\frac{\sigma_{EL}}{\sigma_T} \xrightarrow{s \rightarrow \infty} \frac{1}{2} \quad (5.6)$$

- (iv) There is a forward peak in elastic scattering processes, and a dip=bump structure at large  $|t|$ . The diffraction peak shrinks and the dip moves to smaller  $|t|$  as energy increases.

For an elastic channel  $j$  the authors constructed an amplitude  $M_j(s, \Delta)$  having the above asymptotic properties. They wrote

$$\frac{d\sigma}{dt} = \left| \frac{M_j(s, \Delta)}{s} \right|^2 \quad (5.7)$$

where  $t = -\Delta^2$  (5.8)

$$\text{and } \sigma_T(j) = A_j s^{-\frac{1}{2}} + \frac{4.893}{s} \text{Im } M_j(s, 0) \quad (5.9)$$

The  $s^{-\frac{1}{2}}$  term in e.q. (5.9) was added to patch up the fit to the data at lower energies, since  $M_j(s, \underline{\Delta})$  is supposed to be an asymptotic amplitude.

The model satisfactorily fits all the available hadron-hadron elastic scattering and total cross section data at and above Serpukov energies. It must be pointed out, however, that the  $s^{-\frac{1}{2}}$  term in e.q. (5.9), which is quite arbitrary, is essential to the total cross section fits.

This model is extremely interesting from the point of view that it predicted the rising total cross section, but it seems that the energy region in which it should be valid has not yet been reached. Its interpretation in terms of the theory of hadrons is also unclear.

### 5.3 The Triple Pomeron Vertex

Some authors<sup>(71,72)</sup> have pointed out that the new data can be interpreted in terms of the triple pomeron vertex. It turns out that if this vertex is non-zero at  $t = 0$ , then its contribution to the pp inelastic cross section, and therefore also to the total cross section, rises logarithmically with energy.

On the other hand, it is well known that if the pomeron is a factorising Regge Pole with unit intercept, unitarity forces the triple pomeron vertex to vanish at  $t = 0$ . The two papers differ in their solutions to this problem. Kaidalov et al<sup>(71)</sup> made the assumption that the pomeron intercept is slightly less than unity, whereas Amati et al<sup>(72)</sup> used a pomeron with unit intercept, and imposed unitarity by introducing absorptive cuts in the s channel. Both these models were able to fit the total and differential cross sections, and at present the data are not good enough to differentiate between them.

#### 5.4 The Reggeon Calculus

In chapter 1 we used the Reggeon Calculus to construct the absorption model for the two-reggeon cut. An advantage of this cut prescription is that it introduces no extra free parameters not contained in the pole parametrisation. It is, however, unsatisfactory in some respects, and it might be attractive to try a more phenomenological approach, by parametrising the Gribov Vertex and determining its form by fits to the data. It is then necessary to include more complicated cut terms. Those which contribute to order  $1/\log s$  have been calculated by Ter-Martyrosian, and these are shown in fig. (5.3). The vertices involved are  $g(t)$ , the usual pomeron - two proton vertex,  $N(t, t_1, t_2)$ , the two pomeron - two proton vertex discussed in chapter 1,  $\Gamma(t, t_1, t_2)$ , the three pomeron vertex, and  $C(t, t_1, t_2, t_3, t_4)$ , the five pomeron vertex.

This has been done independently by Pajares and Schiff<sup>(49)</sup> and Sukhatme and Ng<sup>(50)</sup> in two basically similar papers which differ mainly in the parametrisations adopted for the vertices. Both obtained adequate fits to the data with an asymptotic pp total cross section of about 60 mb., somewhat higher than that found in chapter 3. This is a result of the inclusion of the multiple scattering terms.

The authors point out that the rising total cross section and dip-bump structure of the differential cross section are inevitable consequences of the Gribov approach. The slope break is not, however, and in fact is not present if only the two pomeron cut is considered, but is generated by the additional terms in fig.(5.3 (c) - (f)).

In contrast to the previous models discussed, this approach predicts

$$\sigma_{EL} / \sigma_T \xrightarrow{s \rightarrow \infty} 0 \quad (5.10)$$

## 5.5 Discussion and Conclusions

These models are not all incompatible. For example, Amati et al<sup>(72)</sup> used absorptive cuts in their paper to recover unitarity, and might instead have used a Reggeon Calculus model for their cut corrections. Similarly, instead of a simple pole pomeron, the authors<sup>(49,50)</sup> in section (5.4) might have used a more complicated singularity. Either of these procedures, of course, would have produced a model with many free parameters.

The significance of the new data seems to be that some modifications of our ideas about the pomeron are necessary. It should not, however, be forgotten that more precise knowledge about the pomeron at high energies should enable us to obtain more unambiguous information about the mesons at lower energies. To this end it would be extremely useful if conventional accelerators were used for the high-precision experiments on low-energy pp scattering which are now possible. Unfortunately, such experiments are not as prestigious as less precise ones at ultra-high energies.

Perhaps we should have included the pomeron in section (1.2) as one of the problems of Regge Theory. As it was originally invented to explain the apparently constant total cross sections, there seems no reason for the pomeron to retain its simple pole form now that the high energy structure of total cross sections is known to be markedly different from what was formerly thought. The most hopeful results seem to have come from Dual Field Theory, where a pomeron-like singularity emerges as a natural result of the programme. (See, for example, ref. (77)).

In future, Regge phenomenology will be increasingly concerned with very high energies, and particularly inclusive and multi-particle processes. Whilst much useful information will undoubtedly be gained in this way, no complete description of strong interactions will be possible until the problems of two body scattering have been solved, and in particular those discussed in section (1.2). To this end more realistic

cut models are required, as well as a better knowledge of possible low-lying trajectories such as the  $\rho'$ . Finally, until we have more coherent ideas about the nature of the pomeron, all Regge fits will be to a lesser or greater extent ambiguous.

Figures for Chapter 5

- 5.1 The new data on the pp total cross section.
- 5.2 The pp elastic differential cross section at  $s = 2776 \text{ GeV}^2$ .
- 5.3 The Reggeon Calculus diagrams which contribute to order  $1/\log s$ .

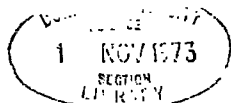


fig. (5.1)

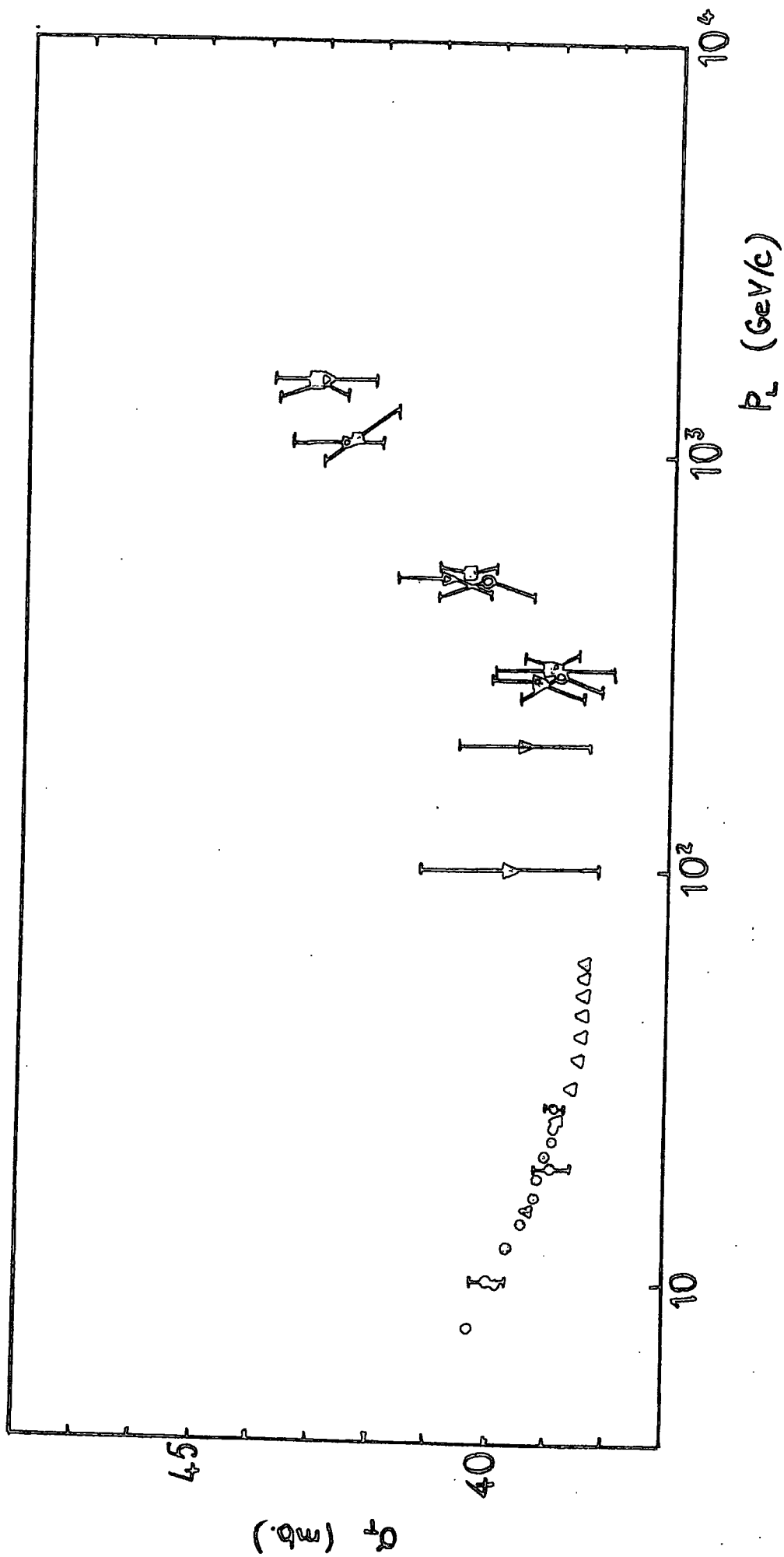


fig. (5.2)

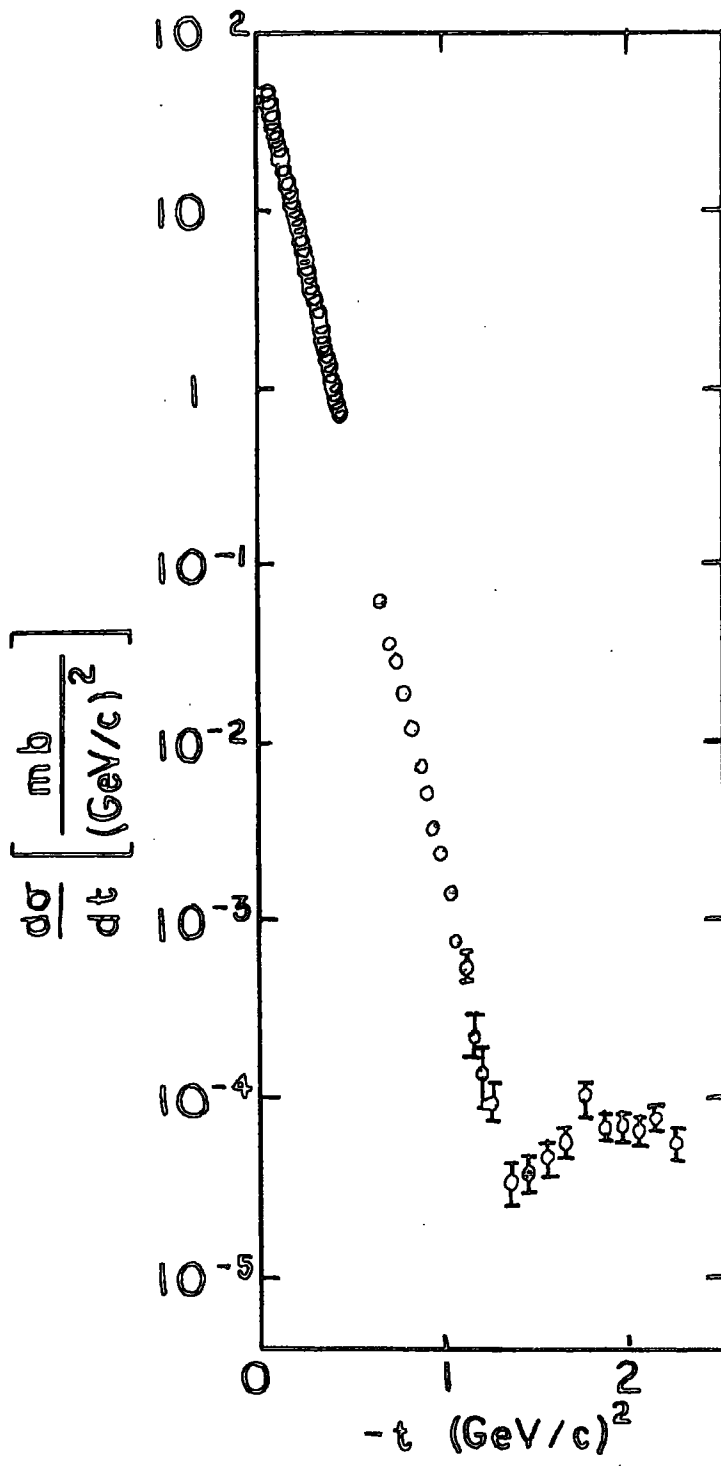
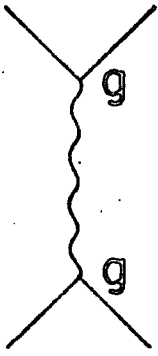
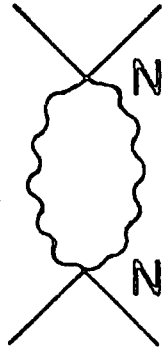


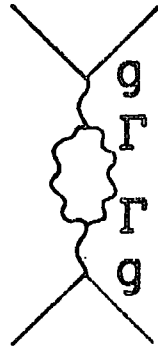
fig. (5.3)



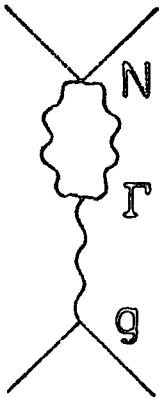
(a)



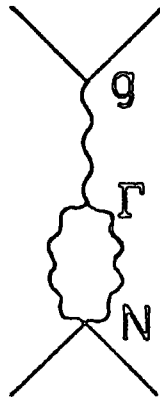
(b)



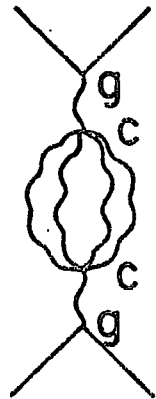
(c)



(d)



(e)



(f)

APPENDIX      ELASTIC SCATTERING KINEMATICS

We consider the process

$$1 + 2 \rightarrow \bar{3} + \bar{4}$$

where  $m(1) = m(3) \equiv m$

and  $m(2) = m(4) \equiv \mu$

Particle (1) is the target, and particle (2) the 'beam'.

The Mandelstam variables  $s$ ,  $t$ ,  $u$  for this process are defined by

$$s = (p_1 + p_2)^2 = (p_3 + p_4)^2 \quad (\text{A.1})$$

$$t = (p_1 + p_3)^2 = (p_2 + p_4)^2$$

$$u = (p_1 + p_4)^2 = (p_2 + p_3)^2$$

Conservation of energy-momentum gives

$$p_1 + p_2 + p_3 + p_4 = 0 \quad (\text{A.2})$$

which implies that

$$s + t + u = 2(m^2 + \mu^2) \quad (\text{A.3})$$

We define the laboratory (LAB) frame by

$$\underline{p}_1(\text{LAB}) = 0 \quad (\text{A.4})$$

and the centre of mass (CM) frame by

$$\underline{p}_1(\text{CM}) + \underline{p}_2(\text{CM}) = 0 \quad (\text{A.5})$$

We call the LAB energy and three-momentum of the beam  $w_L$  and  $\underline{p}_L$  respectively, i.e.

$$p_2(\text{LAB}) = (w_L, \underline{p}_L) \quad (\text{A.6})$$

with  $p_L = \|\underline{p}_L\|$

We call the CM three-momentum of the target  $q$ , i.e.

$$\underline{p}_1(\text{CM}) = -\underline{p}_2(\text{CM}) = q \quad (\text{A.7})$$

In terms of these variables the following relations may be deduced

$$s = m^2 + \mu^2 + 2 m w_L \quad (\text{A.8})$$

and 
$$q = m p_L / \sqrt{s} \quad (\text{A.9})$$

The  $s$  channel CM scattering angle  $\Theta$  is defined by

$$\cos \Theta = - \frac{p_2(\text{CM}) \cdot p_1(\text{CM})}{|p_2(\text{CM})| |p_1(\text{CM})|} \quad (\text{A.10})$$

which reduces to

$$\cos \Theta = 1 + t / 2 q^2 \quad (\text{A.11})$$

The following relations may be obtained

$$\sin^2 \frac{1}{2} \Theta = -t / 4 q^2 \quad (\text{A.12})$$

$$\cos^2 \frac{1}{2} \Theta = 1 + t / 4 q^2 \quad (\text{A.13})$$

It is also useful to introduce a variable  $\rho$ , defined by

$$\rho = (m + w_L) / \sqrt{s} \quad (\text{A.14})$$

or alternatively

$$\rho = (1 + q^2 / m^2)^{\frac{1}{2}} \quad (\text{A.15})$$

REFERENCES

- 1 A.D.Martin, T.D. Spearman Elementary Particle Theory, Northolland, 1970.
- 2 P.D.B. Collins, E.J. Squires Springer Tracts in Modern Physics, vol.45, Springer 1968
- 3 V. Barger, R.J.N. Phillips Phys. Rev. 187 (1969) 2210
- 4 G.V. Dass, C. Michael, R.J.N. Phillips Nuc. Phys. 89 (1969) 549
- 5 W. Rarita et al Phys. Rev. 165 (1968) 1615
- 6 R.C. Johnson, E.J. Squires Phys. Letters 32B (1970) 385
- 7 V. Rittenberg, H.R. Rubinstein Phys. Rev. Letters 25 (1970) 191
- 8 R. Dolen, D. Horn, C. Schmid Phys. Rev. 166 (1968) 1768
- 9 V.N. Gribov, I.Y. Pomeranchuk Phys. Rev. Letters 8 (1962) 343
- 10 V.N. Gribov JETP 26 (1968) 414
- 11 P.V.Landshoff, J.C. Polkinghorne Phys. Reports 5C (1972)
- 12 P.D.B. Collins Phys. Reports 1C (1971)
- 13 R.C. Johnson Durham preprint, Nov. 1971
- 14 R.P. Worden Private communication, May 1973
- 15 H. Harari Phys. Rev. Letters 20 (1968) 1395
- 16 P.G.O. Freund Phys. Rev. Letters 20 (1968) 235
- 17 G. Veneziano Nuovo Cimento 57A (1968) 190
- 18 G. Veneziano International School of Subnuclear Physics, Erice, July 1970
- 19 V. Singh Phys. Rev. 129 (1963) 1889
- 20 S. Mandelstam, L.L. Wang Phys. Rev. 160 (1967) 11490
- 21 S. Mandelstam Nuovo Cimento 30 (1963) 1127,1148
- 22 E. Leader, B. Nicolescu Westfield College preprint, April 1972
- 23 F. Halzen, C. Michael Phys. Rev. Letters 368 (1971) 367
- 24 C. Daum, C. Michael, C. Schmid Phys. Letters 31B (1970) 222
- 25 V. Rittenberg, H.R. Rubinstein Phys. Rev. Letters 25 (1970) 191

26	R.L. Cool et al	Phys. Rev. Letters 17 (1966) 102
	D.V. Bugg et al	Phys. Rev. 16 (1968) 1466
	W. Baker et al	Phys. Rev. 129 (1963) 2288
	W. Galbraith et al	Phys. Rev. 138 (1965) 8913
	A.N. Diddens et al	Phys. Rev. 132 (1963) 2721
	J.N. MacNaughton et al	Nuc. Phys. B14 (1969) 237
	J.A. Danysz et al	Nuc. Phys. B14 (1969) 161
	J.A. Debaisieux et al	Nuovo Cimento 43A (1966) 142
	K.J. Foley et al	Phys. Rev. Letters 11 (1963) 503
	W. DeBaere et al	Nuovo Cimento 45A (1966) 142
	Chih-Yung Chien et al	Phys. Letters 28B (1969) 615
	J. Banaigs et al	Nuc. Phys. B9 (1969) 640
	P.L. Jain et al	Nuc. Phys. B19 (1970) 568
	J. Whitmore et al	Phys. Rev. D3 (1971) 1092
	S. Anderson et al	Phys. Letters 30B (1969) 56
	N. Booth et al	Phys. Rev. Letters 23 (1969) 193
	M. Borghini et al	Phys. Letters 31B (1970) 405
	M. Aderholz et al	Phys. Letters 24B (1967) 434
	J. Gordon et al	Phys. Letters 21 (1966) 117
	D.P. Owen et al	Phys. Rev. 181 (1969) 1794
	V. Chabaud et al	Phys. Letters 38B (1972) 445
	M. Albrow et al	Nuc. Phys. B30 (1971) 273
	R.D. Erlich et al	Phys. Rev. Letters 26 (1971) 925
27	S. Andersson et al	Stonybrook Conf. (1969)
28	F. Hayot, H. Navelet	Phys. Letters 37B (1971) 424
29	M.G. Albrow et al	Nuc. Phys. B30 (1971) 273
30	R.C. Miller et al	Nuc. Phys. B37 (1972) 349
31	F. Wagner, C. Lovelace	Preprint CERN Th 1227, Sept. (1970)
32	R.E. Cutkosky, B.B. Deo	Phys. Rev. 174 (1968) 1859
33	A.D. Martin, R. Perrin	Nuc. Phys. B20 (1970) 287
34	R.E. Cutkosky	Private communication, 1972
35	V. Barger, R.J.N. Phillips, K. Geer	Nuc. Phys. B42 (1972) 29

36 K.J. Foley et al Phys. Rev. Letters 19 (1967) 857  
37 S.P. Denisov et al Phys. Letters 368 (1971) 415  
38 G. Barbiellini et al Oxford Conf. April(1972)  
39 J.D. Jackson, G.F. Hite Phys. Rev. 169 (1968) 1248  
40 A. Kanazawa Hokkaido preprint, Sept. (1970)  
41 K.J. Foley et al Phys. Rev. Letters 11 (1963)  
425, 15 (1965) 45  
42 J.V. Allaby et al Phys. Letters 288 (1968) 67,  
348 (1971) 435  
43 G.G. Beznogikh et al Phys. Letters 308 (1967) 274  
44 M. Holder et al Phys. Letters 358 (1971) 355, 361  
G. Barbiellini et al Phys. Letters 398 (1972) 663  
45 R.A. Carrigan Phys. Rev. Letters 24 (1970) 168  
46 U. Amaldi et al Phys. Letters 448 (1973) 112,  
CERN preprint, (1973)  
47 V. Bartenev et al Phys. Rev. Letters 29 (1972) 1755  
48 S.P. Denisov et al Phys. Letters 368 (1971) 415  
49 C. Pajares, D.Schiff Orsay preprint, May (1973)  
50 U.P. Sukhatme, J.N. Ng Washington preprint, May (1973)  
51 L. Lukaszuk, B. Nicolescu Paris preprint IPNO-TH 73-18 (1973)  
52 E. Leader, U. Maor Phys. Letters 438 (1973) 505  
53 M. Froissart Phys. Rev. 123 (1961) 1053  
54 R.J. Eden Rev. Mod. Phys. 41 (1971) 15  
55 H. Cheng, J.K.Walker, T.T. Wu Phys. Letters 448 (1973) 97  
56 J.S. Ball et al Phys. Rev. Letters 20 (1968) 518  
57 R.J.N. Phillips Nuc. Phys. 82 (1967) 657  
58 M. LeBellac Nuovo Cimento 55A (1968) 318  
59 F. Henyey et al Phys. Rev. 182 (1969) 1579  
60 C. Schmid CalTech Conf. March (1971)  
61 H.H. Rosenbrock Comp. J.3 (1960) 175  
62 H. Rothe Phys. Rev. 159 (1967) 1471  
63 A. Gersten Nuc. Phys. 812 (1969) 537  
64 M. Davier, H. Harari SLAC preprint, (1971)

- 65 Y. Zarmi Phys. Letters 37B (1971) 393
- 66 E.L. Berger, G.C. Fox Preprint UCRL 18886 (1969)
- 67 E.J. Squires Springer Tracts in Modern Physics vol. 57 (1971) 1
- 68 C. Lovelace Caltech Conf. March (1971)
- 69 J.B. Bronzan, C.E. Jones Phys. Rev. 160 (1967) 1494
- 70 A.R. White Nuc. Phys. 850 (1972) 93, 130
- 71 D. Amati, L. Caneschi, M. Ciafaloni Preprint CERN Th 1676, May (1973)
- 72 A.B. Kaidalov et al Moscow preprint, May (1973)
- 73 S.R. Amendolia et al Phys. Letters 44B (1973) 119, CERN preprint, (1973)
- 74 C. Rubbia et al Chicago Conf. Sept. (1972)
- 75 H. Cheng, J.K. Walker, T.T. Wu Chicago Conf. Sept. (1972)
- 76 K.A. Ter-Martyrosian Sov. J. Nuc. Phys. 10 (1970) 600, 715
- 77 C. Lovelace CERN preprint TH 1381, July (1971)

